SERS-based detection methods for screening of genetically modified bacterial strains

Morelli, Lidia

Publication date:
2018

Document Version
Publisher's PDF, also known as Version of record

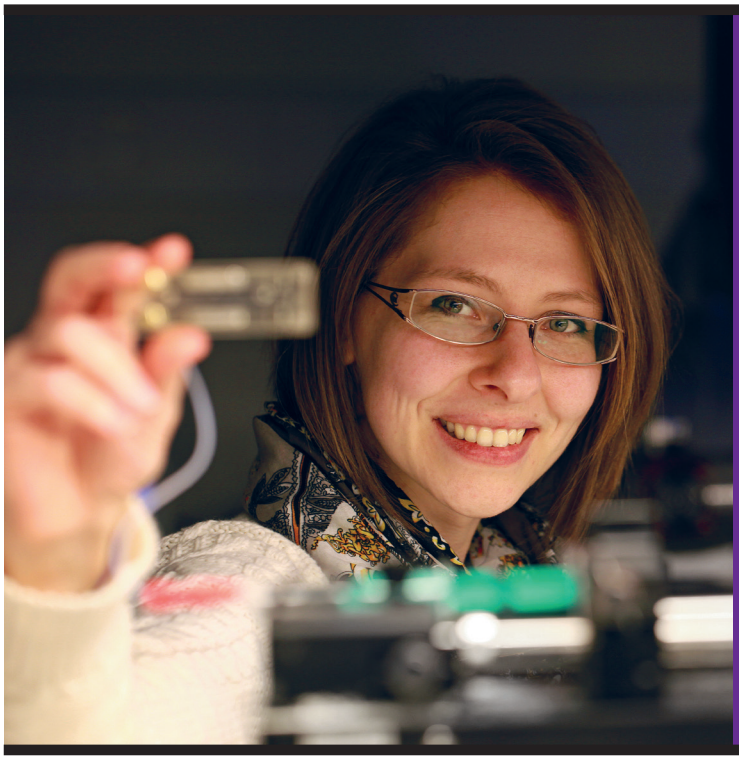

SERS-based detection methods for screening of genetically modified bacterial strains

Lidia Morelli
PhD Thesis December 2017

DTU Nanotech
Department of Micro- and Nanotechnology

SERS-based detection methods for screening of genetically modified bacterial strains

Lidia Morelli

Ph.D. Thesis

December 21, 2017

DTU Nanotech – Department of Micro- and Nanotechnology

Technical University of Denmark

Building 345C

2800 Kongens Lyngby

DENMARK

DTU Nanotech
Department of Micro- and Nanotechnology

To my family, to my boyfriend, to my friends

And, last but not least, to myself

Contents

Preface

This thesis is presented as a partial requirement for obtaining a Ph.D. degree from the Technical University of Denmark (DTU). The project was funded by the Danish National Research Foundation (grant no. DNRF122), by the Villum Fonden (grant no. 9301) and by the European Research Council (grant no. 320535), within the framework of the 'HERMES' project. The work of Christian Bille Jendresen was supported by The Novo Nordisk Foundation (grant no. NNF15OC0015246).

The research was carried out in the Department of Micro- and Nanotechnology (DTU Nanotech) from December 2014 to December 2017. The Ph.D. project was supervised by Professor Anja Boisen and co-supervised by Researcher Kinga Zór and Researcher Tomas Rindzevicius.

Kongens Lyngby,
21st December, 2017
Lidia Morelli

Acknowledgements

First of all, I would like to acknowledge my supervisor, Prof. Anja Boisen, who made possible all the work presented in this thesis. She was a great example of determination and positivity, who first trusted and then supported me throughout the years, constantly encouraging me and backing new ideas. I also acknowledge my co-supervisor, Tomas Rindzevicius, for supporting my growth with proactive suggestions and feedback.

I was lucky enough to spend the years of my PhD with the Nanoprobers, a group of brilliant and creative people, who constantly ensured a comfortable, sharing and trustworthy working environment for personal and scientific growth. I had the pleasure of working closer with some of them, among the others Sune Zoëga Andreasen and Oleksii Ilchenko, learning a lot and getting back a more than productive outcome. Thanks also to Robert Burger, who supervised me during my first year and introduced me to the world of centrifugal microfluidics, never sparing a smile or a kind word. Same for Filo: without your support at the very beginning, I probably wouldn't have had the possibility to stay. I wish you all the best with Blusense, and I am sure a bright future is ahead of you.

Out of Nanoprobes, Prof. Alex Toftgaard Nielsen, Christian Bille Jendresen and Hemanshu Mundhada deserve a special acknowledgement for such a fruitful collaboration; the project would literally not have happened without your meticulous, organized and thorough work at DTU Biosustain.

A special thanks goes to Kinga Zór, the best co-supervisor and mentor I could ask for, without whom I would have probably been lost many and many times. Thanks also to Marco Matteucci for his priceless advice, as a friend and unofficial supervisor. A heartfelt thanks goes to my Master students, Laura Serioli and Francesca Alessandra Centorbi, for putting such commitment in their experimental work. I hope my supervision contributed to your professional growth – at least a little bit – helping you wherever you'll go next. Thanks also to our amazing technicians, Per, Christina and Lotte, for helping us throughout

the years (and sometimes fix our mess as well), to the whole Danchip staff and to the administrative staff here at Nanotech for their invaluable assistance.

Many people contributed to make my stay in Copenhagen warm and comfortable: among them, many Master students – Filomena, Elena, Florence, Giuseppe, Alessandro, Alessia, Giorgia, Eugenia, Alessandra, Erica, Giaele – and many old and new friends – Simone, Yasmin, Bannay, Chiara and Matteo, Chiara and Parid, Marlitt and Lukas, Cristina, William, Adele and Ricca, Marco and Corinna, Ben, Andrea (the best office mate ever!) and Laura. I will never forget our precious evenings and our – sometimes definitely exaggerate – dinners. Thanks for the laughter, the pictures, the memories, and thanks for making me feel like home, even, sometimes, so far away. Out of DTU, thanks to my old and new flatmates – Carsten, Daniel and Bas, who finally made and still make a house feel like home.

Thanks to the few – but golden – who still support me after (or in spite of) knowing me for 10+ years: thanks to Anna, Francesco and Giuliana, for staying, and for keeping my roots still.

Thanks to Fabio, for being there all the time, for all the fun, for travelling together, for helping me through all my difficult moments, and for so much more.

Thanks to my mum, Pina, my dad, Francesco, my brother, Roberto, and my grandma, Maria, for their support, for their unconditional love, and for teaching me the value of honesty and hard work: without all of this, I most probably would not have reached this point in my life. To my grandpa, Paolo, and my great grandma, Rosaria: I hope I inherited a tiny bit of your stubbornness, determination and strength, and I like to think you'd be proud of how I am fighting my way through life.

Abstract

The importance of metabolic engineering has been growing over the last decades, establishing the use of genetically modified microbial strains for overproduction of metabolites at industrial scale as an innovative, convenient and biosustainable method. Nowadays, application areas of microbial factories vary largely, including industrial production of valuable compounds for biofuels, polymer synthesis and food, cosmetic and pharmaceutical industry. The improvement of computational and biochemical tools has revolutionized the synthesis of novel modified microbial strains, opening up new possibilities for rapid genome modification and high-throughput development of large-size microbial libraries. However, there is still a need for fast, high-throughput and real-time screening techniques, in order to speed up the testing of newly produced strains.

In the frame of this PhD project, surface enhanced Raman scattering (SERS) has been identified as a fast and molecule-specific detection technique, increasingly applied to sensing in life sciences. Also due to its great potential for miniaturization and automation, SERS could represent a possible solution for specific, robust and high-throughput sensing in metabolic engineering.

As the main goal of this Ph.D. project, we explored the potential of SERS for quantitative and reproducible screening of genetically modified *E. coli* strains, based on the amount of specific secondary metabolites found in supernatant. However, due to the intrinsic sensitivity of SERS, and due to the matrix complexity of real supernatant samples, a pre-treatment step was needed to exclude salts and other unwanted compounds from detection. Liquid-liquid extraction (LLE) and supported liquid membrane (SLM) extraction were combined with SERS, enabling a robust and quantitative discrimination between different *E. coli* strains, validated with high-performance liquid chromatography (HPLC).

Centrifugal microfluidics, based on the actuation of microfluidic discs by simply controlling a spinning motor, represents an appealing alternative to traditional microfluidics, placing special emphasis on parallelization, short time-to-response and ease of use of the developed devices. We developed a solvent-resistant lab-on-disc (LoD) device, integrating filtration, LLE and SERS-based sensing; besides achieving fast pre-treatment and sensing of supernatant samples on disc, the use of large-scale fabrication

techniques (injection molding and ultrasonic welding) enabled the production of tens of microfluidic modules within two working days, demonstrating the scalability of the developed device.

Resumé på Dansk

Vigtigheden af at kunne regulere og optimere cellulære processer via genmanipulation er vokset de seneste årtier. Brugen af genmodificerede bakteriekulturer er en innovative, praktisk og bæredygtig metode til produktion af metabolitter på industriel skala. I dag bruges sådanne bakteriefabrikker i mange forskellige industrier til production af værdifulde kemikalier til biobrændstof, polymersyntese og fødevarer, kosmetik og i medicinalindustrien. Udviklingen af værktøjer til beregning og fremskridtet indenfor biokemien har revolutioneret syntesen af nye genmodificerede bakteriekulturer og åbnet nye muligheder for hurtig genmodificering og etablering af meget omfattende genbiblioteker for bakterier. Dog er der stadig behov for hurtige og effektive screening-teknikker for at kunne teste disse nye bakterier ligeså hurtigt som de kan udvikles.

I dette ph.d. projekt er teknikken 'surface enhanced Raman scattering (SERS)' blevet brugt til hurtig, molekylespecifik detektion. Muligheden for at formindske og automatisere teknikken gør SERS til en mulig metode til specifik, robust og effektiv screening af bakteriekulturer.

Det overordnede mål for dette ph.d.-projekt var at undersøge SERS teknikkens potentiale til kvantitativ og reproducerbar screening af genmodificerede *E. coli* bakteriekulturer. Potentialet blev vurderet ud fra mængden af en specifik sekundær metabolit der fandtes i supernatanten fra de forskellige bakteriekulturer. Da SERS er en yderst sensitiv teknik og da supernatanten fra en bakteriekultur er yderst kompleks og sammensat, var der behov for at behandle prøven inden detektion. Denne behandling skulle fjerne salte og andre uønskede molekyler. De to behandlingsteknikker 'Liquid-liquid extraction' (LLE) og 'supported liquid membrane (SLM) extraction' blev brugt sammen med SERS for at opnå en robust og kvantitativ skelnen mellem de forskellige *E. coli* bakteriekulturer. Resultaterne blev valideret med den etablerede teknik 'high-performance liquid chromatography (HPLC)'.

'Centrifugal microfluidics', som er en metode baseret på at igangsætte et flow på en disc ved at kontrollere en motor der drejer disc'en rundt er et tiltalende alternativ til traditional 'microfluidics'. Metoden muliggør parallelisering af målinger, korte

responstider og er nem at anvende. Vi har udviklet en opløsningsmiddel-resistent lab-on-disc (LoD) enhed der integrerer filtrering, LLE og SERS detektion. Udover hurtigt at kunne behandle og måle på supernatant prøver, er metoden yderst skalerbar. Med valget af fabrikationsteknikker (injection molding og ultrasonic welding), kan der på to arbejdsdage produceres mere end ti mikrofluid moduler.

List of abbreviations

$[H^+]$	Concentration of H^+ ions in aqueous phase
$[S]_1$	Concentration of the solute S in the aqueous phase
$[S]_2$	Concentration of the solute S in the organic phase
$[S]_{2(HPLC)}$	Concentration of the solute S in the organic phase detected with HPLC
$[S]_{2(SERS)}$	Concentration of the solute S in the organic phase detected with SERS
$[S]_A$	Concentration of S in the acceptor phase
$[S]_D$	Concentration of S in the donor phase
µTAS	Micro total analysis
A	Activity
A^-	Conjugate base of a weak acid
CA	Cinnamic acid
CAD/CAM	Computer-aided design/computer-aided manufacturing
CNC	Computer numerical control
COC	Cyclic olefin copolymer
CPE	Cloud-point extraction
D	Distribution coefficient
DBTL	Design, build, test, learn
DCM	Dichloromethane
DLLME	Dispersive liquid-liquid microextraction
E. coli	*Escherichia coli*
EF	SERS enhancement factor
EtOH	Ethanol
F_C	Centrifugal force
F_{Co}	Coriolis force
F_E	Euler force
HA	Neutral form of a weak acid
HCl	Hydrochloric acid
HLLE	Homogeneous liquid-liquid extraction
HPLC	High-performance liquid chromatography
I_0	Intensity of incident laser

I_R	Raman intensity
I_{Raman}	Intensity of Raman signal
I_{SERS}	Intensity of SERS signal
K	Partition coefficient
K_a	Acid dissociation constant
LLE	Liquid-liquid extraction
LoD	Lab-on-disc
m	Mass
m_{tot}	Total moles of solute S
N_{Surf}	Average number of adsorbed molecules in the scattering volume for SERS
N_{Vol}	Average number of molecules in the scattering volume for Raman
OD_{600}	Optical density at 600 nm
p_0	Ambient pressure
PAL	Phenylalanine ammonia-lyase
PC	Polycarbonate
PCR	Polymerase chain reaction
PDMS	Poly(dimethyl siloxane)
pHCA	*p*-Coumaric acid
Phe	Phenylalanine
PLS	Partial least squares
PMMA	Poly(methylmetacrylate)
PP	Poly(propylene)
PS	Poly(styrene)
PSA	Pressure sensitive adhesive
q	Fraction of solute left in the aqueous phase after LLE
r	Radius
RIE	Reactive ion etching
SDME	Single-droplet microextraction
SERS	Surface-enhanced Raman scattering
SLM	Supported liquid membrane
SPE	Solid phase extraction
t	Time
TAL	Tyrosine ammonia-lyase
TRY	Titer, rate, yield
Tyr	Tyrosine

UV	Ultraviolet
V	Volume of a gas bubble in a compressed or expanded state
V_0	Volume of a gas bubble at p_0
V_1	Volume of aqueous phase
V_2	Volume of organic phase
α_1	Fraction of HA in the aqueous phase
α_A	Fraction of HA in the acceptor phase
α_D	Fraction of HA in the donor phase
Δp_C	Centrifugal pressure
Δp_e	Capillary pressure at equilibrium
Δp_I	Maximum capillary pressure before bursting of the capillary valve
Δp_{pn}	Pneumatic pressure
θ_e	Equilibrium contact angle
θ_I	Maximum contact angle before bursting of the capillary valve
ν	Spinning frequency
ρ	Density
σ	Surface tension
σ_R	Raman cross-section
ω	Angular velocity

List of useful definitions

Bacterial supernatant	Liquid sample obtained by centrifugation and/or filtration of bacterial aliquots after a certain culture time.
Design	The process of choosing chemical processes, materials, microfluidic operations and fabrication techniques involved in the creation of a complex microfluidic system, while respecting given specifications.
High-throughput	Processing a high number of samples within a short time, often through the use of automated systems.
Lab-on-disc	Microfluidic device embedding complex fluidic networks on a polymeric disc, actuated by a spinning motor
Large-scale production	Production of a commodity in high numbers through industrial plants and machinery. It is characterized by mechanization and automation, and it aims at the sale of goods in large volumes.
Liquid-liquid extraction (LLE)	Separation process based on the diffusion of a solute from a first liquid phase to a second one, based on the respective affinity. Important factors are the pH of the aqueous phase, the volume ratio between the phases and the solvent choice.
Metabolic engineering	The science of manipulation of enzymatic, transport and regulatory functions of the cell for metabolite overproduction or improvement of the cellular properties.
Micro total analysis (μTAS) system	Miniaturized system integrating multiple functional elements, such as sample pre-treatment and sensing, to provide a sample-in/answer-out approach.

Microfluidic operation	A particular fluidic task, such as filtration, valving, mixing or emulsification.
Platform cell factories	Well-known microorganisms used for development of novel pathways.
Proof-of-principle strain	The reconstruction of a pathway for overproduction of a compound in a platform cell factory.
Quantitative analysis	The process of identifying the amount of a compound in a sample.
Raman spectroscopy	A vibrational spectroscopic technique based on the inelastic scattering of light. A Raman spectrum of a sample illuminated by an incident laser contains information about the structure, crystallinity, orientation and amount of Raman active molecules.
Sample pre-treatment	Operations and manipulations carried out before instrumental determination to clean-up the sample, or to isolate or enrich the desired compounds. Some researchers distinguish between sample preparation (chemical operations) and pre-treatment (mechanical and basic treatments).
Supported liquid membrane (SLM) extraction	Separation process based on the diffusion of a solute from a donor to an acceptor aqueous phase. A porous membrane, impregnated with a non-volatile organic solvent, is placed between the phases. Important factors for separation are the membrane material, the organic solvent and the donor and acceptor pH.
Surface-enhanced Raman scattering (SERS)	Enhancement of Raman signal of molecules adsorbed or close to a metallic nanostructured surface. The material, size and shape of the SERS active surface are relevant for generating a plasmonic resonance phenomenon between the incident light and the substrate.

List of publications

Paper I	**Detection of *p*-coumaric acid from cell supernatant using surface enhanced Raman scattering** L. Morelli, C. B. Jendresen, K. Zór, T. Rindzevicius, M. S. Schmidt, A. T. Nielsen, A. Boisen *Procedia Technology*, vol. 27, pp. 190–192, 2017
Paper II	**Surface Enhanced Raman Scattering for Quantification of *p*-Coumaric Acid Produced by *Escherichia coli*** L. Morelli, K. Zór, C. B. Jendresen, T. Rindzevicius, M. S. Schmidt, A. T. Nielsen, and A. Boisen *Analytical Chemistry*, vol. 89, no. 7, pp. 3981–3987, Apr. 2017
Paper III	**Injection molded lab on disc platform for screening of genetically modified *E. coli* using liquid-liquid extraction and surface enhanced Raman scattering** L. Morelli†, L. Serioli†, F. A. Centorbi, C. B. Jendresen, M. Matteucci, O. Ilchenko, D. Demarchi, A. T. Nielsen, K. Zór, A. Boisen Manuscript submitted to *Lab on a Chip*
Paper IV	**Simultaneous detection and quantification of mixtures of bacterial metabolites using surface enhanced Raman scattering** L. Morelli, F. A. Centorbi, C. B. Jendresen, D. Demarchi, A. T. Nielsen, K. Zór, A. Boisen Manuscript to be submitted to *Analytical and Bioanalytical Chemistry*
Paper V	**Quantification of a bacterial secondary metabolite by SERS combined with SLM extraction for bioprocess monitoring** L. Morelli, S. Z. Andreasen, C. B. Jendresen, A. T. Nielsen, J. Emnéus, K. Zór, and A. Boisen *The Analyst*, vol. 142, no. 23, pp. 4553–4559, 2017.

† The authors contributed equally to the work

Contributions to the papers

Paper I	I designed, planned and performed the SERS experiments. I wrote the paper.
Paper II	I designed the extraction protocol, I designed, planned and performed the SERS experiments, I wrote the MatLab script and evaluated the results. I wrote the paper.
Paper III	I designed, planned and performed SERS experiments. I supervised and collaborated with Ph.D. student Laura Serioli, who significantly contributed to the design, fabrication and optimization of the microfluidic platform. I supervised the work of MSc student Francesca Alessandra Centorbi, who contributed to SERS experiments and data analysis, also helped by PostDoc Oleksii Ilchenko. I evaluated the data and wrote the paper.
Paper IV	I designed and planned SERS experiments. I supervised the work of MSc student Francesca Alessandra Centorbi, who contributed to experiments and SERS data analysis, also helped by PostDoc Oleksii Ilchenko. I evaluated the data and wrote most of the paper.
Paper V	I performed SERS experiments on samples pre-treated by Ph.D. student Sune Zoëga Andreasen through his SLM microfluidic device. I evaluated the data through my MatLab script and wrote most of the paper.

Bacterial samples were provided by Researcher Christian Bille Jendresen, who also performed part of HPLC data analysis in all the papers.

I also acknowledge the constructive and constant contribution of Researcher Kinga Zór in brainstorming, scientific discussion, experimental planning and revision of manuscripts throughout the Ph.D. project.

List of conference contributions and other works

I	**Detection Of Bacterial Metabolites Through Dynamic Acquisition From Surface Enhanced Raman Spectroscopy Substrates Integrated In A Centrifugal Microfluidic Platform** O. Durucan, L. Morelli, T. Rindzevicius, R. Burger, M. S. Schmidt, A. Boisen *The 19th International Conference on Miniaturized Systems for Chemistry and Life Sciences (μTAS)*, October 25 – 29 2015, Gyeongju, Korea *(POSTER)*
II	**Parallelized System For Biopolymer Degradation Studies Through Automated Microresonator Measurement In Liquid Flow** A. C. Ceccacci, L. Morelli, F. G. Bosco, R. Burger, C.-H. Chen, E.T. Hwu, A. Boisen *The 19th International Conference on Miniaturized Systems for Chemistry and Life Sciences (μTAS)*, October 25 – 29 2015, Gyeongju, Korea *(POSTER)*
III	**Surface Enhanced Raman Spectroscopy Detection Of p-Coumaric Acid From Cell Supernatant Using Gold-Capped Silicon Nanopillar Substrates** L. Morelli, C. B. Jendresen, K. Zór, T. Rindzevicius, M. S. Schmidt, A. T. Nielsen, A. Boisen *Biosensors 2016: 26th Anniversary World Congress On Biosensors,* May 25 – 27 2016, Gothenburg, Sweden *(POSTER)*
IV	**Challenges In The Integration Of Silicon SERS Substrates Into A Polypropylene Injection Moulded Microfluidic Chip** L. Serioli, L. Morelli, M. Matteucci, K. Zór and A. Boisen *43rd International Conference on Micro and Nanotechnology (MNE),* September 18 – 22 2017, Braga, Portugal *(POSTER)*

V	**Extraction And SERS-Based Detection Of Bacterial Metabolites In Mixture On A Centrifugal Microfluidic Device** L. Morelli, L. Serioli, F. A. Centorbi, M. Matteucci, D. Demarchi, K. Zór and A. Boisen *The 21st International Conference on Miniaturized Systems for Chemistry and Life Sciences (μTAS)*, October 22 – 26 2017, Savannah, Georgia, US *(POSTER)*
VI	**Blu-Ray-Based Micromechanical Characterization Platform For Biopolymer Degradation Assessment** A. C. Ceccacci, C.-H. Chen, E.-T. Hwu, L. Morelli, S. Bose-Goswami, F. Bosco, S. Schmid, A. Boisen *Sensors and Actuators B: Chemical*, vol. 241, pp. 1303–1309, 2017 *(FULL PAPER)*

1 Introduction

1.1 Motivation

Metabolic engineering was born as a science in the early 90's, defined as the direct modulation of cellular activities by manipulation of enzymatic, transport and regulatory functions, for metabolite overproduction or improvement of cellular properties [1]. Over the last decades, this field has gained more and more importance for production of food additives, biofuels and pharmaceuticals, focusing both on the optimization of existing processes and on the development of new ones [2]. The reasons behind the success of metabolic engineering are the versatility of the processes and the biosustainability of microbial-produced compounds. In fact, compounds of interest are often synthetized by using renewable substrates, when the chemical synthesis or extraction from natural resources are too complex or time and resource consuming [3]. Therefore, this approach is convenient and cost-effective, also at industrial scale.

The development of an effective microbial strain for industrial production consists in the development of a *proof-of-principle* strain, which is the implementation of an effective overproduction pathway in a host microorganism, and its subsequent upscaling for industrial fermentation, meeting specific titer, rate and yield requirements in order to balance production costs. The optimization of a *proof-of-principle* strain requires numerous cycles of design, building and testing of strains, resulting in a costly and time-consuming process, which can last up to several years [2]. While bioinformatic methods are routinely used for fast design and modeling of metabolic pathways, and new technologies have contributed to rapid genome modification, there is still a need for fast, real-time screening techniques to speed up the testing step [4]. Current analytical techniques for testing newly developed strains (e.g. gas chromatography, high-performance liquid chromatography) are robust and accurate, but they require long separation procedures, expensive instrumentation operated by skilled personnel, and long optimization protocols [4].

Thanks to its appealing advantages, Raman spectroscopy is being increasingly used as a detection method in life sciences [5]. It is a fast, molecule-specific, non-destructive and label-free technique, suitable for collecting information from non-transparent samples, even in small quantities [6]. Besides investigation of biological macromolecules [7] and physiology of cells and biological tissues [8], Raman spectroscopy was also applied to bioprocess monitoring, through the analysis of nutrients in industrial fermentation [9].

However, Raman detection and quantification of molecules in complex media can be challenging, especially at low concentrations. High laser power and long acquisition time are required, possibly damaging the organic molecules of interest; furthermore, fluorescence can cover the Raman signal in biological samples. Surface enhanced Raman scattering (SERS) is a technique able to increase the Raman signal of a molecule of several orders of magnitude, through the use of metallic nanostructured surfaces [10]. Thanks to the plasmonic properties of SERS active surfaces, a significant enhancement of the incident electromagnetic field is generated in the nanogaps, called *hotspots*, between adjacent nanoparticles; in this way, when a molecule is located in or close to a hotspot, its Raman signal is significantly increased [11]. The SERS signal can be observed with a lower laser power and shorter acquisition time than Raman, and signal intensity can overcome fluorescence of biological samples. Thanks to these advantages, the potential of SERS for analytical applications in life sciences is currently being explored [12]–[14]. Industrial applications of SERS have been limited by issues like non-uniformity and instability of SERS substrates, leading to irreproducible measurements and challenges in the quantification process. Therefore, the development of uniform and stable substrates is crucial for proper sensing and quantification. As a solution for uniformity across a large surface, Schmidt *et al*. [15] developed a SERS substrate, based on silicon metal-capped nanopillars, which is uniform at a wafer scale. Additionally, SERS is characterized by a molecule-specific signal, a sensitive and fast acquisition, and it has great potential for miniaturization and automation, representing a possible answer to the need for specific, robust and time-effective sensing in metabolic engineering.

A big effort towards miniaturization and automation of analytical processes was made in the last decades, since the concept of micro total analysis systems was first introduced in the early 90's. Micro total analysis (μTAS) systems aim at downscaling complex and

well-established analytical systems to miniaturized devices and develop new assays for μfluidics, enabling a sample-in/answer-out analysis on a small footprint, with low amounts of samples, chemicals and solvents [16]. Portability, high throughput, fast response, ease of use and low analyte volumes are crucial advantages of μTAS systems, achieved with miniaturized devices embedding complex fluidic chambers and microchannels. However, these systems also require the addition of complex and bulky pumps for fluidic actuation, which decrease their usability and add significant complexity. Centrifugal microfluidics has emerged as an alternative to traditional microfluidics [17]. Centrifugal microfluidic devices, also called lab-on-discs (LoDs) are polymeric discs implementing complex microfluidic operations, actuated through centrifugal forces. Fluidic handling is performed by simply controlling a spinning motor, without the need for external pumps. Additionally, complex microfluidic operations can be combined and performed in parallel on the same disc, enabling high-throughput and miniaturized analytical processes. Many LoDs were reported for a number of biomedical and diagnostic applications [18], incorporating several detection principles, e.g. colorimetry, optomagnetism and electrochemistry [19], together with fluidic handling on the same platform. However, their potential for screening in metabolic engineering is not well-represented yet [20].

In this scenario, the aim of the Ph.D. project is to explore and develop novel SERS-based methods for the study of bacterial metabolites, combined with centrifugal microfluidics. The overall goal is to provide a robust tool for quantitative and fast microbial screening as an alternative to the standard analytical techniques, in order to help biotechnologists in speeding up the development of novel engineered strains.

1.2 Summary of the research

Strains of *Escherichia coli* (*E. coli*), genetically modified to produce different amounts of *p*-coumaric acid (pHCA) and cinnamic acid (CA), were used as a case of study for SERS-based screening. pHCA and CA are small Raman active molecules, precursors of many phenolic compounds and therefore commercially relevant in cosmetic [21], food [22] and pharmaceutical industry [23]. The discrimination between different strains was based on

the quantitative evaluation of the mentioned secondary metabolites in bacterial supernatant, always validated through HPLC results.

In **Paper I**, SERS substrates were used to detect pHCA directly from supernatant of producing and non-producing *E. coli* strains. As a first step, we showed that the amount of salts in solution was responsible for a proportional fouling of SERS signal of pHCA; however, sample dilution also decreased sensitivity, due to the dilution of the compound of interest. A trade-off between salt dilution and decrease of sensitivity was found with a 10-fold dilution of supernatant with ultrapure water. Droplets of diluted bacterial supernatant were directly poured on freshly prepared SERS-active surfaces and used for detection. With this simple technique, we detected a qualitative difference between producing and non-producing strains, confirmed by HPLC results.

However, it was demonstrated that the leaning mechanism of nanopillars works best if the substrates are wetted by an organic solvent instead of an aqueous solution [24]. Additionally, the described approach was not able to exclude salts and other molecules from SERS sensing.

Matrix complexity is a well reported problem for SERS sensing, due to the inherent sensitivity of this technique. Approaches based on surface functionalization [25], labeling [26] and sample pre-treatment [27] have been developed to increase the selectivity and sensitivity of SERS-based assays. In our work, we implemented a simple manual pre-treatment step, based on liquid-liquid extraction (LLE), prior to SERS sensing. As described in **Paper II**, LLE enabled the exclusion of salts and interfering compounds through the partition of pHCA into a dichloromethane (DCM) organic phase. Droplets of DCM extracts, enabling optimal wetting of SERS substrates, were used for detection and quantification. Thanks to the improved sensitivity, we successfully discriminated between different *E. coli* strains based on the amount of produced pHCA, and validated the results with HPLC.

Interestingly, SERS quantification was performed on DCM extracts of both pHCA spiked bacterial growth medium and real supernatant samples. In case of real supernatant samples, SERS signal was proportional to pHCA concentration only after further dilution of the extracts with DCM. Without dilution, instead, a fouled signal was collected, possibly due to the complexity of sample matrix, even after LLE. Therefore, the work proved that a

quantitative use of SERS is possible and robust, but important considerations must be done about sample pretreatment and matrix complexity according to the specific case.

Paper III describes the adaptation of the manual LLE assay to be performed on a centrifugal microfluidic platform. The paper describes the design, development and fluidic operation of a lab-on-disc (LoD) device enabling filtration, LLE and SERS sensing of bacterial aliquots. The main challenges during LoD fabrication were the design of a DCM-resistant platform and the integration of a silicon SERS chip in the microfluidic design, compatibly with the high-throughput fabrication techniques available at DTU Nanotech, namely injection molding and ultrasonic welding. The LoD device was used to discriminate between different bacterial strains based on the amount of pHCA in supernatant, also demonstrating the importance of filtration of bacteria for quantitative sensing. A partial least squares (PLS) data analysis method was successfully used to enable correct quantification of both spiked medium and real supernatant samples.

In **Paper IV**, we extended the application of the manual LLE/SERS assay presented in **Paper II** to the quantitative evaluation of mixtures of compounds with a similar molecular structure and similar spectral features. Supernatant samples of *E. coli* strains modified to produce both pHCA and CA in different amounts were pre-treated with manual LLE and tested with SERS. Discrimination of overlapping spectral features and correct quantification were achieved with the application of a PLS model.

In **Paper V** we investigated the combination of SERS-based sensing with a different pre-treatment technique, namely supported liquid membrane (SLM) extraction. Similarly to **Paper I**, SERS detection of pHCA had to be performed on aqueous extracts containing salts, due to the working principle of SLM extraction. However, the flow-based SLM extraction assay was implemented on a robust, custom-made microfluidic chip, which enabled up to more than 13-fold pHCA enrichment. Thanks to the significant SLM enrichment, the interference of acceptor salts was effectively compensated by diluting samples with EtOH, without affecting sensitivity. *E. coli* strains grown with different medium compositions were quantitatively differentiated, again based on their different pHCA production.

1.3 Organization of the thesis

The thesis is divided into 6 chapters, guiding the reader through the process of design, development and characterization carried out during the Ph.D. project. The chapters provide an overview of the state of the art in the main scientific topics and research fields which were the focus of the Ph.D. project (metabolic engineering, Raman spectroscopy, sample pre-treatment and centrifugal microfluidics) and a basic introduction to the theory involved. Additionally, the microfluidic operations included in the LoD device are described in detail, together with the materials and the fabrication methods used.

Chapter 2 introduces the concept of metabolic engineering and discusses the current challenges about high-throughput screening in the process of strain development and optimization. **Chapter 3** provides an overview of applications of Raman spectroscopy and SERS sensing and describes the basic principles behind them. The chapter focuses on the origin of the Raman and SERS phenomena, on the interpretation of Raman and SERS spectra and on addressing reproducibility issues during SERS acquisition to achieve a robust quantitative sensing. Furthermore, the application of Raman spectroscopy to the quantification of metabolites and nutrients in liquid samples of bacterial supernatant is described. **Chapter 4** describes a few examples of common pre-treatment techniques, highlighting their advantages and disadvantages. The chapter justifies the choice of LLE and SLM extraction to be combined with SERS-based sensing, and relates the choice of materials and chemical parameters to basic theoretical considerations for both the techniques. **Chapter 5** defines the concepts of μTAS systems and LoDs, explaining their advantages through examples and several applications. The relevance and potential of the LoD technology applied to metabolic engineered is discussed, and the design process of the microfluidic device is described. Based on brief theoretical considerations, the main fluidic operations implemented on disc are analyzed in detail and the materials and fabrication methods are described. **Chapter 6** concludes the thesis with a summary of the results achieved and possible further developments. The **Appendix** contains the relevant published, submitted and to be submitted scientific works produced throughout the Ph.D. project.

2 Bacterial factories: an overview

The cultivation of microorganisms in order to obtain useful products is a very ancient practice; for thousands of years, in fact, mankind used microorganisms for fermented food and beverages and, in the last century, microorganisms were used for harvesting antibiotics and a number of chemical compounds at industrial scale [28], [29].

However, it was only in the last few decades that metabolic engineering was born as a science. According to the definition given by the *Metabolic Engineering* journal (Elsevier), it is *"the science of direct modulation of metabolic pathways for metabolite overproduction or the improvement of cellular properties"*. In more detail, Bailey [1] defined it for the first time in 1991 as *"the improvement of cellular activities by manipulation of enzymatic, transport and regulatory functions of the cell with the use of recombinant DNA technology"*. Thanks to novel bioinformatics and mathematical modeling tools, new insights were reached about the inner microbial metabolism, and more directed DNA modifications could be introduced. Since then, a dramatic increase in the number of processes and applications has spread, ranging from pharmaceuticals to foods and additives, through biofuels and chemical industry, focusing attention both on optimization of existing bioprocesses and on development of new ones [2].

The reason behind such success is the yet-to-be-discovered full potential of bio-based production in terms of production of new compounds and biosustainability. In fact, compounds of interest can be too complex to be chemically synthetized or not convenient to be extracted from natural sources [2]. Moreover, production of chemicals through microorganisms is often based on the use of renewable substrates, such as starch, sucrose, cellulose, resulting in a more sustainable process compared to traditional ones, often based on fossil fuels, thus leading to a reduced environmental footprint [3]. Therefore, bio-based production can be more convenient and cost-effective than chemical synthesis, especially at industrial scale.

The process of engineering microbial pathways to optimize the production of a desired compound is very complex. The preferred route for development of new bioprocesses is the engineering of so called *platform cell factories*. In other words, development of new

pathways is preferentially done through a limited number of well-known microorganisms. Important advantages of this approach include a deep characterization in terms of microbial genetics and physiology, and full availability of tools for genome editing and gene expression.

Different microorganisms are preferred according to the field of application. For instance, *Aspergillus niger* and *Bacillus subtilis* are used for production of industrial enzymes, due to their efficient protein secretion; Chinese hamster ovary (CHO) cells are commonly used for secretion of glycosylated proteins in the pharmaceutical field, and *Corynebacterium glutamicum*, *Escherichia coli* and *Saccharomyces cerevisiae* are used for production of biofuels and other chemicals. However, this is not a strict classification. For instance, in Tab. 2.1 the reader can find a few examples of small molecules synthetized by engineered *E. coli*, which can find applications in different fields, besides the proposed categorization.

Tab. 2.1: Examples of industrial applications of *E. coli* metabolic engineering (extracted from [30]**,** [31] **and** [32]**).**

Application	Examples	References
Biofuels	Bioethanol, 1-Propanol, 1-Butanol, Isobutanol	[33], [34], [35], [36]
Food industry	L-Lactic acid, Pyruvate, Acetate, L-Phenylalanine, L-Tryptophan	[37], [38], [39], [40], [41]
Cosmetic industry	D-Lactic acid, L-Valine, CoQ10, L-Serine	[42], [43], [44], [45]
Pharmaceutical industry	Taxadiene, Echinomycin, Anthracyclines, Theophylline, Amorphadiene, Glucaric acid	[46], [47], [48], [49], [50], [51]
Polymer synthesis	L-Tyrosine, Succinic acid, Adipic acid, *p*-Coumaric acid, Cinnamic acid	[52], [53], [54], [55]

Among the listed molecules, in **Paper I – III** and **V** we exploited different sample pretreatment and sensing possibilities for quantification of *p*-coumaric acid produced by *E. coli* as a case of study. In **Paper IV** we investigated the possibility of simultaneous

quantification of *E. coli* secondary metabolites with a similar chemical structure, namely *p*-coumaric acid and cinnamic acid.

2.1 Microbial factories development: the DBTL cycle

The typical process of modern strain development and optimization is described in Fig. 2.1 as the Design-Build-Test-Learn (*DBTL) cycle*, including the following steps:

a) *Design*: the desired metabolic pathway is designed and the necessary DNA modifications are translated into assembly instructions;
b) *Build*: the pathway is implemented into the microorganism through synthetic biology tools;
c) *Test*: the developed biological system is tested for its ability to perform the desired function;
d) *Learn*: the scientist gathers information and evaluates the previous steps, in order to further optimize them and restart the cycle.

Following these steps, many cycles of strain construction and optimization may be repeated, in order to obtain sufficiently efficient production of the desired metabolites through incremental improvements.
When a new bioprocess is developed, the initial goal is to identify, if possible, an already existing pathway producing a certain molecule. If this pathway exists, the aim is to optimize and maximize the production of the molecule in the host organism. If this is not possible, the biosynthetic pathway must be transferred to a heterologous host, or chimeric pathways must be constructed. Nowadays, powerful bioinformatics tools for DNA and RNA sequencing are routinely used in this phase for fast design and modeling of metabolic pathways, only limited by the computational power of available calculators [57].

Once a metabolic model is designed, the pathway must be reconstructed into the desired host organism through DNA segments encoding the enzyme expression and regulation mechanisms for enzyme production. In this case too, new technologies have

contributed to a significant speed-up through low cost gene synthesis and rapid genome modification [58], [59].

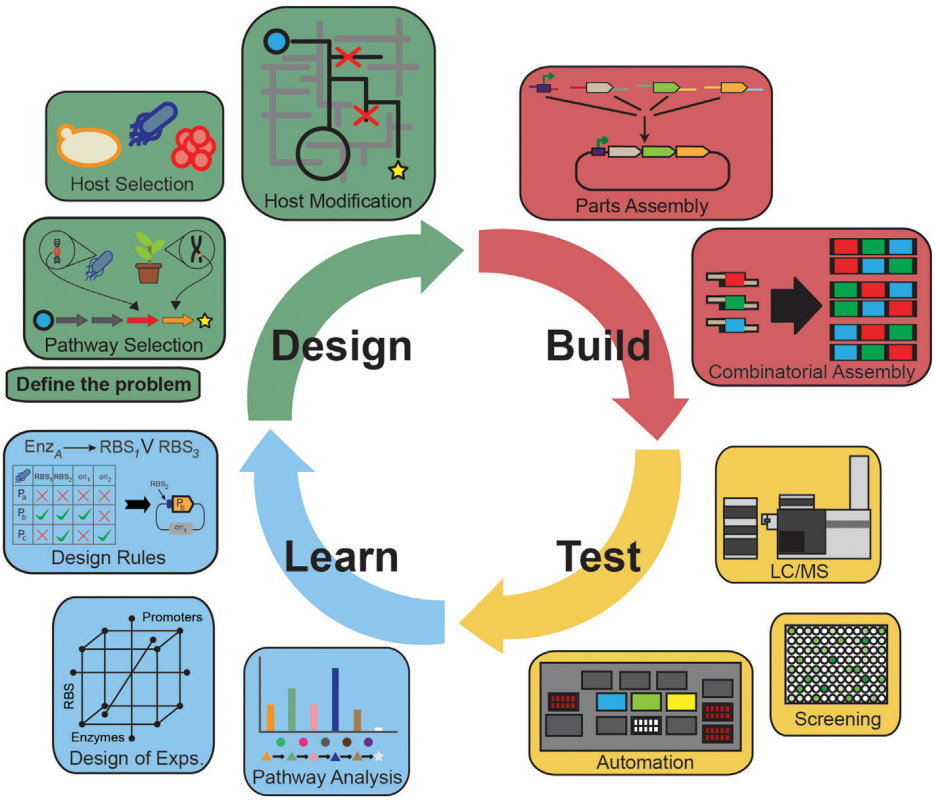

Fig. 2.1: Scheme of DBTL cycle, reprinted from [56] **with permission.**

Due to the complexity of microbial metabolism, many genetic modifications are needed not only to boost the desired process, but also to prevent the competing or limiting ones [56]. The reason behind this difficulty is the tight regulation of microbial metabolism through a number of interconnected mechanisms at levels of gene expression, enzyme activity and stability, substrate import and product export. Therefore, big libraries of engineered microorganisms need to be tested in terms of successful integration or exclusion of genes, strain growth and physiology, and quantification of the final products, in order to find the best performing strain. Depending on the results, all the steps can be evaluated and optimized towards the next iteration. Therefore, testing is a crucial step in

the DBTL cycle. However, it was also described as the bottleneck of the entire process, since the same throughput, robustness and generalization developed in the Design and Build steps cannot be observed here [4], [60]. Significant effort was made in the last decades to address the need of high-throughput and novel sensing techniques, in a complex research process that is still ongoing, which was also one of the goals of this Ph.D. project.

2.2 Analytics for metabolic engineering

The first step for overproduction of a certain compound is the development of a *proof-of-principle* strain, namely the reconstruction of an effective metabolic pathway in a platform cell factory. Once the *proof-of-principle* strain is established and eventually patented, the process can be transferred to a cell factory for commercial production. However, in order to balance the costs of the fermentation process, the strain must be cost-effective and therefore meet industrial requirements in terms of titer (total amount of product in supernatant), rate (production per unit of time) and yield (amount of product per unit of substrate consumed), called TRY requirements. Both the development of a proof-of-principle strain and its optimization towards industrial TRY requirements are costly processes, and can last many years [2].

According to the development stage, analytical techniques with different features are required. Flexible and robust identification and quantification are needed in the first development phase, whereas high-throughput sensing is preferred during TRY optimization [56].

For quantification of metabolites and initial pathway validation during *proof-of-principle* development, chromatographic separation methods (e.g. gas chromatography, liquid chromatography or high-performance liquid chromatography) are commonly coupled to UV detection and/or mass spectroscopy [61]. These well-established techniques are powerful because they enable accurate sensing and quantification of one or more target molecules, and detection protocols can be flexibly adapted to different compounds. Furthermore, their robustness makes them good validation tools for newly developed assays, as it was done in the presented work with HPLC (**Paper I – V**). However,

flexibility and robustness are balanced by a relatively low throughput, long separation procedures and expensive instrumentation [4].

To achieve the desired throughput during TRY optimization, some examples of screening and selection techniques are colorimetric, UV absorbance or fluorescent assays in micro-titer plates, fluorescent-activated cell sorting or *in vivo* biosensor-driven assays [62]. The throughput of these tools is in the order of 10^4 or more samples per day. However, many compounds lack appropriate fluorophores or chromophores, and this requires the development of quantitative assays based on more complex chemical modifications [56].

In this context, we aim at developing quantitative and integrated sensing tools which can be used for fast pre-screening in the first development steps, as an alternative to standard sensing techniques. Crucial features for this purpose are specific identification, ease of use and time effective protocols.

3 Raman spectroscopy and surface enhanced Raman scattering

Raman spectroscopy is a vibrational spectroscopic technique based on the inelastic scattering of light. When a light beam is used to illuminate a sample, the incident light interacts with the material and generates vibrations specific to the molecular structure of the sample. This molecule-specific information can be obtained by collecting the spectrum of scattered light, i.e. the Raman spectrum. Therefore, Raman is particularly suitable for chemical and physical characterization of materials, semi-quantitative analysis and identification of unknown samples [11].

The number of reported applications of Raman spectroscopy has increased exponentially over the last few decades, thanks to its appealing advantages. In fact, Raman spectroscopy is a non-destructive, label-free technique which can be used to collect data from very small samples (Raman microscopy can be performed with a resolution of a few square μm) and non-transparent solid samples, even in harsh conditions [6]. Applications of Raman spectroscopy can be found in several fields like materials, forensic [63] and environmental science as well as in biology and medicine. This technique has been largely applied to the study of polymers [64] measuring polymer deformation [65], crystallinity [66], tribology [67], chirality [68] and polymer/polymer interfaces [69], for both structural studies and on-line monitoring of industrial processes [70]. Applications for studying ceramics [71] and glasses [72] have also been developed. In addition, spectroscopic environmental monitoring of water quality [73], atmospheric pollution and air particulate [74] were also performed. Raman spectroscopy was even applied to the study of ancient paintings, pigments and dyes in archaeology [75].

Due to the molecule-specific and non-destructive nature of Raman spectroscopy, particular interest was recently focused on life science applications [5]; few examples in the field are investigation of proteins [7], lipids [76] and nucleic acids [77], and interactions between drugs and DNA [78]. The physiology of cells and biological tissues has been investigated [8], [79], exploring new methods for biomedical applications.

Raman-based diagnostics is currently drawing more and more attention, with numerous examples of tissue analysis for cancer diagnosis [80], monitoring of nutrients [81], and assays for detection of biomarkers [82] and pathogens [83] in biological fluids.

Although Raman is a versatile and relatively simple technique, some significant issues in sensing of biological samples are related to the low level of Raman signal. Since the probability of a Raman scattered photon is only 1 out of 10^6 - 10^8 incident photons, high laser power (tens or hundreds of mW) and long acquisition intervals (in the order of minutes) are needed to achieve an acceptable signal-to-noise ratio. However, this can degrade organic molecules and stress or damage living cells and tissues. Furthermore, many biological matrices present strong fluorescence emission, which can cover the weak Raman signal. In some cases the use of photobleaching [84] or near-infrared lasers can lower fluorescence [85], however the issue cannot always be solved.

Surface-enhanced Raman scattering (SERS) is a technique able to enhance Raman signal of several orders of magnitude (typically to 10^5 – 10^6) [10] through the plasmonic properties of nanostructured metallic surfaces. When a SERS active surface is irradiated by a laser, the incident electromagnetic field is locally enhanced in points called *hotspots*, which depend on surface roughness. For instance, hotspots can be located in the nanogaps between aggregated nanoparticles. When an analyte is located in or close to a hotspot, it undergoes a much stronger excitation, and its Raman signal significantly increases [11].

SERS can be observed with lower laser power (in the order of 10^{-1} – 10^0 mW) and shorter acquisition time (fractions of seconds) compared to Raman, and it can overcome fluorescence. It is an intrinsically sensitive technique, enabling detection of molecules in solution at low concentrations or even at single-molecule level [86].

Due to these advantages, the potential of SERS is currently being explored in many fields, including analytical applications in biology. Both functionalized and non-functionalized nanoparticles, for instance, have been used to study a wide variety of mammalian cells [12] as well as tissues [87]. SERS nanoparticles have been used to study biological macromolecules, such as DNA and proteins, often relying on a specific surface functionalization [88]. Several examples can be found in literature about SERS-based isolation and identification of pathogens from human blood [13], [89], discrimination of bacteria [14] and identification of biofilms [90].

Drawbacks like non uniformity and instability of SERS substrates, irreproducibility of measurements and difficult quantification have limited industrial applications of SERS so far. However, due to the molecule-specific nature of the signal, the sensitivity and the fast acquisition typical of SERS-based sensing, and given its potential for miniaturization and automation when integrated in an analytical device, the potential of SERS is yet to be exploited in many industrial applications. In the field of metabolic engineering, for instance, an automated SERS-based setup could meet the need for high-throughput and robust sensing and be used as an alternative analytical tool for fast screening during strain development. While SERS active surfaces have been used to investigate bacterial lysates [89], secreted metabolites [91] and growth media [92]–[94], in the frame of this Ph.D. project we were the first, to the best of our knowledge, to implement SERS-based quantitative screening of bacterial strains.

In **Paper II** and **IV** a quantitative screening of *E. coli* strains was performed based on the amount of produced secondary metabolites and the assay was validated with HPLC. Liquid-liquid extraction (LLE) was used as a pretreatment step prior to SERS sensing. All the samples were manually treated in parallel, for a total processing time of 35 min, and collected, for an acquisition time up to 5 min per sample, leading to a significant time gain compared to HPLC analysis time (about 15 min per sample).

In **Paper III**, LLE and SERS were integrated on an automated centrifugal platform. The processing time on disc was 10 min per sample, but up to 4 samples could be treated at the same time.

In **Paper V**, SERS sensing was combined with supported liquid membrane (SLM) extraction, implemented on a microfluidic chip. Although the processing time was 20 min for each sample, at least two microfluidic chips could be used in parallel, significantly reducing the processing time per batch of samples.

3.1 Nature of Raman scattering

Raman scattering is a physical phenomenon experimentally detected for the first time by Raman and Krishnan in 1923 [95]. In their original experiment, schematically represented in Fig. 3.1, Raman and Krishnan focused sunlight through a telescope

objective on samples made of liquids or dust-free vapors, in order to have powerful illumination. Then, they used a combination of complementary blue-violet and yellow-green filters to observe the sample. When placing both filters between the incident light and the sample, all the visible wavelengths were extinguished; therefore no light hit the sample. Instead, when placing one filter between the incident light and the sample, and the other one between the sample and the observer, they could observe a different light weakly scattered through the sample (Fig. 3.1). This experiment demonstrated the basic principle of Raman spectroscopy, i.e. inelastic light scattering.

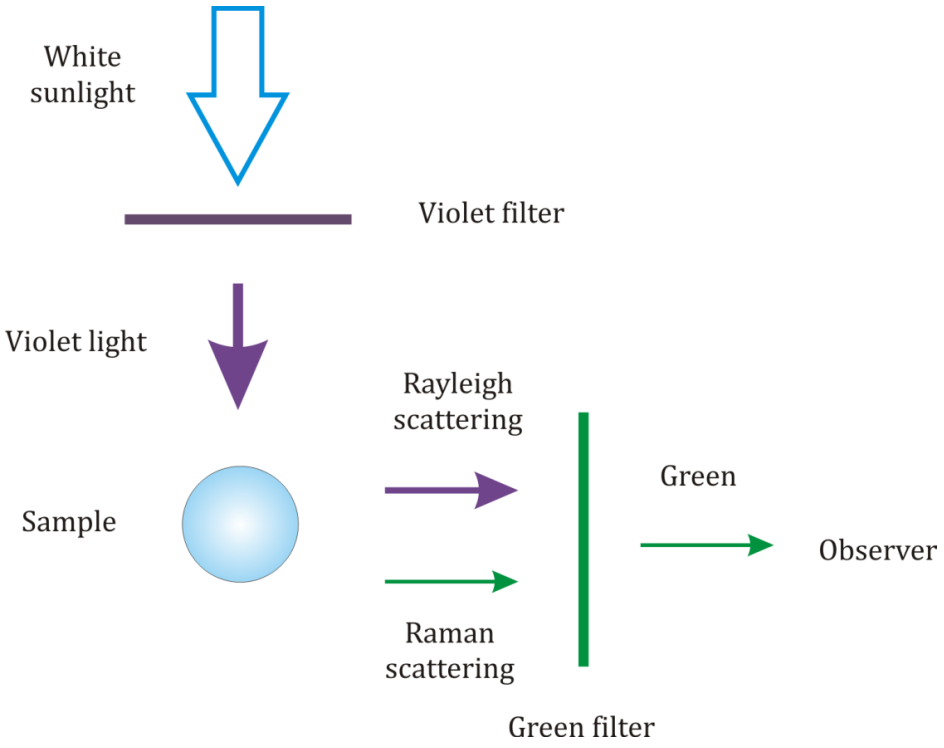

Fig. 3.1: Scheme representing Raman and Krishnan's experiment: a sample is illuminated with a focused sunlight beam, and a combination of filters is used for observation. The violet and green complementary filters, when combined together, completely extinguish the incident light. When placing a violet filter between the incident light and the sample, and a green filter between the sample and the observer, only the light scattered with a wavelength different than the incident one can be observed.

When shining a light beam on a sample, photons can interact with electrons and nuclei in different ways: they can be absorbed, scattered, or pass through the sample without any interaction. Vibrational spectroscopy, and therefore Raman spectroscopy, is based on

light-matter interactions which cause the motion of the nuclei in the observed sample. In other words, the energy required to excite molecules to a different vibrational state can be measured. Referring to the scheme in Fig. 3.2, most molecules at room temperature are at ground state, which is the state at the lowest vibrational energy level (m). When a sample is excited with light covering a range of frequencies, and when a photon matches the energy difference between two different vibrational states (n-m), the photon is absorbed and the molecule is excited to a higher vibrational state (n). The absorption (loss) of this specific frequency is detected through a comparison between the incident light and the light passing through the sample, and it is specific to the molecule; this mechanism is used for absorption spectroscopy.

Raman spectroscopy, instead, exploits the interactions between a light source and a sample resulting in inelastic scattering of photons. The incident light can be described as a propagating oscillating dipole; when it passes over a molecule, the light polarizes and distorts its electron cloud, exciting the molecule to a higher energy state. This temporary interaction results in a short-lived molecule state (*virtual state* in Fig. 3.2), characterized by a deformed electron cloud and no significant nuclear movement.

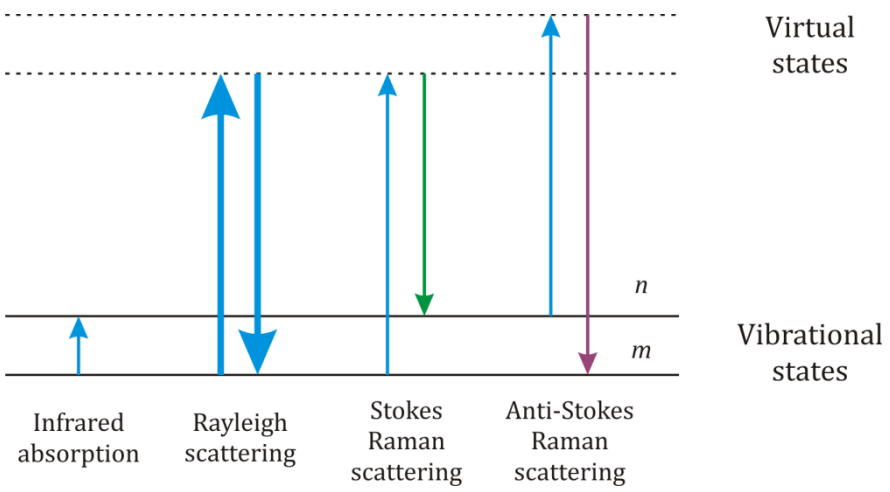

Fig. 3.2: Jablonski diagram representing quantum transitions for infrared absorption and Rayleigh, Stokes and anti-Stokes scattering.

The energy of the virtual state depicted in Fig. 3.2 only depends on the energy of the incident light, and, unlike absorption, does not have to match the energy difference between different vibrational states. For this reason, monochromatic lasers can be used for illumination in Raman spectroscopy.

The light is immediately released as scattered radiation; in most cases, the electron cloud relaxates without generating any nuclear movement. In this case there is no significant change in energy of the scattered light compared to the incident beam (Rayleigh scattering). Once every 10^6 – 10^8 times, nuclear motion is generated by the interaction, and the light is scattered at a different energy. The scattered light can have lower energy, if it interacted with a molecule at the ground state, or in few cases higher energy, if the molecule was already at an excited vibrational state (Stokes and anti-Stokes scattering, respectively). Since the relative intensities of the two phenomena depend on the populations of the various states of the molecule, anti-Stokes scattering is much less intense than Stokes scattering, and usually only the latter is recorded.

3.2 Interpretation of Raman spectra

The intensity of light scattered by a sample can be represented as a Raman spectrum, as depicted in Fig. 3.3. The x axis, representing the *wavelength* or *Raman shift*, is commonly expressed in cm^{-1}. The Raman shift is the difference between the wavelength of the scattered light and the one of the incident light. Therefore, the spectrum is centered in 0, and the Stokes scattering, which is usually represented, has negative wavelength values. As a common use among spectroscopists, the minus sign and the Δ symbol, representing the wavelength difference, are omitted. The y axis represents signal intensity, which can be expressed in counts per second or other units, according to possible data processing or normalizations.

Important parameters in the interpretation of Raman spectra are amplitude and position of Raman bands. The position, as previously explained, depends on the energy difference between two specific vibrational states of the molecule, and therefore is specific to the molecule itself.

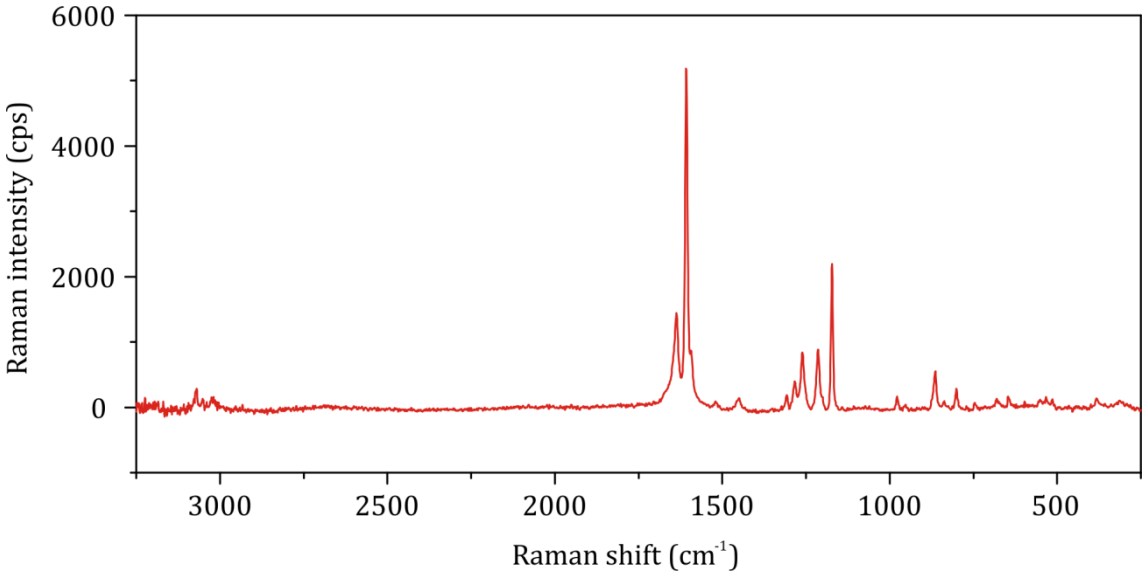

Fig. 3.3: Raman spectrum of p-coumaric acid between 250 and 3250 cm^{-1} after baseline correction. The spectrum was obtained with a 780 nm laser with 10 mW power, a 10x objective, and averaged over 3 exposures of 10 s each.

In principle, if N is the number of atoms of a molecule, the number of degrees of freedom of the molecule is 3N – 6, and 3N – 5 for linear molecules. We should expect the same number of modes of vibrations, and therefore the same number of Raman peaks. However, not all the vibrational modes are Raman active, due to the existence of selection rules between Raman and infrared spectroscopy. In general, only vibrational modes which generate a significant polarization of the electron cloud will give Raman bands, whereas large variations of dipole moment (i.e. displacement of nuclei with different electronegativity) will give absorption bands. Therefore, some modes could be absent or less significant in Raman spectroscopy. Furthermore, as it happens in more complex molecules, a larger number of atoms can be involved in a single vibrational mode. For instance, when two or more bonds are close together in a molecule and have similar energy, they can interact, and it is the result of the interaction between different groups of atoms which is actually detected in the Raman spectrum.

A common approach to the interpretation of Raman spectra is to break down vibrations of groups of atoms into features that are common to many molecules, and match a peak to the vibration, in a process called *peak assignment*. Nowadays, molecular mechanics and

infrared/Raman vibrational spectra can also be studied through software simulations (e.g. GaussView and Gaussian, Gaussian Inc., Wallingford, CT, US). Although not always exact, simulations can help in graphically examining the main displacements contributing to a certain peak, especially in complex molecules [11].

Furthermore, it is possible to find in literature frequency ranges where Raman peaks of single or group vibrations can be typically expected. In general, light atoms (X – H) and strong bonds (-N=C=O, -C=O, -C=N, -C=C-) have peaks at higher frequencies, whereas heavy atoms, weak bonds, molecular and lattice vibrations have peaks at lower frequencies. Organic molecules usually have characteristic patterns of carbon-carbon and carbon-nitrogen vibrations in the region between 1500 and 500 cm^{-1}, commonly called *fingerprint region*. In Fig. 3.4 the reader can find few examples of single and group vibrations and expected intensities between 900 and 1700 cm^{-1}.

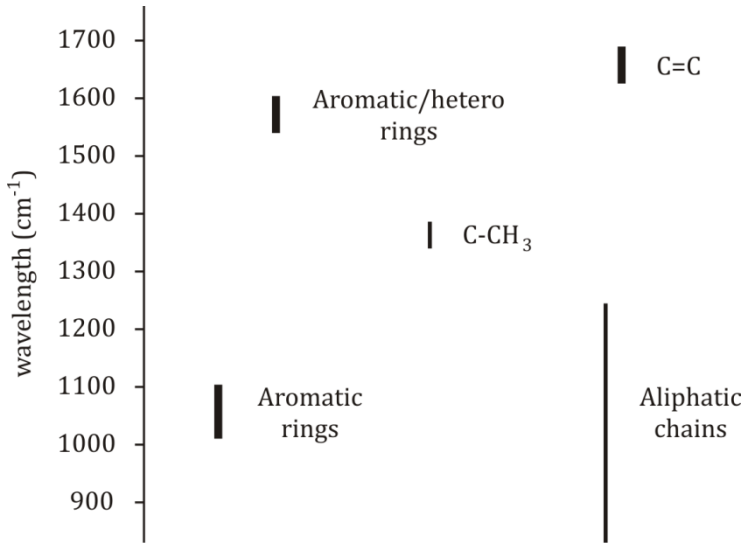

Fig. 3.4: Single and group vibrations and possible intensities of Raman peaks, extracted from [11]**. The thickness of the vertical lines represents the expected intensity of the peaks, whereas the length represents the expected wavelength range.**

As an example of peak assignment, the Raman peaks of p-coumaric acid (pHCA) experimentally obtained in Fig. 3.5 correspond to the vibrational modes listed in Tab. 3.1.

As expected, a C=C vibrational mode is detected at 1636 cm^{-1}, and vibrations related to the aromatic ring can be found at 1606, 1260 and 1172 cm^{-1}.

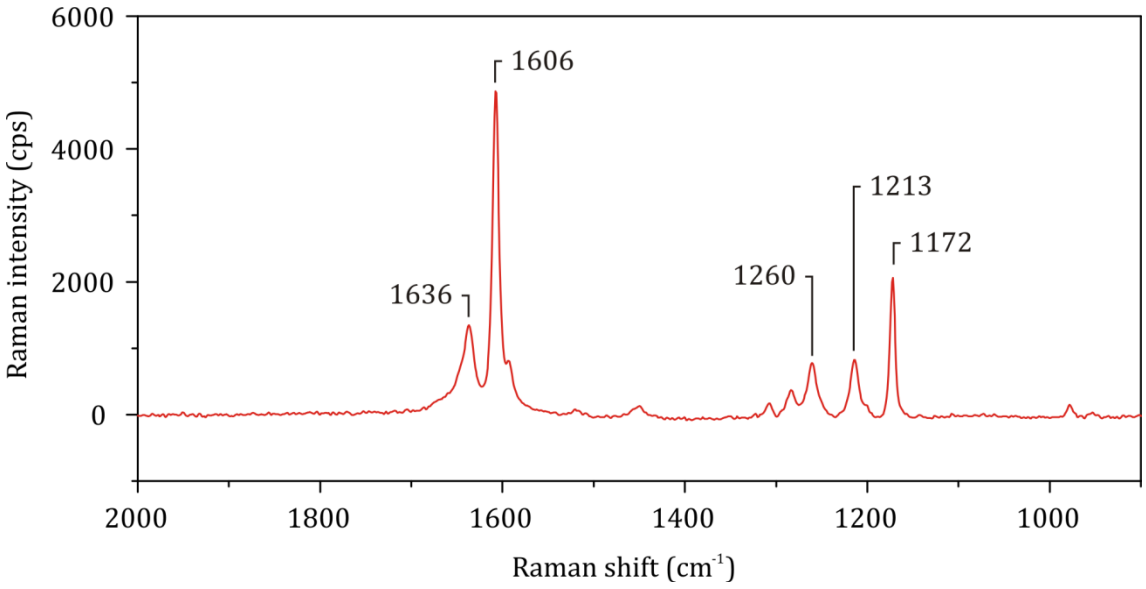

Fig. 3.5: Raman spectrum of p-coumaric acid between 900 and 2000 cm^{-1} after background correction. The spectrum was obtained with a 780 nm laser with 10 mW power, a 10x objective, and averaged over 3 exposures of 10 s each.

Tab. 3.1: Assignment of the main Raman peaks of p-coumaric acid in the fingerprint region, extracted from [96]**. The atoms and the bonds mainly involved in each mode are specified, with *ar* standing for aromatic ring.**

Raman shift (cm^{-1})	Intensity	Assignment
1636	medium	$\nu(CC)_{C=C}$
1606	very strong	$\nu(CC)_{ar}$
1260	medium	$\beta\ (OH)_{ar}$
1213	medium	$\beta\ (CH)$
1172	strong	$\beta(CH)_{ar}$

Besides theoretical considerations, Raman cross-section (σ_R) is an important empirical parameter for the estimation of peak intensity, proportional to the probability of an incident photon to be Raman scattered at a certain Raman-shift [97]. Raman signal (I_R) is directly proportional to the Raman cross-section according to the following equation:

$$I_R \propto I_0 \sigma_R \quad \textbf{Eq. 3.1}$$

with I_0 representing the intensity of the incident laser. For some molecules, Raman cross-section is low, and high laser power is needed to obtain a detectable Raman signal. However, some samples, such as biological molecules, cannot be analyzed at high power due to molecule degradation and burning. A way to compensate for the low Raman cross-section is to locally enhance the electromagnetic field by using surface-enhanced Raman scattering.

3.2.1 Raman for quantification of nutrients and metabolites

Unpublished material, please see the attachment "Papers and unpublished material" for content.

3.3 Surface-enhanced Raman scattering

Surface-enhanced Raman scattering, commonly referred to as SERS, makes use of metallic nanostructured surfaces to enhance the Raman signal by several orders of magnitude [10]. The most common definition of SERS enhancement factor for a SERS substrate is given by the following equation [109]:

$$EF = \frac{I_{SERS}/N_{Surf}}{I_{Raman}/N_{Vol}} \quad \textbf{Eq. 3.2}$$

where I_{SERS} is the intensity of SERS signal, N_{Surf} is the average number of adsorbed molecules in the scattering volume[‡] for the SERS experiment, I_{Raman} is the intensity of the Raman signal and N_{Vol} is the average number of molecules in the scattering volume for the

[‡] The scattering or sampling volume is a cylinder of diameter $D = 4\lambda f/\pi d$ and length $L = 16\lambda f^2/\pi d^2$, with λ = laser wavelength, d = diameter of unfocussed laser beam and f = focal length of focussing lens [11].

Raman experiment. Therefore, SERS enhancement is proportional to the ratio between SERS and Raman signal, and it can reach values up to 10^{14} – 10^{15} for single molecules [86].

This strong enhancement of Raman signal was observed for the first time by Fleischmann *et al.* [110] in 1974, when studying the signal of pyridine adsorbed to the roughened surface of a silver electrode. Since then, intense research was focused on developing theories to explain SERS enhancement; today, the most widely accepted theory is a combination of an electromagnetic and a charge transfer effect [111].

The electromagnetic effect involves an electromagnetic coupling between the incident electric field and the nanostructured metal surface. When a single metal nanoparticle is illuminated by a laser source, the conduction electrons begin to oscillate coherently across the metal surface against the direction of the incident electric field (Fig. 3.8a). These coherent oscillations are called *surface plasmons*, and they result in a redistribution of the electromagnetic field at the surface of the nanoparticle. When many nanoparticles aggregate together, the single electromagnetic fields can interfere coherently with each other, creating particularly strong enhancement *hotspots* at the gaps between two adjacent nanoparticles (Fig. 3.8b). Therefore, when a molecule is placed in one of these hotspots, it is excited by a strong oscillating electromagnetic field and its Raman signal is strongly enhanced. In particular, the effect is extremely pronounced when molecules are situated in the vicinity of the metal surface, i.e. within a few nanometers.

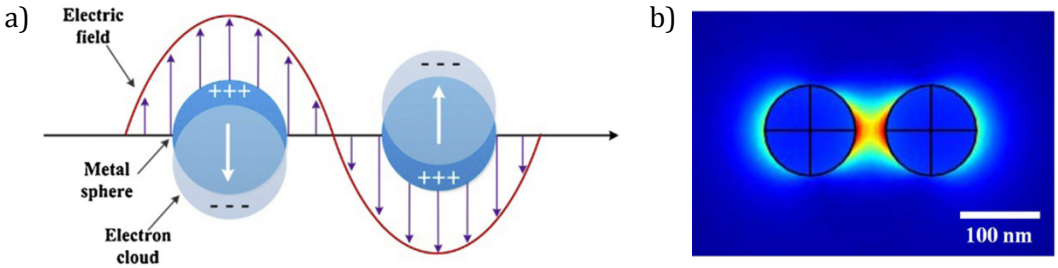

Fig. 3.6: a) Redistribution of conduction electrons at the surface of a nanoparticle interacting with an oscillating electric field [112]**. b) Constructive interference of the local enhanced electromagnetic field between two adjacent nanoparticles** [113]**.**

The charge transfer effect, instead, involves the formation of a bond between the molecule and the metal surface. This bond is believed to enable transfer of charge from the metal to the analyte, leading to a significant increase of the molecule polarizability. As opposed to the electromagnetic effect, enhancement due to charge transfer is only possible for analytes directly adsorbed onto the metal surface.

Due to the combination of electromagnetic and charge transfer effect, SERS technique works best for small molecules which are physically or chemically adsorbed to the metal surface.

Due to the complexity of SERS phenomenon, SERS spectra can be difficult to interpret. As explained, the generation of SERS peaks depends on the interaction between the analyte and the metal surface. Therefore, the nature of the SERS substrate, the orientation of the molecule towards the surface and the strength of absorption can influence both width and position of SERS peaks, and certain vibrational modes can even appear or disappear.

For instance, Fig. 3.9 shows a SERS spectrum obtained from a droplet of pHCA in EtOH dried on a gold-capped silicon nanopillar substrate. Compared to the Raman spectrum of pHCA in Fig. 3.5, peaks are broader, and the small peaks between 1200 and 1310 cm^{-1} are replaced by two wider peaks at 1250 and 1369 cm^{-1}. Nevertheless, the Raman peaks at 1636, 1606 and 1172 cm^{-1} are maintained in the SERS fingerprint, with small frequency shifts.

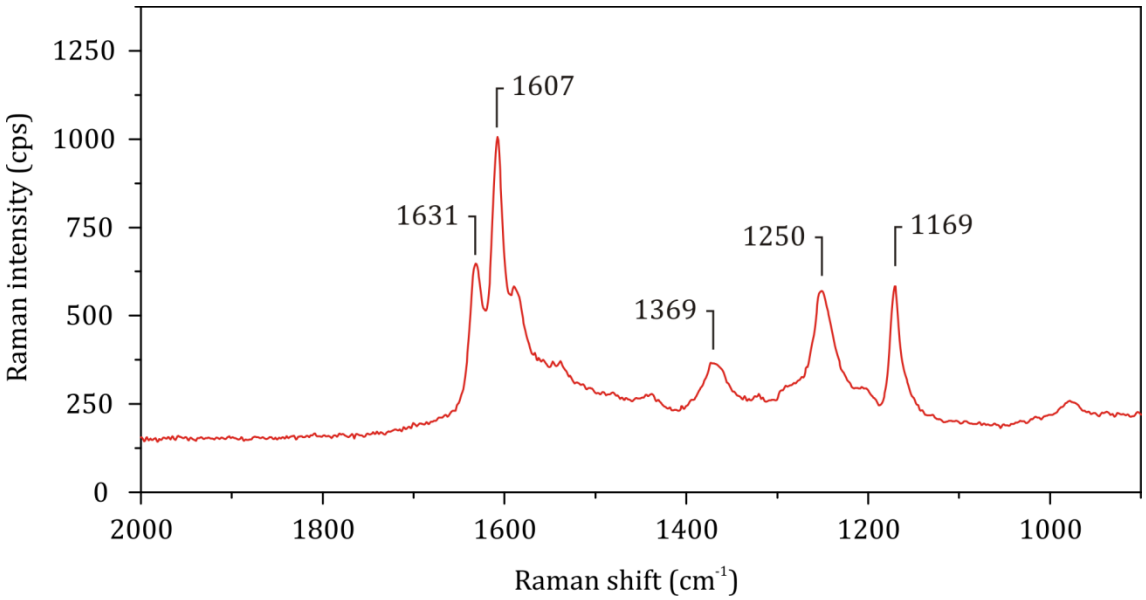

Fig. 3.7: SERS spectrum of 100 µM pHCA in EtOH dried on a gold-capped silicon nanopillar substrate. The spectrum was obtained with a 780 nm laser with 0.1 mW power, a 10x objective, and averaged over 3 exposures of 3 s each.

In more detail, the peak at 1169 cm^{-1} was chosen as a characteristic peak for qualitative and quantitative analysis of pHCA. In fact, vibrations around 1600 cm^{-1} are common to many organic molecules, which could interfere with pHCA detection in complex solutions. The chosen peak, instead, proved particularly pronounced and related to pHCA concentration, and quantification of pHCA was successfully performed based on the height of this peak in both **Paper II** and **V**.

3.3.1 Fabrication of SERS substrates

When designing SERS substrates, certain requirements regarding material, size and shape must be considered.

Surface plasmons are characterized by a resonance frequency at which the coupling between the incident electric field and the nanoparticle is more efficient, leading to a better enhancement of the local electromagnetic field. Therefore, it is important to match the resonance frequency of the substrate with the wavelength of the incident light.

The resonance frequency is influenced by the size of the nanoparticle, which should be smaller than the wavelength of the incident light, and by the dielectric properties of the material. Metals such as gold and silver have a resonance frequency in the visible region; therefore these metals are suitable for SERS with common visible Raman lasers [114].

The goal of each substrate is to ensure the creation of hotspots, where the analyte of interest can be located and therefore sensed with optimal sensitivity. Furthermore, characteristics such as chemical stability, ease of preparation, reproducibility and spatial uniformity of hotspots are extremely important for a good SERS substrate. Many examples of SERS substrates were reported in literature, mainly divided in colloidal suspensions of nanoparticles with different shapes (e.g. spherical, cubic, triangular, rectangular [115] and star-shaped [113]) and structural solid substrates (nanospheres on a surface [116], silicon/polymer nanocones [117], nanocylinders [118], nanoholes [119]).

In the frame of this Ph.D. project, substrates based on gold-capped silicon nanopillars were extensively used for SERS-based sensing [15], [120]–[122].

The fabrication process is depicted in Fig. 3.10. Randomly distributed silicon nanopillars are obtained on the surface of a silicon wafer (Fig. 3.10a) through a maskless reactive ion etching (RIE) process (Fig. 3.10b). During the RIE process, the reactive gases (a combination of SF_6 and O_2 in this case) are ionized in the reaction chamber by a strong electric field, and subsequently accelerated towards the silicon surface, where a physical and chemical etch takes place. The density, shape and height of silicon nanopillars can be controlled by changing the chamber pressure [121], the composition of the reactive gases and the etching time [120]. After etching, a short O_2 plasma cleaning step can be performed to remove any residue of reactive species still present on the silicon surface, in order to reduce the background signal before metal deposition [120].

The second and last step is e-beam assisted metal evaporation (Fig. 3.10c). A thin layer of metal is deposited on the silicon surface, resulting in the creation of metal caps at the top of the nanopillars (Fig. 3.10c, d and e).

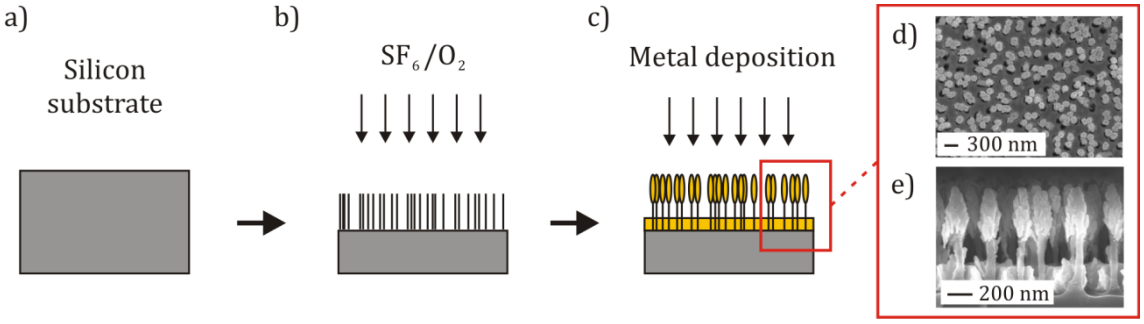

Fig. 3.8: Fabrication process of metal-capped silicon nanopillars. The reactive ion etching process, obtained through acceleration of SF_6/O_2 on the surface of a silicon substrate (a) creates randomly distributed silicon nanopillars (b). An e-beam assisted metal evaporation step creates metal caps on top of the nanopillars (c). SEM images representing the top (d) and side view (e) of gold-capped nanopillars.

The main feature of this substrate is represented by the leaning of adjacent nanopillars when liquid is applied and dried onto the surface. The leaning enables the creation of hotspots between adjacent nanopillars, resulting in an increased SERS signal compared to the non-leaning substrate [15]. Another feature is represented by the shape of the metal caps, which generates another hotspot at the interface with the silicon nanopillar [122]. This means that signal enhancement is delivered not only to the analytes between leaning nanopillars, but also to the analytes adsorbed underneath the metal caps.

Due to these features, the optimal working condition is achieved when a liquid sample is dried on the active surface, and the analyte of interest is trapped in the hotspots between leaning nanopillars. Fouling or crystallization of salts on the nanopillar surface should be avoided, in order to achieve proper leaning and maximize SERS signal. Additionally, liquid samples in organic solvents were proven to enable better leaning [24] and better wetting of nanostructures, also increasing the possibility of distributing analytes underneath the metal caps and therefore increasing SERS signal.

In **Paper I**, SERS sensing was performed on a droplet of bacterial supernatant diluted with ultrapure water. It was observed that exposure to atmosphere and wafer dicing substantially decreased the wettability of the substrates over days. As a result, the droplet could not spread and the signal was completely covered by salts accumulating over a small spot (not shown). Proper spreading of the aqueous droplet, and therefore a useful SERS signal, was observed only on freshly fabricated, non-diced wafers up to 24 h from

fabrication. However, even in this case, the presence of crystallized salts resulted in poor sensitivity.

In **Paper II** and **IV**, the samples were treated with liquid-liquid extraction (LLE), employing dichloromethane (DCM) as the organic extraction phase. This technique enabled extraction of the analytes of interest in DCM while leaving salts and other interfering compounds in the aqueous phase. SERS signal, as opposite to **Paper I**, was collected from a droplet of organic phase. No salt crystals were observed on the substrates in this case, and proper wetting was possible even months after substrate fabrication, substantially improving the usability of the assay.

The microfluidic design of the Lab on Disc (LoD) presented in **Paper III** enabled fast DCM wetting and subsequent drying of the SERS chip, reproducing the same wet/dry experimental conditions for leaning nanopillars in batch experiments.

In **Paper V** we showed that a combination of supported liquid membrane (SLM) extraction and SERS-based sensing enables enrichment and quantification of pHCA in bacterial supernatant. As depicted in Fig. 2 in **Paper V**, pHCA was extracted in the aqueous acceptor phase, which was not suitable for optimal SERS sensing. Therefore, EtOH was added to each sample in order to improve surface wetting.

3.4 Quantitative Raman and SERS

The study of peak position and relative peak intensities of a SERS spectrum can give specific information about the molecular structure of the analyzed sample, and therefore be used for identification and other qualitative analysis. However, peak intensity is also proportional to the concentration of the molecule in the sample, which enables quantitative SERS analysis.

When using SERS for quantitative sensing, as in the scope of our work, reproducibility can be affected by many issues related to the substrate (reproducibility, stability, spatial uniformity), to sample handling (e.g. distribution of the analyte on the SERS surface, focus and alignment of the sensing surface), and to the instrument (different calibration outcome from day to day, laser lifetime, temperature drift).

Reproducibility issues related to the SERS substrate were addressed by using a reproducible, spatially uniform and stable gold-capped nanopillar substrate [120]. As described in **Paper II**, the in-wafer deviation of SERS signal based on characteristic pHCA peak in DCM was found to be approximately 11%, which was considered acceptable. In order to compensate for in-batch and batch-to-batch variation, we collected a new calibration curve for each wafer.

The analyte distribution on the surface was uniformed by adding a sufficient amount of sample to cover the whole 4x4 mm^2 SERS chip. For instance, in **Paper II** and **IV**, the measurements were performed on 5 µL droplets of DCM samples. Due to the high volatility of DCM, a smaller droplet tended to evaporate before covering the whole chip, leading to a non-uniform signal over the droplet area. Furthermore, handling DCM volumes smaller than 5 µL proved challenging. In case of the EtOH diluted samples analyzed in **Paper V**, a 2 µL volume was already sufficient to cover the whole chip.

Efforts were made to standardize the acquisition procedure in order to have a reproducible focusing method and a significant acquisition area on each SERS chip. In **Paper II**, as depicted in Fig. 3.11a, a map of 25 points with a 500 µm step (2x2 mm^2 area), was always collected from the center of the chip, after focusing by eye on the top right corner of the SERS chip. In **Paper III – V** a different Raman instrument with a maximum xy step of 100 µm was used. Therefore, acquiring a 2x2 mm^2 area would lead to the acquisition of an excessive amount of spectra per dataset. In this case, smaller maps were collected from random spots on the SERS surface, after focusing in the center of the chip (Fig. 3.11b).

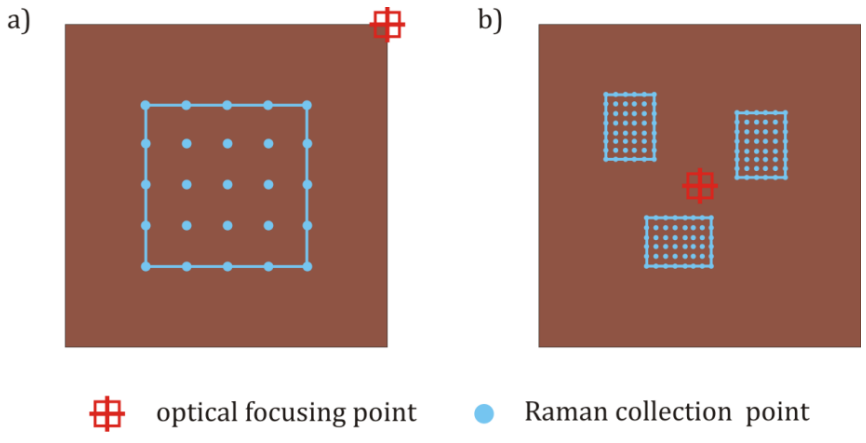

Fig. 3.9: a) Map acquisition on a 4x4 mm² SERS chip in Paper II and b) in Paper III – V. The red symbol represents the optical focusing point, whereas the blue dot represents the spatial location of the collection points in each map.

Day-to-day instrument performance issues were addressed by calibrating the Raman system prior to each experiment and by collecting and comparing calibration samples for every experiment.

3.4.1 Data analysis

A large variety of analysis techniques can be used for quantitative analysis of SERS spectra.

Simple quantification methods correlate the peak height or area to the analyte concentration. Whereas peak area is generally more suitable for well-resolved peaks and can improve robustness in case of irregularly shaped or wide peaks, peak height can reduce the effect of overlapping peaks. As explained in Paragraph 3.3, the peak at 1169 cm^{-1} was chosen as a characteristic peak for pHCA in **Paper II** and **V**, and quantification was based on peak height due to the close presence of other shoulders and wide peaks (e.g. at 1250 cm^{-1}).

The estimation of peak height performed in **Paper II** and **V** involved the following steps:

1) A polynomial baseline correction was performed on each SERS spectrum of each map. The purpose was to better identify outliers and improve averaging in the following steps.
2) Outliers were removed from each map. For a correct estimation, the standard deviation of the spectra of each map was calculated at each wavelength in the fingerprint region. The wavelength with the highest standard deviation was identified and used to discard spectra with a lower significance level than 0.05.
3) Average and standard deviation were calculated for each map.
4) A linear baseline correction was performed on the average spectrum in the peak region (between 1150 and 1190 cm^{-1}). It was observed that if the linear baseline

correction was performed on SERS spectra without prior averaging, the estimation of pHCA at low concentrations was worse, due to the signal noise.

5) Peak height was calculated at 1169 cm^{-1}.
6) Signal intensity and pHCA concentration were correlated with a linear regression model, enabling quantification of unknown samples.

In **Paper III** and **IV** we present quantification based on a partial least squares (PLS) model, automatically implemented through the software TQ Analyst (version 9.2, Thermo Fisher Scientific Inc., Waltham, MA, US). PLS was applied for the quantification of pHCA alone in **Paper III**, of a mixture of pHCA and CA in **Paper IV** and mixture of different salts, nutrients and metabolites in the Raman experiment described in Paragraph 3.2.1.

The PLS algorithm is a statistical approach to quantitative analysis, capable of separating the contributions of analytes with overlapping spectral features, or with chemical interactions resulting in a non-linear correlation between concentration and signal intensity. To build a PLS model of a Raman or SERS dataset, calibration samples with a known number of components and known concentrations must be given as input. Validation samples, which are treated as unknown samples, must also be included in order to evaluate the goodness of the model. The correlation between the concentration of each component and the signal intensity is performed on selected spectral regions where the components show significant vibrational peaks. Other signal processing tools, such as smoothing, first or second derivative and baseline correction of spectra can be used to improve the model. It is possible to verify the correct separation of the analyte spectral contributions by inspecting the spectra of pure components, as done in Supporting Information in **Paper III** and **IV**.

4 Sample pre-treatment in analytical chemistry

When aiming at detecting an analyte in a sample matrix, the analytical procedure consists of a series of steps such as sampling, sample pretreatment, identification and quantification of target compounds, and data analysis. This chapter will be focused on sample pre-treatment and preparation prior to detection, a fundamental step for a robust and reproducible analysis [123].

This part of the analytical process has a great influence on the time required for analysis and the quality of results obtained [124]. In fact, sample pre-treatment was estimated to represent two-thirds of the analysis time and to be the source of most experimental errors and discrepancies between laboratories [125]. Very often, sample pretreatment is still a tedious and time-consuming process involving repeated manual manipulations, which can be a source of contamination and can result in the loss of target analytes. This is a major issue especially in trace analysis, where extensive extraction, purification and up-concentration steps need to be performed, resulting in complex extraction protocols [126]. Additionally, these sample pre-treatment protocols are mostly performed offline, often generating large amounts of waste, and thus affecting both the throughput and the environmental footprint of the analytical procedure.

When selecting and developing a sample pre-treatment procedure, this needs to be tailored for the specific application, taking into consideration the sample matrix, the target analyte, the detection method and the purpose of the analysis (e.g. detection of specific target molecules versus comprehensive profiling). For the choice of solvents and chemicals, it is important to consider both the sensitivity and compatibility of the detection method with the pre-treatment method in use. Finally, considerations must be done about costs, analysis time, usability and possibility of miniaturization and automation of the process. Developing and optimizing a sample pretreatment procedure is

Tab. 4.1: Overview of the most common extraction techniques for liquid samples, extracted from [125].

	Extraction technique	Selectivity	Suitable for semipolar compounds	Enhancement factor	Extraction time	Automation	Simplicity	Ruggedness/ repeatability	Cost
Liquid phase	LLE	++	+++	Low	2 – 30 min	Low	High	Moderate	Low
	SLM	+++	++++	High	5 – 120 min	Moderate	Moderate	Good	Low
Sorbent phase	SPE	+++	++++	Moderate	2 – 10 min	High	Moderate	Good	Moderate
	Column chromatography	++++	++++	Moderate	10 – 40 min	High	Moderate	Good	Moderate

a complex task, since, in fact, there is no universal technique suitable for all kinds of samples, analytes and applications.

When analyzing small molecules in bacterial aliquots, for instance, procedures like filtration and centrifugation are commonly used to remove bacteria and physical debris from the sample [55]. Then, in most cases, an additional sample pre-treatment step might be needed according to the detection method, to further clean up the sample or to extract a specific molecule from the sample [45], [55], (**Paper II – V**).

The traditional categorization of extraction techniques depends on the nature of the sample to be analyzed (gaseous, liquid or solid) [125]. Due to the large variety of currently available and continuously developed techniques, a complete review is beyond the scope of this work. Therefore, we limited our overview to the most common techniques for extraction/sample cleanup of liquid samples, aiming at the analysis of liquid supernatant samples (Tab. 4.1).

Among these, a categorization can be made between liquid phase and sorbent phase extraction.

Liquid phase extraction techniques are separation methods based on the partition of an analyte between two immiscible liquid phases. The mass transfer depends on the

affinity of the component towards each phase [127]. The most established and well-known technique is liquid-liquid extraction (LLE), which is a separation process depending on the mass transfer of the component to be separated from a first liquid phase to a second one. In general, nonpolar compounds tend to be more soluble in nonpolar organic solvents, whereas charged molecules tend to stay in the aqueous phase. It can be used for extraction of nonpolar or semipolar compounds from salt solutions into an organic phase (**Paper II** – **IV**), or for extracting polar compounds into an aqueous phase [127].

The most traditional tool for LLE is the separatory funnel (Fig. 4.1a): an aqueous and an organic phase with different densities are inserted in the funnel. Once the funnel is closed, it is slowly inverted to increase the exchange surface without forming emulsions. Then, the stopcock is opened to separate the phases, starting from the heavier one, and the extraction can be eventually repeated. The same mechanism can be implemented in a channel, where the organic and aqueous phases are mixed with a turbulent flow and then separated based on their density difference. Many industrial systems, such as columns, centrifugal contactors (Fig. 4.1b) and mixer-settlers (Fig. 4.1c), have been developed and optimized with the purpose of fast phase mixing and separation on industrial scale [128].

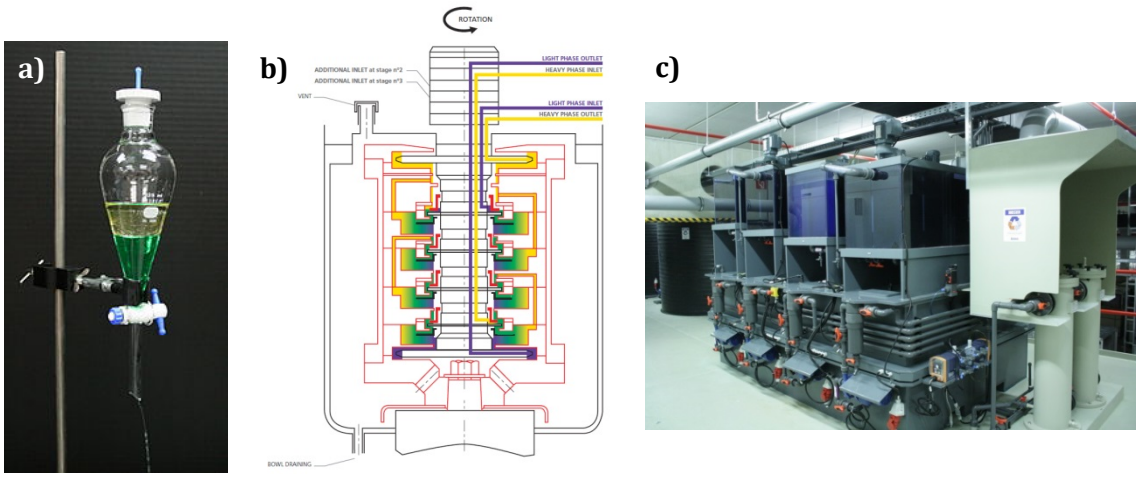

Fig. 4.1: (a) Separatory funnel, commonly used for LLE. The funnel is made of glass, whereas the stopcock and the seal are commonly made of Teflon, particularly resistant to a wide range of organic solvents. (b) Complex cross section of an industrial centrifugal extractor and (c) bulky industrial mixer-settler equipment.

LLE has been successfully used for industrial applications over the last few decades as a very robust separation technique for the recovery of industrially relevant compounds from fermentations [129]. However, new LLE applications have been recently explored, such as extraction of drugs and vitamins from biological samples for forensic science and diagnostics [130]–[132], and extraction of metabolites from microbial culture medium, for signaling [133] and metabolomics studies [134], [135], (**Paper II** - **IV**).

LLE is a rather simple, well-established and widespread technique, with a large amount of available literature and data. Common disadvantages are the usage of large amounts of toxic solvents in big scale processes, the need for several extraction steps to reach good extraction efficiency and time-consuming manual operations.

Many variations of LLE were developed to minimize the amount of organic solvent and maximize the interface between phases. For instance, single-droplet microextraction (SDME) only uses a small droplet of organic solvent (Fig. 4.2a). Few μL of extraction solvent are suspended at the tip of a syringe and exposed to a liquid or gaseous sample for a certain time at a defined temperature. After extraction, the droplet is removed and transferred to the analytical instrument [136]. Other techniques, such as dispersive liquid-liquid microextraction (DLLME) (Fig. 4.2b), cloud-point extraction (CPE) [137] and homogeneous liquid-liquid extraction (HLLE) [138], aim at the formation of finely dispersed microemulsions, or even a virtually infinite interface, starting the extraction in a homogeneous solution. Among others, extraction of organic pollutants [139], [140], proteins [137] and aminoacids [138] were reported with these techniques.

Besides still requiring repeated manual steps, these methods also involve additional surfactants and/or dispersers, as well as additional steps for creation and sedimentation of the emulsion, adding complexity to the overall system.

The research towards the reduction of organic solvents and samples has generated numerous microfluidic devices for performing LLE [141]. Microfluidics represents an ideal environment for LLE due to high surface-to-volume ratios, small amounts of sample required and waste produced, automated fluidic handling and integration of complex fluidic operations in a single platform [142]. Since the first example of microfluidic LLE developed by Sato *et al*. [143], applications have been reviewed in the production of fine chemicals [144], in medical detection [145] and environmental monitoring [146].

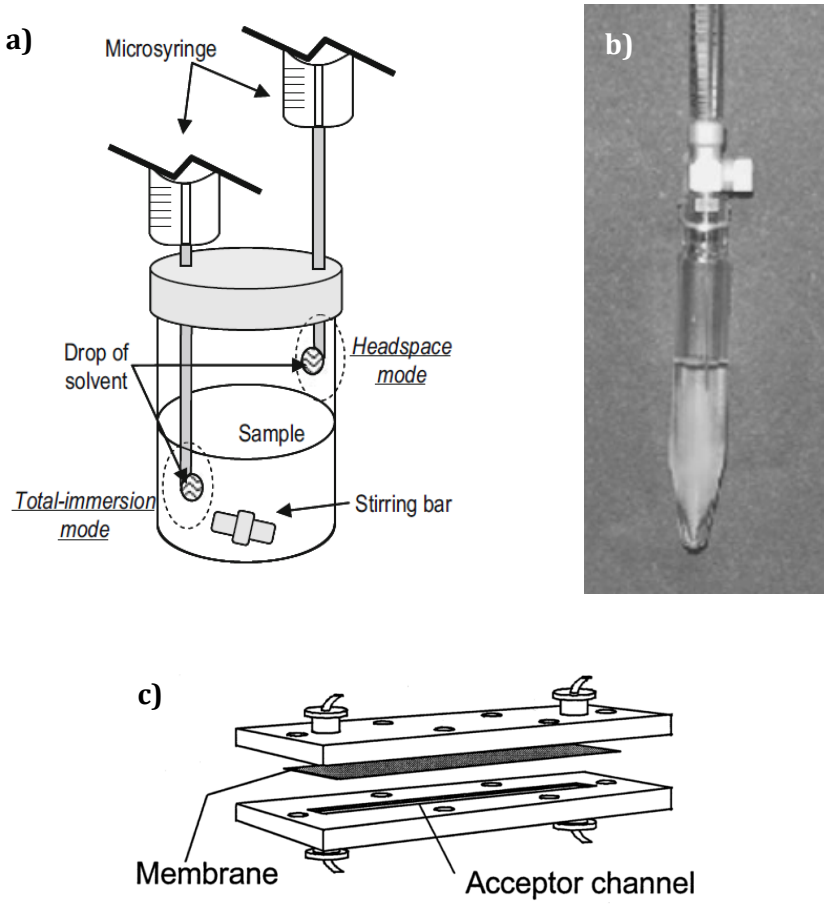

Fig. 4.2: (a) SDME working principle: a droplet of few µL of an extraction solvent is exposed to a stirred liquid (or gaseous) sample for a certain time and temperature. After extraction, the droplet is retracted and analyzed. (b) Rapid injection of an extraction solvent mixed with a disperser, creating a fine emulsion into an aqueous sample. (c) Microfluidic device for SLM extraction, embedding a porous membrane between the channels containing the donor and acceptor phase. Reprinted from [136]**,** [139] **and** [155] **respectively, with permission.**

Membrane-supported extractions, instead, use porous or non-porous membranes to perform a selective extraction and enrichment [147]. In case of supported liquid membrane (SLM) extraction, a porous hydrophobic membrane, placed between donor and acceptor aqueous phases, is impregnated with the extraction solvent of choice [148]. The analyte diffuses from one phase to the other through the impregnated pores of the membrane, undergoing both a solvent extraction and a size-exclusion filtration. With proper control of donor/acceptor pH, membrane material and organic solvent, flow-based

SLM extraction can enrich the analyte even hundreds of times, proving advantageous for detection at low concentrations [22].

Numerous environmental and bioanalytical applications of membrane-based extraction have been reviewed throughout the years [147], [150], due to important advantages such as tunability, use of low amounts of solvent, ease of use and possibility of automated in-line enrichment [151]. Applications of microfluidic SLM devices also include detection of pollutants in water samples [152], biomolecules and drugs in blood plasma [153] and urine [154] and, as reported in **Paper V**, for monitoring different culture conditions of genetically modified microorganisms, based on the extraction and enrichment of secondary metabolites from supernatant.

However, disadvantages of SLM extraction include the fabrication of the extraction device itself (Fig. 4.2c), which requires careful design and implementation, and memory effects, which can affect subsequent extractions if the membrane is not properly maintained.

Sorbent phase extraction techniques use a solid (or stationary) phase to temporarily bind the analyte(s), which is then eluted by a liquid (or mobile) phase [123].

Traditional solid phase extraction (SPE) is based on the surface affinity between a solid phase and an analyte in solution. The solid phase, made of functionalized silica or polymer particles, is packed in cartridge-like devices. A typical SPE procedure involves several steps, including initial cartridge conditioning with a proper buffer, addition of the sample, washing of the undesired impurities and elution of the compounds of interest (Fig. 4.3a). Subsequent elutions with solvents at different polarity enable chemical separation of the sample components, according to their affinity to the solid phase. SPE can be used to selectively retain the analytes of interest from the sample, which are later recovered by elution, or to retain the undesired impurities, removing them from the eluted sample.

Different kinds of SPE can be distinguished, according to how compounds are retained by the solid phase [156], [157]:

- *Normal phase* (polar modified solid phase, nonpolar liquid phase): it is used to retain polar analytes, mainly through hydrogen bonding, dipole-dipole and dipole-induced dipole interactions. Such analytes are then eluted with a more polar solvent than the originary sample matrix.

- *Reversed phase* (nonpolar modified solid phase, polar liquid phase): it is used for retention of mid- or nonpolar analytes through interactions with the hydrophobic functional groups at the surface of the solid phase (mainly van der Waals or dispersion forces). The compound is then eluted with a nonpolar solvent.
- *Ion exchange* (charged groups on solid phase): it is used to retain anionic or cationic compounds in solution, mainly by electrostatic attraction with charged functional groups at the silica surface.

SPE is a widely used technique because it is suitable for both polar and nonpolar analytes with a wide variety of sorbents, enabling a high degree of customization according to the specific needs. Many sorbent cartridges are commercially available with detailed documentation, also packed in miniaturized and disposable devices such as syringes or micropipette tips, enabling the usage of small amounts of sample and eluents [156].

However, some drawbacks are the cost of disposables, the high number of manual steps to be performed and the need for sample pretreatment and pH control prior to extraction. Additionally, reproducible packing of solid phases into custom-made devices is difficult [158], representing a challenge for a microfluidic implementation of SPE. In spite of the disadvantages, examples of microfluidic SPE were reported for separation of biomarkers [159] and matrix clean-up for detection of trace elements [160].

The principle of packed SPE columns is applied to column chromatography and coupled to a wide range of analytical procedures. In column chromatography, the stationary phase is packed into columns of different diameter according to the sample volume to be analyzed. The mobile phase is continuously eluted through the column, and the individual components of the sample are eluted one at a time. The retention time of each eluted component depends on the physico-chemical features of both liquid phase (polarity, flow rate) and solid phase (surface chemistry, particle size, column diameter), influencing the ability of a column to separate different components [161]. The eluent flow can be driven by gravity or, in case of tightly packed columns with small-sized particles, an external pressure can be applied to overcome the flow resistance. The fractions of eluent containing different components can be collected by means of a fraction collector or

continuously analyzed by a UV or fluorescence spectrophotometer, or a mass spectrometer, enabling quantitative analysis.

Automated systems using column chromatography for separation and quantitative sensing include high-performance liquid chromatography (HPLC) (Fig. 4.3b). HPLC is a well-established technique with countless applications in research, diagnostics [162], [163], food industry [164] and, as mentioned in **Chapter 2**, in metabolic engineering for strain development and optimization. Moreover, due to its robustness, HPLC is an excellent tool for validation of newly developed quantification methods. In fact, in **Paper II – V** and in **Chapter 3** we validated our SERS and Raman-based quantification of pHCA and CA through a reversed-phase HPLC procedure.

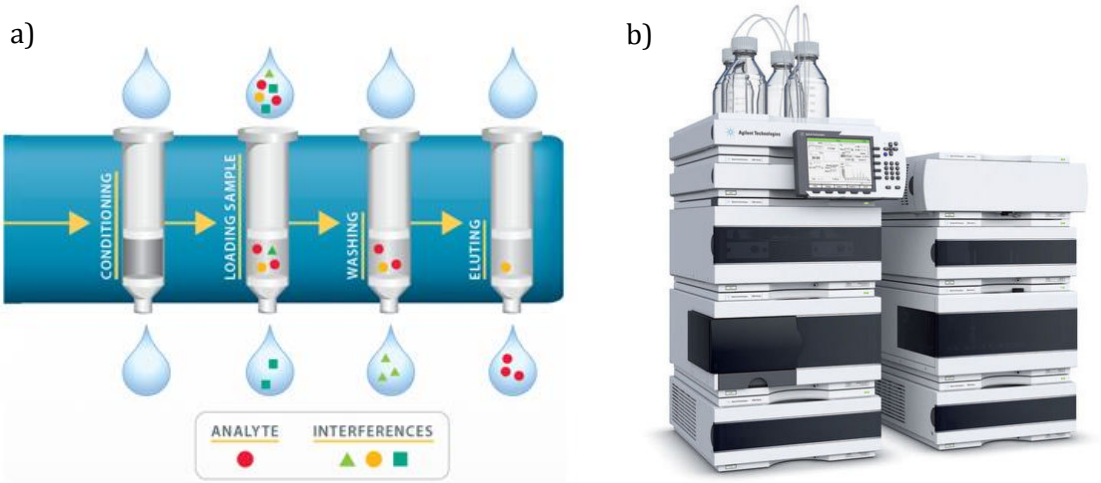

Fig. 4.3: (a) Typical SPE procedure, involving cartridge conditioning, sample loading, washing and elution of the analyte of interest. Image reprinted from www.johnmorris.com.au (b) HPLC system, produced by Agilent©.

However, HPLC requires a bulky and costly instrumentation, which must be operated by skilled personnel. Moreover, the optimization of sensing protocols can be challenging, and the time-to-result per sample can vary from minutes to tens of minutes, limiting the overall throughput.

4.1 Motivation for the choice of sample pre-treatment

As demonstrated in **Paper I**, direct SERS detection of analytes in a complex matrix is challenging, due to the presence of interfering compounds and salts fouling the active surface. Therefore, there is a need for a fast, selective and SERS-compatible sample pre-treatment step prior to SERS sensing. The following specifications were considered for the choice of the optimal pre-treatment technique:

- Exclusion of compounds which have overlapping spectral features with the SERS signal of the target analytes.
- Removal or reduction of salt content in the sample, to avoid fouling of the SERS-active surface.
- Enable detection in organic solvent or in aqueous sample diluted with an organic solvent, since the SERS signal is best enhanced when the silicon nanopillars are wet by a droplet of organic solvent [165].
- Possibility of integration of the sample pre-treatment procedure on a lab on disc (LoD) platform, combined with SERS-based sensing.

In this perspective, sorbent phase techniques were excluded due to difficult microfluidic integration. In fact, the reproducible packing of a stationary phase on microfluidic discs would introduce significant complexity to the fabrication process [158], [160]. Furthermore, the microfluidic complexity of a LoD implementing repeated washing and elution steps combined with SERS sensing would increase exponentially.

Among the liquid phase extraction techniques, LLE was chosen for extraction of pHCA (**Paper II**) and CA (**Paper IV**) from bacterial samples and for adaptation to the LoD device (**Paper III**), due to its simplicity and ruggedness as a common extraction method for phenolic compounds [126], [166]–[170].

SLM extraction, too, was found to be a suitable extraction method for phenolic compounds [171], and advantages such as analyte enhancement and robustness and ease of use of a microfluidic implementation were particularly appealing for its combination with SERS sensing (**Paper V**).

4.2 Liquid-liquid extraction

The enzymatic reactions used as cases of study in **Paper I – V** are depicted in Fig. 4.4: pHCA and CA were synthetized by deamination of the substrates needed for the reaction, i.e. Tyr and Phe respectively [55]. Genetically modified *E. coli* expressing TAL and PAL enzymes gradually processed the substrates to produce pHCA and CA during culture. Therefore, Tyr and Phe could be found in supernatant at significant concentrations at different time points during incubation, and they could interfere with the SERS signals of the compounds of interest (**Paper II – V**). Hence, the goal was to extract pHCA and CA while excluding Tyr, Phe and also salts, which fouled the SERS signal by crystallizing on the active surface (**Paper I**).

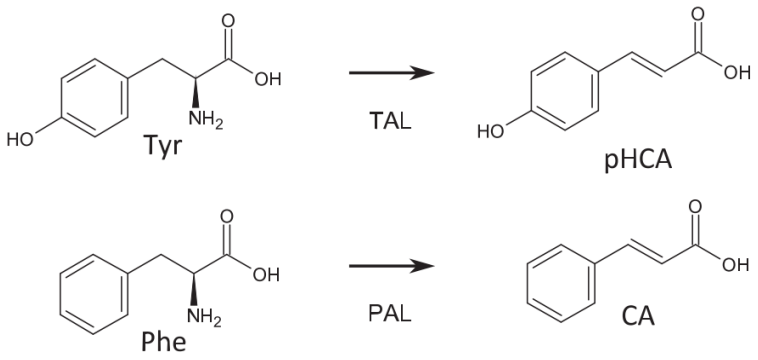

Fig. 4.4: Tyrosine ammonia-lyase and Phenylalanine ammonia-lyase, which synthetize pHCA and CA from Tyr and Phe respectively.

As previously explained, LLE enables the partition of an analyte between two immiscible phases, according to the affinity of the analyte towards each phase. A common case is represented by the extraction of an analyte from an aqueous to an organic phase. According to its density, the organic phase can be found on top or underneath the aqueous phase, as depicted in Fig. 4.5.

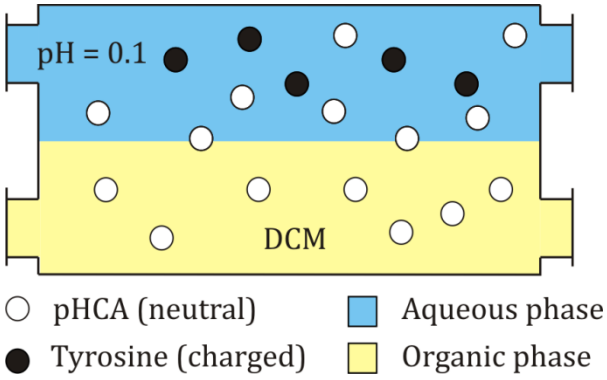

Fig. 4.5: Partitioning of an analyte between two immiscible liquid phases. In this example, the organic phase (DCM, yellow) is denser than water (blue), therefore it is placed at the bottom of the chamber.

The partition of the analyte between the phase 1 (aqueous phase, blue in Fig. 4.5) and 2 (organic phase, yellow) at equilibrium depends on the partition coefficient, K [161]:

$$K = \frac{A_{S_2}}{A_{S_1}} \approx \frac{[S]_2}{[S]_1} \qquad \textbf{Eq. 4.1}$$

Where A_{S_1} and A_{S_2} are the activities of the solute in phase 1 and 2, and $[S]_1$ and $[S]_2$ are the corresponding concentrations.

Considering that neutral species are more soluble in organic solvents, and charged species are more soluble in aqueous solutions, the pH of the aqueous phase is a crucial parameter to control for an advantageous partition.

In our case of study (Fig. 4.4), the analytes of interest (pHCA and CA) were weak acids, neutral at low pH. At the same time, the undesired compounds (Tyr and Phe) had a NH_2 group, positively charged at low pH. Therefore, a careful choice of a low pH could exclude substrates, salts and other charged molecules from the organic phase, while extracting the compounds of interest (Fig. 4.5). The importance of a low pH for pHCA (and CA) extraction was experimentally confirmed by observing that DCM extracts of non-acidified aqueous samples did not give any pHCA signal (not shown).

When dealing with a species that has more than one chemical form, such as the mentioned weak acids, the distribution coefficient D is used instead of K:

$$D = \frac{total\ concentration\ in\ phase\ 2}{total\ concentration\ in\ phase\ 1} \quad \textbf{Eq. 4.2}$$

Considering the example of pHCA, whose neutral form HA has a partition coefficient K between the organic and aqueous phase, and assuming that its conjugate base A^- is only soluble in the aqueous phase, D becomes:

$$D = \frac{[HA]_2}{[HA]_1 + [A^-]_1} \quad \textbf{Eq. 4.3}$$

Substituting $K = [HA]_2/[HA]_1$ and the acid dissociation constant $K_a = [H^+][A^-]_1/[HA]_1$ into Eq. 4.3, D becomes:

$$D = \frac{K \cdot [H^+]}{K_a + [H^+]} = K \cdot \alpha_A \quad \textbf{Eq. 4.4}$$

where α_A is the fraction of the neutral form HA in aqueous phase. Therefore, if $\alpha_A \approx 1,\ D \approx K$.

This principle was applied to maximize the partition of pHCA and CA in the organic phase. The aqueous samples were always acidified at a very low pH ($\sim$ 0.1), much lower than pK_a for both pHCA (pK_a of 4.9 for -COOH and 9.35 for -OH, [172]) and CA (pK_a of 4.4, [173]), in order to maximize the fraction of neutral pHCA and CA in aqueous phase. In this way, we could assume that no dissociated analyte was left in the aqueous phase, and that $D \approx K$.

In **Paper II** and **IV** the LLE process was developed and characterized for extraction of pHCA and CA. As a first step, the organic extraction phase was chosen. Non-volatile solvents, such as n-octanol, were excluded, due to the need for quick drying of samples on the SERS chips. Then, LLE was performed on pHCA spiked medium with different solvents (i.e. DCM, diethyl ether, ethyl acetate) in **Paper II**. As shown in Fig. S-2 (Supporting Information, **Paper II**), DCM showed a better result compared to ethyl acetate. Additionally, extraction from control supernatant was performed, and a higher

background in the region peak was found when extracting with diethyl ether compared to DCM (Fig. S-3). For these reasons, DCM was chosen for LLE in all the experiments.

LLE of pHCA and CA was characterized in terms of extraction efficiency, a parameter closely related to the partition coefficient K, defined as:

$$\%\ extr\ eff = \frac{[S]_2}{[S]_i} \cdot 100 \qquad \textbf{Eq. 4.5}$$

where $[S]_i$ is the initial sample concentration, known in spiked samples. In general, it is possible to calculate the extraction efficiency through models and solubility data, or it can be found in literature for analytes in well-characterized extraction systems. However, its value can also be easily calculated by experimentally measuring the amount of extracted analyte in each phase.

For the calculation of the extraction efficiency, LLE was performed on pHCA and CA spiked growth medium, and the extraction efficiency was measured with both SERS and HPLC. $[S]_{2(SERS)}$ (i.e. pHCA concentration in DCM extracts) was directly measured through SERS acquisition of DCM extracts. However, HPLC was not suitable for the elution of volatile and water immiscible DCM samples, hence $[S]_{2(HPLC)}$ was calculated by measuring pHCA in the aqueous phase before ($[S]_i$) and after extraction ($[S]_1$). Assuming that the total number of moles was maintained in the system, $[S]_{2(HPLC)}$ was calculated as $[S]_i - [S]_1$. Fig. 4.6 (**Paper II**) shows a good correlation between SERS and HPLC quantification of pHCA in DCM extracts. The graph in Fig. 4.6 also shows that the extracted amount of pHCA was close to 10% of the starting concentration in all the analyzed samples, for a $K \sim 0.1$. Knowing the dynamic range of the SERS sensor (3 to 50 μM) (**Paper II**), the obtained extraction efficiency enabled correct quantification up to a concentration of 500 μM in the starting samples, and further dilution of the extracts enabled quantification of up to 800 μM pHCA in bacterial supernatant. The same procedure was repeated for CA, obtaining an efficiency of 86% (**Paper IV**).

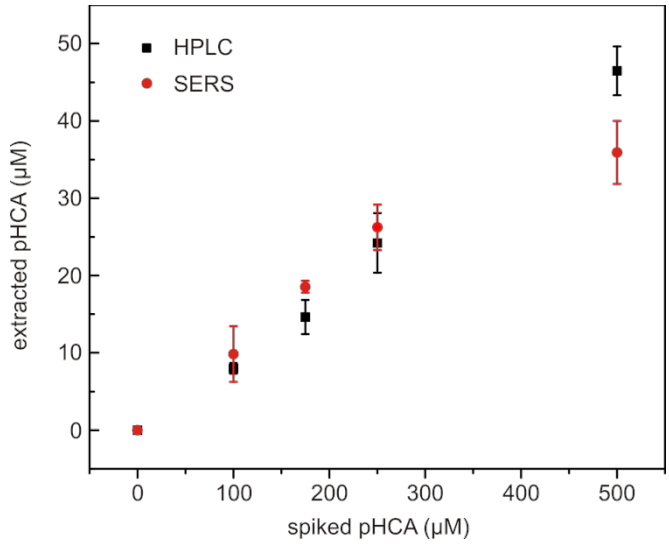

Fig. 4.6: Extracted amount of pHCA from spiked samples of bacterial growth medium measured with both HPLC and SERS. Reprinted from Paper II with permission.

The outcome of LLE is also influenced by the volume of both liquid phases. If a solute S with a m number of total moles and a partition coefficient K is extracted from V_1 mL of phase 1 to V_2 mL of phase 2, and q is the fraction of solute left in phase 1 after extraction, we have:

$$[S]_1 = \frac{qm}{V_1} \qquad \textbf{Eq. 4.6}$$

And

$$[S]_2 = \frac{(1-q)m}{V_2} \qquad \textbf{Eq. 4.7}$$

It is possible to calculate the fraction q of the solute remaining in aqueous phase after one extraction:

$$q = \frac{V_1}{V_1 + KV_2} \qquad \textbf{Eq. 4.8}$$

and after n extractions:

$$q^n = \left(\frac{V_1}{V_1 + KV_2}\right)^n \qquad \textbf{Eq. 4.9}$$

It can be demonstrated that many small extractions are more efficient than just one with the same volume of solvent; for this reason performing several extraction steps is a common practice. Nevertheless, as previously explained, SERS enabled effective quantification in the relevant concentration range after just one extraction step. Furthermore, limiting the number of extraction steps to just one significantly reduced the complexity of LLE implementation on the LoD described in **Paper III**.

In **Paper III** we investigated the effect of different DCM/sample volume ratios on the SERS signal of pHCA. Fig. 4.7 shows the normalized SERS intensity of the characteristic pHCA peak with different DCM/sample ratios. It can be observed that the signal increases with decreasing DCM/sample ratios until 1, and it does not change significantly at smaller ratios. According to Eq. 4.8, the fraction of extracted S increases when increasing the DCM/sample volume ratio, which means that more solute is extracted when using a higher volume of organic phase. However, the collected SERS signal is proportional to pHCA *concentration* (Eq. 4.7), which decreases with higher V_2, coherently with the results in Fig. 4.7.

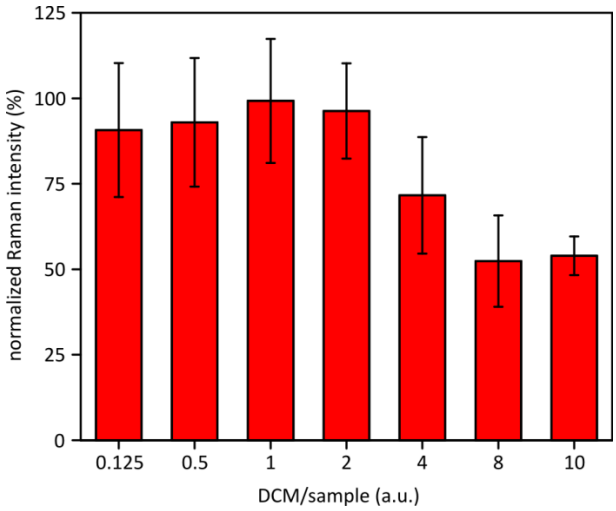

Fig. 4.7: Normalized Raman intensity of the characteristic pHCA peak for various DCM/sample ratios. Reprinted from Paper III with permission.

The plateau reached at ratios smaller than 1 is explained when substituting $K \sim 0.1$ in Eq. 4.8. With the volumes and concentrations used in the experiment, it was calculated

that the extracted pHCA was 24 µM, 22 µM and 14 µM at ratios of 0.125, 1 and 8 respectively. Therefore, in case of low K, a significant decrease in DCM/sample ratio does not lead to a proportional signal improvement, while overcomplicating sample handling in case of very small sample volumes.

4.3 Supported liquid membrane extraction

The working principle of a typical membrane unit for SLM extraction is depicted with the target analyte, pHCA and the interfering compound, Tyr, in Fig. 4.8. The top chamber, containing a flowing donor phase, is separated from the bottom chamber, containing a stagnant acceptor phase, by a porous hydrophobic membrane impregnated with an organic solvent. The result is a three-phase system with an organic phase placed in between two aqueous phases. The porous membrane has different functions: it physically separates the two aqueous phases, it holds and confines the organic solvent into its pores, and it prevents extraction of macromolecules bigger than the pore size.

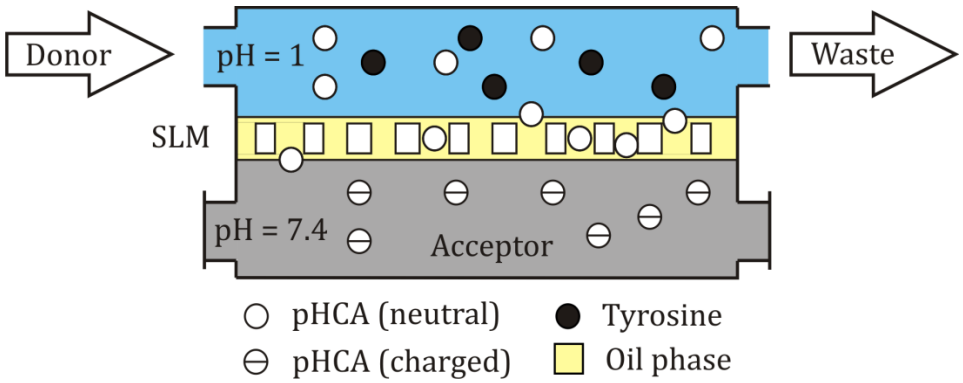

Fig. 4.8: Scheme depicting the working principle of SLM extraction in the particular case of pHCA extraction from a complex matrix. Reprinted from Paper V with permission.

Referring to Fig. 4.8, permanently charged compounds, as well as compounds that are charged at low pH, such as Tyr (pK_a of 2.2 for -COOH, 9.21 for $-NH_3^+$ and 10.46 for -OH), are excluded from the membrane. As previously mentioned, acidic analytes, such as pHCA,

are uncharged in the acidic donor, therefore they are extracted into the organic phase. Since the acceptor phase is a basic solution, the extracted compounds are immediately dissociated at the interface between the membrane and the acceptor, preventing it from diffusing back into the membrane. The result is an irreversible transport of pHCA from the donor to the acceptor. Furthermore, since the captured analyte is in a different (dissociated) state in the acceptor than in the donor, the concentration gradient of the diffusing (neutral) species is largely unaffected by the acceptor, where the compound can be significantly and irreversibly enriched. For the same reason, small neutral compounds can be also extracted, but they cannot be enriched since their concentration in the acceptor cannot exceed the one in the donor.

The choice of donor and acceptor pH must be done considering that the mass transfer is proportional to the concentration difference over the membrane [148]:

$$\Delta[S] = \alpha_D[S]_D - \alpha_A[S]_A \qquad \textbf{Eq. 4.10}$$

where $[S]_D$ and $[S]_A$ are the concentrations of S in donor and acceptor, and α_D and α_A are the fractions of the uncharged forms in each phase. Therefore, it is maximized if α_D is close to 1 and α_A is close to 0. As a rule of thumb, the acceptor pH should be 3.3 points higher than the pK_a of the acidic analyte in order to work in this condition [174].

These considerations were applied to the design of the SLM extraction system in **Paper V**, where SLM extraction was combined with SERS-based sensing. SLM extraction was implemented through an easy to handle, robust and reproducible microfluidic device. In this case, the aqueous acceptor phase, containing the extracted pHCA, had to be diluted with EtOH to be compatible with SERS sensing. This enabled proper wetting of SERS substrates as well as dilution of the acceptor salts. The enrichment of pHCA achieved by the developed SLM device was able to overcome the decrease in sensitivity due to EtOH dilution, proving compatibility between SLM extraction and SERS-based sensing. Additionally, a proper washing technique enabled a reduction of the memory effects (Fig. S2, Supporting Information, **Paper V**), resulting in a robust and reproducible extraction (Fig. 4, **Paper V**).

5 Centrifugal microfluidics

As illustrated in the previous chapter, sample pre-treatment is a crucial part of the analytical process when aiming at the detection of a target analyte in a sample matrix. The optimal sample pre-treatment method can significantly improve the accuracy and sensitivity of the detection. However, it is often a sequence of tedious and time-consuming manual steps, prone to errors and generating large amounts of waste [123].

Since the introduction of microfluidics [175], a significant effort has been invested towards the automation and miniaturization of sample pre-treatment methods over the last decades [176] to achieve reliable, easy to use devices requiring low sample, solvent and reagent volumes. Besides the adaptation of sample pre-treatment procedures in microscale, focus has been directed towards the integration of sample handling steps with detection in so called *micro total analysis* (μTAS) systems. This expression was formulated to identify integrated and miniaturized systems performing a complete analysis, from sample pre-treatment to sensing [16].

μTAS systems have been developed and applied for cell and protein analysis, pathogen/disease detection, drug screening, forensic and environmental analysis [16], [177].

Miniaturization and parallelization, characteristic of microfluidic systems, represent useful features when aiming at high-throughput screening in metabolic engineering. Research has been growing in this sense, with the application of microfluidic devices to microbial culture and/or monitoring of nutrients [178] or secreted metabolites [179]–[181].

In spite of the small footprint of microfluidic devices, they often require complex fluidic actuation systems, which reduce their usability and increase their complexity. Centrifugal microfluidics has recently emerged as an alternative technology for complex microfluidic assays [17]. Since the first examples of centrifugally driven tools dating back to the 60's [182], [183], this technology has raised more and more attention for analytical

applications, aiming at portability, high throughput, short time-to-response and ease of use.

Lab-on-disc (LoD) systems are microfluidic devices in the form of a CD, embedding complex fluidic networks and simply actuated by controlling a spinning motor. In fact, one of the main advantages of centrifugal microfluidic systems, compared to the traditional pressure driven ones, is the absence of pumps. Furthermore, several microfluidic units can be implemented on the same disc and actuated with the same centrifugal force at the same time, increasing the throughput and reproducibility of the assay. The use of centrifugation as the main actuation principle also avoids the formation of bubbles and makes discs particularly suitable for fluidic operations such as sedimentation, which are commonly performed with a centrifuge [184].

Thanks to the versatility of LoDs, complex assays have been implemented for a number of biomedical applications, including blood analysis and diagnostics [18]; many examples of cell handling, PCR and immunoassays were reported [185]–[187], and colorimetric, optomagnetic and electrochemical detection techniques have been used for sensing [19].

In spite of the advantages provided by LoD devices, there are only a few reports on the application of this technology for microbial screening. Significantly, Kim *et al*. [20] reported a centrifugal microfluidic platform for quantitative screening of genetically modified microalgae, based on the amount of produced lipids, extracted with LLE.

In this Ph.D. project a LoD device was developed for screening different strains of genetically engineered *E. coli*, based on the amount of secondary metabolite pHCA, extracted with LLE (**Paper III**).

There are a few reports about LLE on LoD in literature, mostly based on non-volatile organic solvents compatible with most common polymers [20], or using external actuation systems, such as lasers for burning sacrificial valves or pneumatic pumps [188]. In our LoD device, instead, a LLE assay was implemented without any external component, and the choice of a solvent-resistant polymer (PP) enabled the fabrication of a platform resistant to extremely harsh solvents, such as DCM. Additionally, large-scale fabrication techniques (injection molding and ultrasonic welding) were used, resulting in a fast and scalable fabrication process.

A SERS-based detection unit, based on a gold-capped silicon nanopillar substrate, was also integrated on the platform, in order to achieve a real μTAS system. There are reports on SERS-based detection on LoD in literature; however, they are mostly based on nanoparticle aggregation [189], which is more prone to irreproducibility than solid SERS substrates [190].

5.1 Microfluidic design of the LoD

The design of a centrifugal microfluidic platform is a complex process, where several specifications need to be considered, and the optimization of the developed system is often achieved through repeated trial and error cycles.

The microfluidic design of the LoD presented in **Paper III**, combining LLE sample pre-treatment with SERS sensing, was the result of several considerations, summarized in Fig. 5.1. The application (LLE + SERS for quantification of pHCA in bacterial samples) determined the choice of the chemicals used on the platform.

The usage of harsh chemicals in the LLE assay (HCl and DCM, **Paper II**) and the optical sensing technique (SERS), led to the choice of a solvent-resistant and optically clear polymer. At the same time, the polymer had to be compatible with the available fabrication methods (injection molding and ultrasonic welding).

In turn, the chosen fabrication methods introduced geometric constraints to the design of the fluidic elements (e.g. size of the microfluidic slide, depth and disposition of chambers and channels) and to the embedding of SERS active substrates.

Moreover, the following generic criteria were applied when designing the LoD platform:

- Maximize multiplexing (i.e. maximize the number of parallel fluidic modules implemented on the same disc)
- Enable a complete analytical procedure on the same disc (i.e. implement calibration together with sample pre-treatment)
- Keep fabrication and fluidic operation simple (i.e. avoid the addition of external active components)

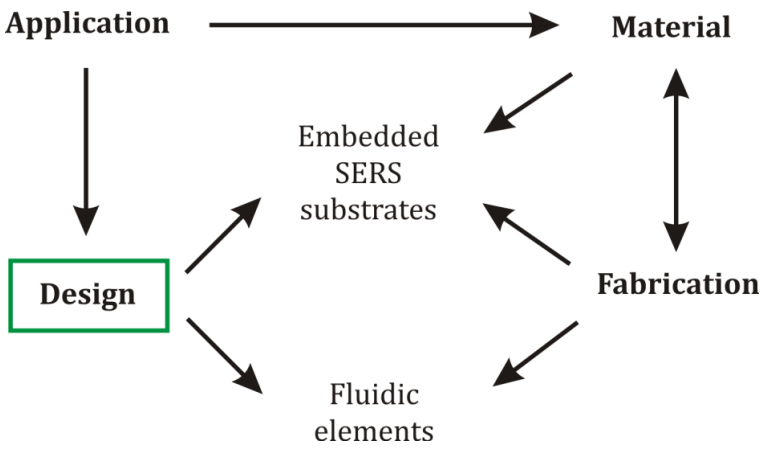

Fig. 5.1: Scheme representing the factors considered for the design of the LoD presented in Paper III.

The result of these considerations was the modular LoD shown in Fig. 5.2a, composed by microfluidic slides made of layers of poly(methylmetacrylate) (PMMA), pressure sensitive adhesive (PSA) tape and injection molded clear poly(propylene) (PP), enabling both calibration and sample pre-treatment/SERS sensing.

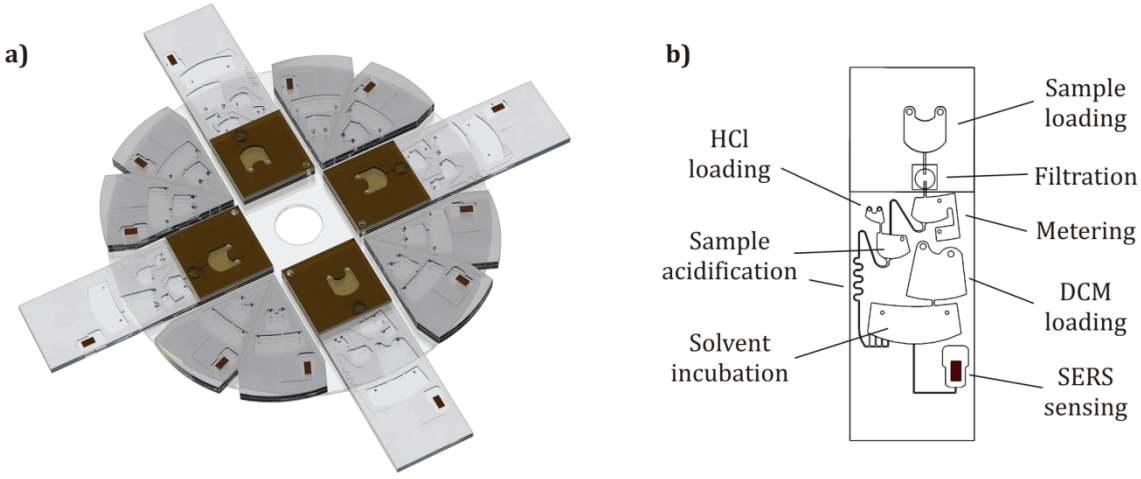

Fig. 5.2: (a) 3D render (realized by Ph.D. student Laura Serioli) of the LoD device. The LoD is composed by 4 assay modules (rectangular slides) and 8 calibration modules (triangular slides) assembled on a PMMA disc. (b) Assay steps implemented on the assay module.

According to the experimental protocol reported in **Paper II**, the steps for manual LLE and SERS-based sensing of bacterial samples were:

- Sample filtration
- Sample acidification
- Solvent incubation
- Wetting and drying of SERS chip with organic extracts

The same steps were adapted to the LoD, thanks to the microfluidic design in Fig. 5.2b.

In the next paragraphs more details will be provided about microfluidics theory, implementation and combination of microfluidic operations (filtration, valving, mixing and pneumatic pumping) in the presented design and the chosen fabrication techniques. A more detailed description of LoD microfluidic operation is given in **Paper III**.

5.1.1 Centrifugal microfluidics theory

For the design of fluidic operations it is important to understand the forces controlling the fluid motion on a centrifugal platform. These are usually divided into *intrinsic forces*, generated by the presence or absence of centrifugation, and *extrinsic forces*, generated by external means (e.g. magnetic, electric or external pneumatic forces that bring particles or fluid into motion). In our work we limited our overview to the intrinsic forces, sub-classified into *pseudo forces* and *non-pseudo forces*.

Pseudo forces are inertial forces arising from the centripetal acceleration acting on the rotating device. The main forces acting on a point-like mass m on a centrifugal microfluidic device are centrifugal force ($\boldsymbol{F}_C$), Coriolis force ($\boldsymbol{F}_{Co}$) and Euler force ($\boldsymbol{F}_E$), described by the following vectorial equations [17]:

$$\boldsymbol{F}_c = -m\boldsymbol{\omega} \times (\boldsymbol{\omega} \times \boldsymbol{r}) \qquad \textbf{Eq. 5.1}$$

$$\boldsymbol{F}_{Co} = -2m\boldsymbol{\omega} \times \frac{d}{dt}\boldsymbol{r} \qquad \textbf{Eq. 5.2}$$

$$\boldsymbol{F}_E = -m\frac{d}{dt}\boldsymbol{\omega} \times \boldsymbol{r} \qquad \textbf{Eq. 5.3}$$

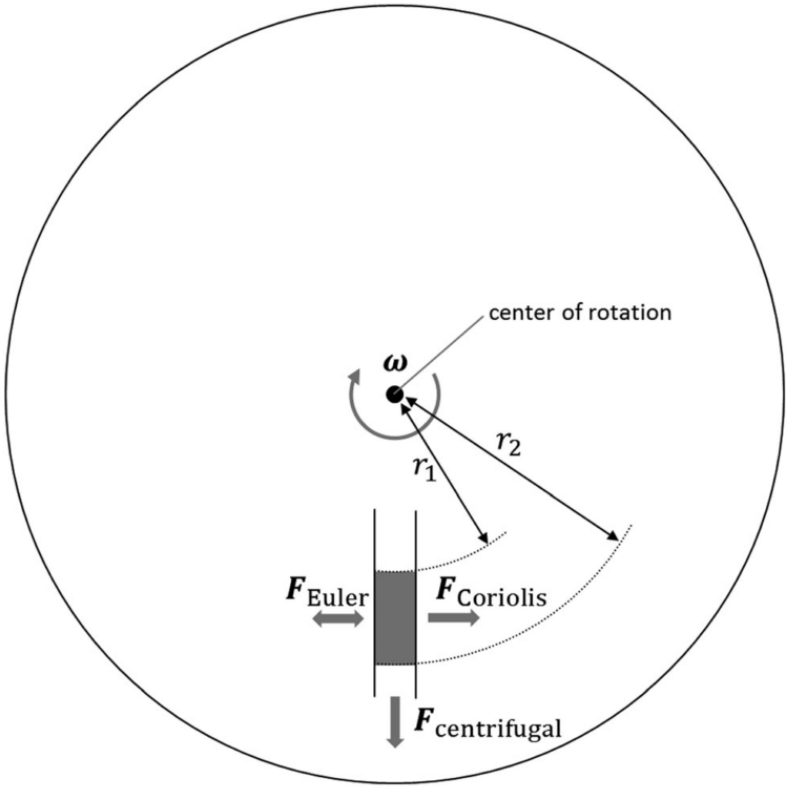

Fig. 5.3: Pseudo forces acting on a liquid column of height $r_2 - r_1$ on a centrifugal platform. The centrifugal force drives the fluid radially outwards, whereas Coriolis force is perpendicular to both ω and fluid velocity. Euler force is proportional to angular acceleration and deceleration. Reprinted from [17] **with permission.**

However, scalar differential pressures are more convenient than vectorial forces for the design of fluidic elements on a disc. For instance, a liquid column of density ρ is subject to a centrifugal pressure given by:

$$\Delta p_C = \frac{1}{2}\rho\omega^2({r_2}^2 - {r_1}^2) \qquad \textbf{Eq. 5.4}$$

where r_1 and r_2 are the radial distances from the center of the top and bottom of the column respectively, as also shown in Fig. 5.3. Interestingly, Δp_C only depends on the height of the column (given by r_1 and r_2) and not on the channel section.

Non-pseudo forces include capillary force and pneumatic force, exerted by a pressurized gas bubble on a LoD. Capillary force in a circular channel is driven by a Δp_e described by the Young-Laplace equation [191]:

$$\Delta p_e = \frac{2\sigma cos\theta_e}{r} \quad \textbf{Eq. 5.5}$$

where σ is the surface tension of the fluid, θ_e is the equilibrium contact angle and r is the channel radius. If the channel is hydrophilic ($\theta_e < 90°$), it will be self-primed by spontaneous imbibition. If the channel is hydrophobic ($\theta_e > 90°$), an external force must be applied to fill it.

The pneumatic force is described as [17]:

$$\Delta p_{pn} = p_o \left(\frac{V_0}{V} - 1\right) \quad \textbf{Eq. 5.6}$$

where p_o is the ambient pressure, V_0 is the volume of a gas bubble at p_o, and V is the gas volume in a compressed or expanded state.

5.1.2 Filtration

When performing an analytical process on a centrifugal microfluidic platform, separation of interfering residues, undesired particles or organisms (e.g. cells) is a fundamental step. For instance, plasma needs to be separated from whole blood in case of biomarker analysis [192], whereas undesired suspended particles or cells can clog the microchannels and significantly affect sensitivity when measuring pollutants or cell metabolites [193], [194].

Separation of undesired particles is usually performed manually and off-line, leading to a significant bottleneck in automating analytical processes. For example, a manually performed centrifugation and/or filtration step needs to be executed prior to HPLC analysis on bacterial aliquots, in order to remove bacteria from the sample [55]. In this Ph.D. project, we could overcome the need for manually performed centrifugation and/or filtration with the implementation of an automated filtration step on the fluidic platform, significantly reducing sample handling. In fact, due to the sensitivity of SERS-based sensing, removal of bacteria was a crucial step in order to reduce the amount of interfering compounds (Fig. 6, **Paper III**).

Two common approaches for separation on centrifugal microfluidic platforms are *sedimentation* and *filtration*, based on particle mass and size respectively.

With sedimentation, heavy particles are driven radially outwards by the centrifugal force, according to their mass (Eq. 5.1). The fluidic design directs the cells towards the bottom of a chamber or a well, while the clean supernatant is removed (Fig. 5.4). The sediment can then be excluded from analysis or be used for different purposes, such as cell count in blood samples.

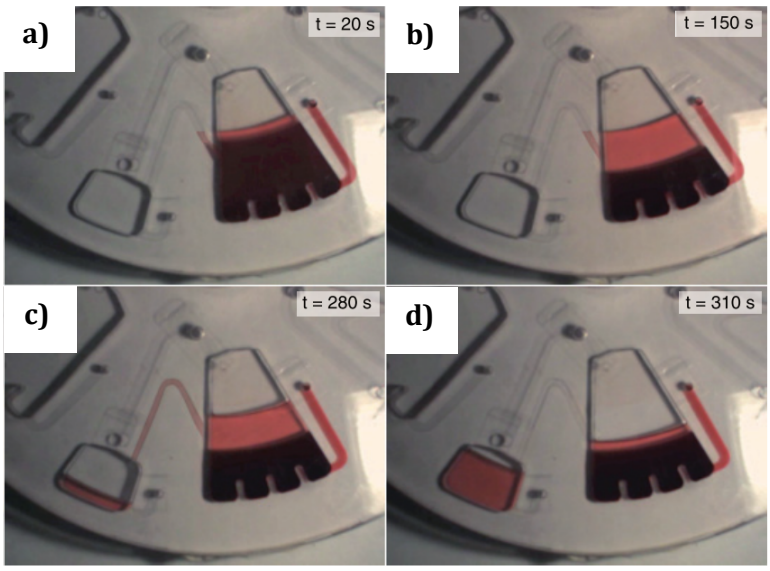

Fig. 5.4: Isolation of plasma from whole blood. (a), (b) Centrifugal force gradually drives red blood cells towards the bottom of the sedimentation chamber, underneath the level of the siphon inlet on the left of the chamber. (c) The disc slows down and the siphon is primed; (d) only plasma is transferred to the second chamber when accelerating again. Reprinted from [192] **with permission.**

Filtration, instead, is based on particle exclusion according to their size. Filtration can be performed through progressive geometric restrictions of the fluidic channels or, in case of smaller particles or bacterial cells, the liquid sample can be constrained to pass through a membrane filter embedded in the fluidic path. As reported by Czugala *et al.* [193], solid particles in turbid water samples were effectively trapped by a progressive restriction of the channel down to a height of 86 μm. Membrane filtration, instead, was used to remove bacteria from water samples [195] or even selectively filter circulating tumor cells from a whole blood sample [196].

Although examples of both sedimentation and membrane filtration were reported on LoD, sedimentation may not be able to completely remove fine particulate, and particles could be uptaken during the siphon priming. Therefore, membrane filtration was implemented in **Paper III**.

The sealing of the membrane filter is important to prevent leaking and therefore ensure correct filtration. The membrane can be sealed through solvent-assisted bonding (Fig. 5.5), thermal bonding (i.e. by applying high temperature and pressure to the membrane) [195], or, as presented in **Paper III**, by embedding the membrane between two layers of PSA tape (Fig. 5.6a).

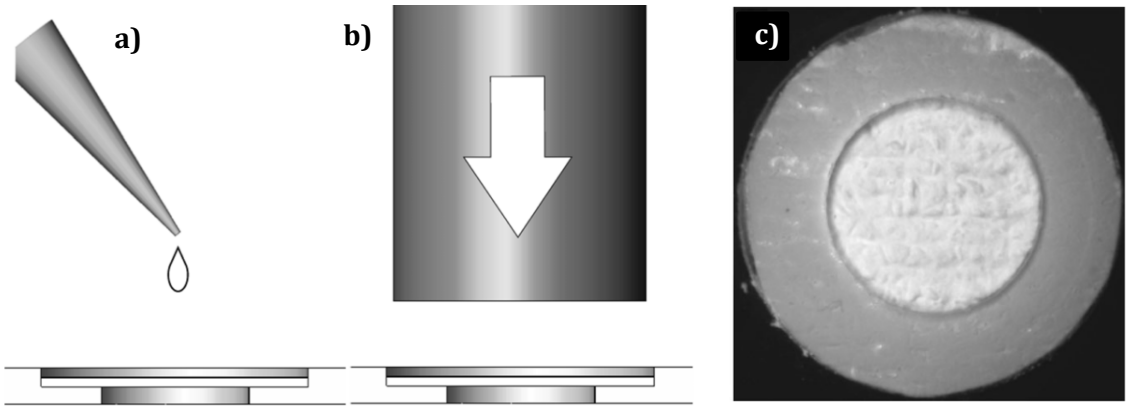

Fig. 5.5: Example of membrane integration in a polycarbonate (PC) microfluidic chamber. A droplet of acetone is poured on the membrane (a), subsequently pressed against the chamber (b). PC melts and seals the edges of the membrane, which become transparent (c). Reprinted from [196] **with permission.**

The advantage of the latter method is that it is very fast, simple and effective to implement. The effectiveness of the filtration of *E. coli* was tested by mimicking bacteria with 1 µm diameter microbeads, easily visible by eye, at a concentration of 10^{10} beads/mL, which is approximately twice the *E. coli* concentration at a typical OD_{600} = 5 after 24 h of culture. The microbeads (Dynabeads® MyOne™ Carboxylic Acid, Thermo Fisher Scientific) were filtered through a cellulose acetate membrane (0.2 µm pore size, Whatman™) at a spinning speed of 60 Hz for 2 min. As shown in Fig. 5.6b and c, the microbeads were completely trapped by the membrane, leaving a transparent sample in the bottom chamber, without any significant clogging of the membrane.

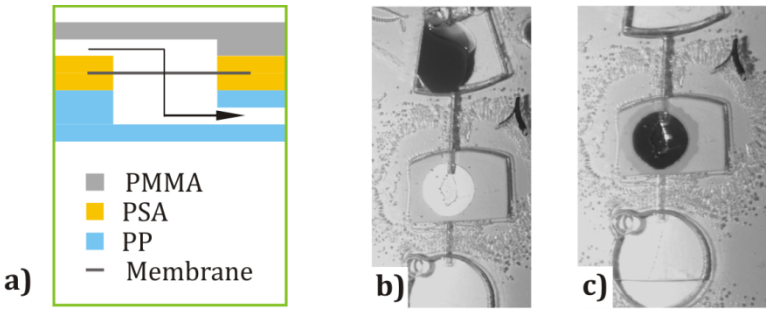

Fig. 5.6: (a) Scheme representing a filtration membrane embedded between two layers of PSA tape, indicated in yellow, with an arrow indicating the direction of the sample through the membrane. Scheme reprinted from Paper III with permission. 20 µL of microbeads solution flowing through a hydrophilic membrane filter, before (b) and after (c) filtration.

5.1.3 Metering

Most of the microfluidic processes require the handling of a precise amount of sample. Metering and aliquoting are two widely employed microfluidic operations for this purpose. A simple metering structure consists in an input connected to a well with a known volume, which redirects the excess fluid into a waste chamber (Fig. 5.7) [197]. The reproducibility of metering largely depends on the precise fabrication of the chamber and waste walls. For instance, laser ablation creates V-shaped walls, as explained in Paragraph 5.2.1, deviating from the designed volume of the metering chamber. Additionally, in case of very sharp and small features, such as the waste overflow, the polymer can melt in an

uncontrolled way, introducing a significant error. For these reasons, micromilling and molding techniques are preferred for such applications.

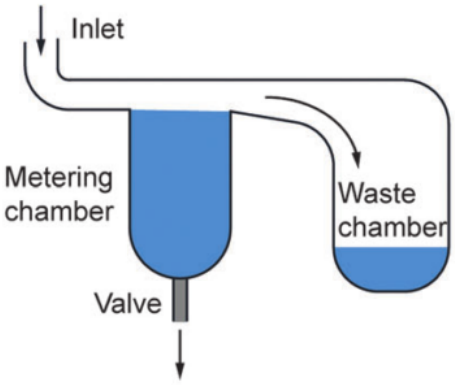

Fig. 5.7: Basic metering principle: the sample flows into a metering chamber and the excess volume overflows in a waste chamber. A valve can be placed at the bottom of the metering chamber to enable further fluidic processing. Reprinted from [17] **with permission.**

In the case of the microfluidic design used in this work, it was observed that an unknown portion of the liquid sample was absorbed by the membrane filter, as also indicated by the wet border around the round filtration chamber in Fig. 5.6c. Therefore, a simple metering chamber with an overflow waste was implemented in the PP microfluidic slide after filtration (Fig. 5.10d).

Metering can be used as the last step before analysis, or, as in our case, it can be combined with a valve at the bottom of the metering chamber to enable further fluidic processing. Examples of valves combined with metering units are hydrophobic valves [198] and capillary siphons [199].

5.1.4 Valving

Valving is one of the most essential fluidic operations on a centrifugal platform, because it controls the flow and regulates fluidic actuation. According to the design of the valve, it regulates the flow by stopping the fluid at high or low spinning speed, or it can even be actively opened when needed.

Valving can be classified into *passive* and *active valving*. Passive valving only relies on the forces acting on disc (e.g. centrifugal pressure, capillary force or pneumatic pressure), whereas active valving requires external active elements. For the design of a simple LoD device, passive valving is advantageous because it avoids the addition of external elements, which add complexity to the system [17].

Among the large variety of passive valves available, we included capillary and siphon valves in our microfluidic design. The *capillary valve* uses the effect of a liquid meniscus pinned at the diverging end of a channel, as shown in Fig. 5.8. The meniscus stops the flow until the applied centrifugal pressure (Eq. 5.4) overcomes the capillary pressure opposed by the interface, given by:

$$\Delta P_I = -\frac{2\sigma cos\theta_I}{r} \qquad \textbf{Eq. 5.7}$$

where θ_I is the maximum contact angle the meniscus can withstand before bursting. A deeper analysis of the dependency of the burst pressure on the fluid contact angle, channel section and outlet design was developed, among others, by Cho *et al*. [191].

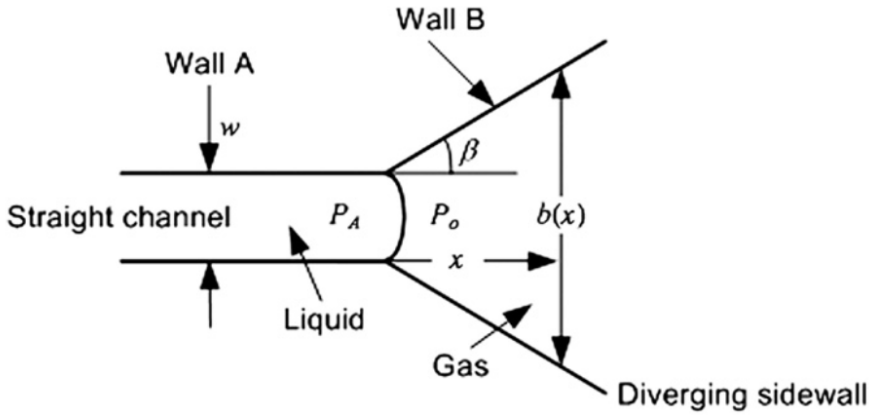

Fig. 5.8: Top view of a capillary valve. Reprinted from [191] **with permission.**

Special hydrophobic coatings can be sprayed or dispensed at the outlet of the channel if the wetting properties of the liquid do not enable the formation of a stable meniscus, or just to increase the burst pressure [198], [200].

The *siphon valve*, instead, connects an inlet and an outlet chamber through an S-shaped hydrophilic channel, as shown in Fig. 5.9. At high spinning speed, the shape of the channel prevents the liquid from flowing towards the outlet chamber (Fig. 5.9(1)). The fluid can move over the siphon crest only at low spinning speed, when the inward capillary pressure is stronger than the outward centrifugal pressure (Fig. 5.9(2)). After the fluid reaches the siphon outlet, the inlet chamber can be emptied by rotating the disc at high speed again (Fig. 5.9(3) and (4)).

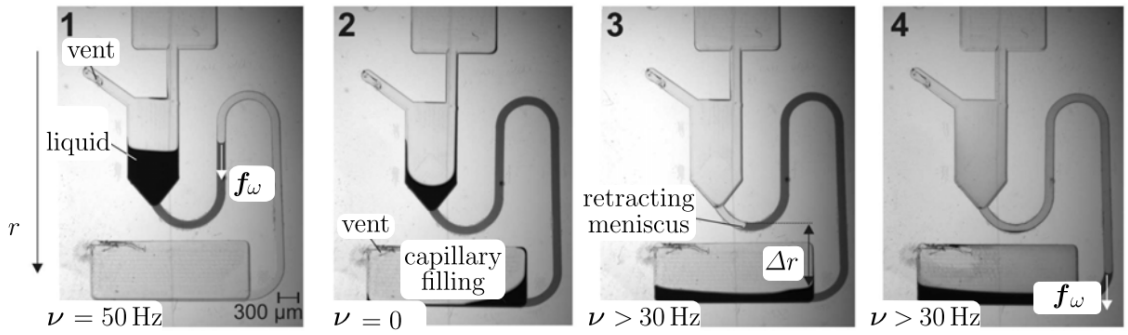

Fig. 5.9: Working principle of a siphon valve. Reprinted from [201] **with permission.**

Based on these considerations, while capillary valves stop the flow at low speed and burst when accelerating the disc, siphon valves stop the flow at high speed, and need a temporary state of low speed to be primed and subsequently opened. Combinations of serial siphons and capillary valves can be found in literature, demonstrating the possibility of fluid control over several cycles of accelerations and decelerations in complex designs [202].

In the developed device a simple combination of hydrophilic siphons (wetted with Tween© 20, Sigma Aldrich) and capillary valves was used. Since filtration and metering happen simultaneously at high pressure, a siphon valve at the bottom of the metering chamber was the most suitable choice to stop the liquid during metering (Fig. 5.10d). When stopping the disc for HCl loading, the siphon could prime, and the sudden disruption (i.e. capillary valve) at the end of the siphon prevented uncontrolled filling of the mixing chamber (Fig. 5.10b and d). The same principle was applied to the serpentine siphon connecting the mixing and the incubation chamber (Fig. 5.10c).

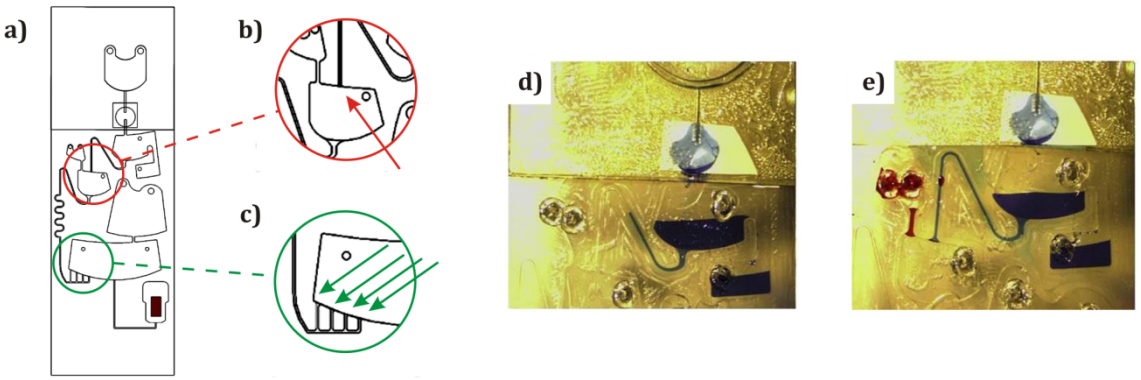

Fig. 5.10: (a) Fluidic scheme of the microfluidic slide. The capillary valves at the end of the hydrophilic siphons are indicated in (b) and (c). (d) When filtering and metering the sample (blue dye) at high spinning speed, the siphon valve confines the sample in the metering chamber. (e) When stopping the disc to load HCl (red dye), the sample primes the siphon and stops at the outlet, due to capillary valving. Adapted from Paper III with permission.

5.1.5 Mixing

It was demonstrated that microchannels up to 0.5 mm diameter on a centrifugal microfluidic platform always maintain a laminar flow regime [203]. Therefore, the microfluidic design should implement features to speed up mixing, either by enhancing the diffusion process or by creating fluidic turbulence on disc. La *et al.* [204] modeled and characterized a simple mixing process in a centrifugal force-based serpentine micromixer, finding that effective mixing could be achieved even with microchannels shorter than 1 cm. In fact, a combination of the Coriolis force, centrifugal force and fluidic inertia enabled effective mixing in the microchannel, due to its serpentine shape (Fig. 5.11a).

Since the LLE assay developed in **Paper II** includes an acidification step, where HCl is added and mixed with the sample, we implemented a similar serpentine channel in our LoD. At first, partial mixing was achieved through the simultaneous and turbulent emptying of the two streams into the common mixing chamber (Fig. 5.11b, top right). Then, the serpentine siphon, connecting the mixing chamber to the incubation chamber, enabled complete mixing prior to solvent incubation (Fig. 5.11b).

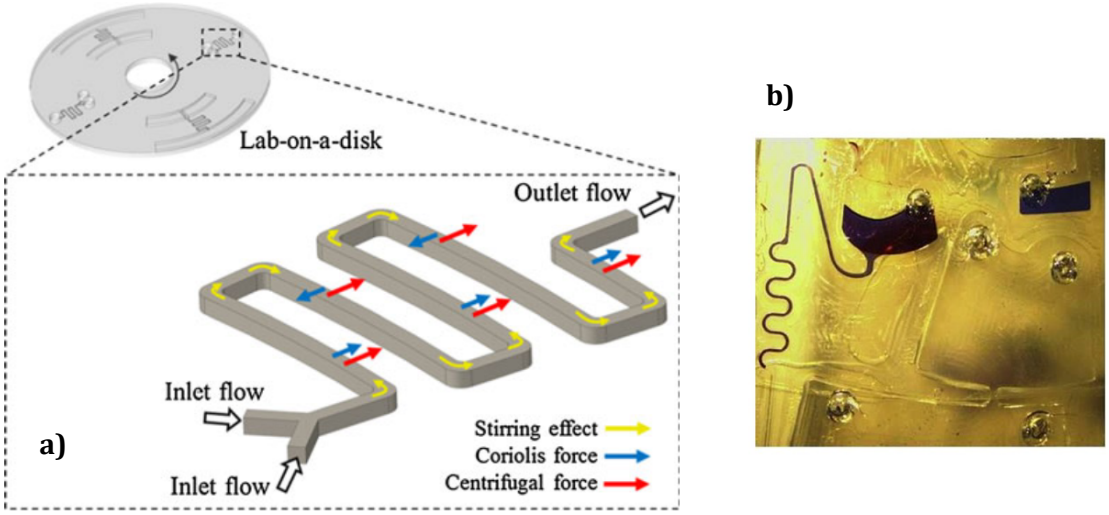

Fig. 5.11: (a) Schematic of the forces acting on the fluids into a serpentine siphon. Reprinted from [204] **with permission. (b) Priming of serpentine siphon before solvent incubation. Reprinted from Paper III with permission.**

As mentioned in **Chapter 4**, phase mixing is an important step in LLE. Many variations of LLE were developed with the purpose of increasing the exchange surface between phases by dispersion. In our microfluidic device we applied an emulsification principle, analogous to the one reported by Schuler *et al.* [186], in order to disperse small bubbles of aqueous phase in the organic phase.

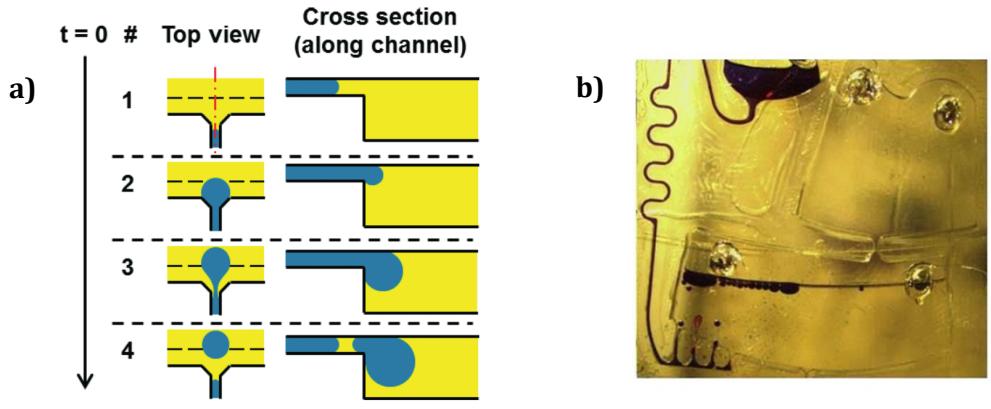

Fig. 5.12: (a) Principle of centrifugal emulsification, reprinted from [186] **with permission. (b) Formation of bubbles of aqueous sample in DCM. Reprinted from Paper III with permission.**

As shown in Fig. 5.12a, two fluids of different density are involved in the emulsification process. The inlet channel, introducing the least dense fluid at the bottom of the chamber, has a sudden disruption that generates a bubble, which is pushed to the top when applying centrifugal pressure. Analogously, the four outlets of the serpentine siphon enabled the creation of aqueous bubbles through the DCM phase during the first seconds of phase mixing on our LoD (Fig. 5.12b).

5.1.6 Pneumatic pumping

The principle of pneumatic pumping was first introduced in centrifugal microfluidics by Gorkin *et al*. [205]. The mechanism is based on the storage and release of pneumatic energy, as illustrated in Fig. 5.13.

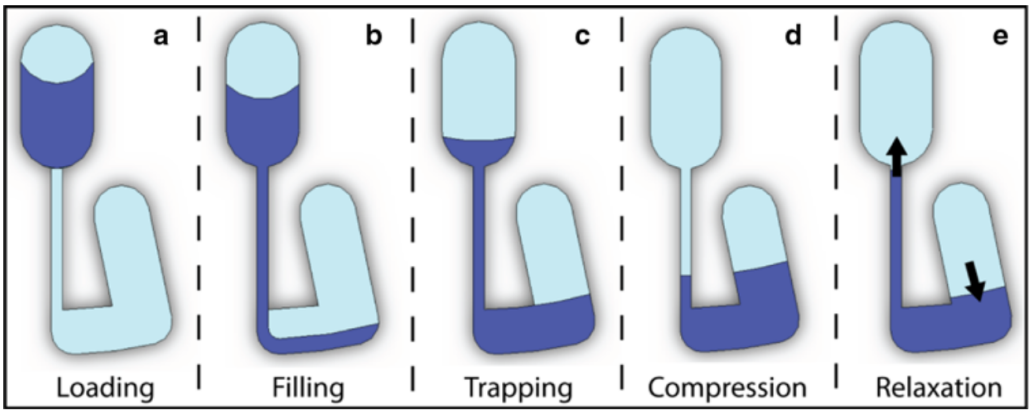

Fig. 5.13: (a) Loading of the sample. (b) Increasing the spinning speed, the sample fills the inlet channel and (c) traps air into the dead-end pneumatic chamber. (d) Further acceleration compresses the trapped air, which expands (e) by decelerating the disc. Reprinted from [205] **with permission.**

The fluid, initially loaded in the loading chamber (Fig. 5.13a), is pushed into the dead-end pneumatic chamber (Fig. 5.13b and c). At high spinning speed, the fluid traps and compresses the air in the pneumatic chamber (Fig. 5.13d). When lowering the spinning speed, the pressure on the pneumatic chamber is released, causing the trapped air to expand and push the liquid backwards (Fig. 5.13e). Gorkin *et al*. developed a theoretical

model for pneumatic pumping, describing the dependency of the liquid column height on the spinning speed, and applied it to cascade priming of hydrophobic siphons [206].

The principle of pneumatic actuation is advantageous because it overcomes a substantial limitation of centrifugal microfluidics, represented by the unidirectional liquid actuation, without any external actuation device of surface modification. However, the pneumatic chamber needs space on disc, which is a disadvantage in case of repeated siphoning or small footprint microfluidics.

Pneumatic actuation was also applied to control the wetting of the base of a chromatographic/filtration element embedded on disc [207], [190], or to repeatedly wet an immunoassay antigen array through repeated cycles of acceleration and deceleration [187]. Analogously, we applied pneumatic actuation to rapidly wet the surface of the SERS chip embedded in the sensing chamber, and push the solvent back to let the chip dry (Fig. 5.14). Fast wetting was needed to reduce the contact time between the tape (used for SERS chip integration) and the organic solvent, in order to minimize tape degradation.

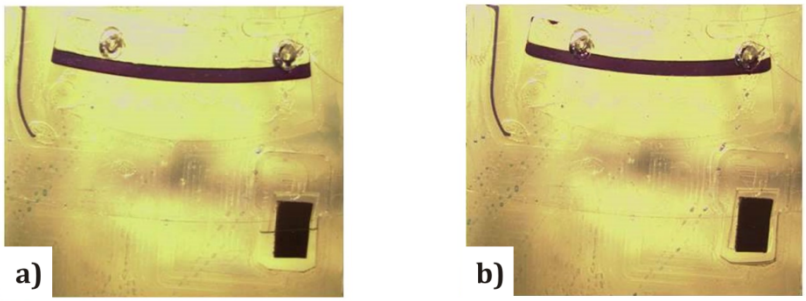

Fig. 5.14: (a) Organic solvent wetting the SERS chip in the sensing chamber at high spinning speed (ν = 45 Hz). (b) The solvent is pushed back at lower speed (ν = 12.5 Hz). Reprinted from Paper III with permission.

5.2 Fabrication of the LoD

Early microfluidic devices were mostly made of materials such as glass, quartz or silicon and predominantly involved microelectronic fabrication methods [208]. However, many applications demanded disposable microfluidic devices in order to avoid sample

contamination, or rapid prototyping techniques to enable fast design and optimization cycles. Therefore, an increasing trend towards polymer-based microfluidics represented the solution to this problem, additionally supported by the progress in polymer chemistry and polymer fabrication, which had already been developed for the production of a wide variety of low-cost common laboratory items (e.g. Eppendorf tubes, pipette tips, culture flasks, etc.) [209]. PDMS soft-lithography, introduced by Duffy *et al*. [210], first enabled the design and fabrication of an elastomeric microfluidic device in less than 24 h, while keeping a significantly low channel resolution (<20 µm in [210]). This innovation led to an exponential growth of research activities in this area, although some reviewers pointed out the increasing gap with the materials and methods used in industry (namely thermoplastic materials and injection molding) [209].

Tab. 5.1: Overview of chemical resistance and fabrication techniques of polymers for microfluidic applications (extracted from [209] **and** [211]**).**

Polymer	Resistant against	Not resistant against	Fabrication technique
PMMA	Acids, bases, oil, petrol	Alcohols, acetone, organic solvents	Laser ablation, hot embossing, injection molding, x-ray lithography
PC	Alcohols, acids	Hydrocarbons, ketones, KOH	Injection molding, hot embossing, laser ablation
PP	Acids, bases, alcohols, organic solvents, fats	Petrol, hydrocarbons	Injection molding
PS	Bases, alcohols	Concentrated acids, ether, hydrocarbons	Injection molding, hot embossing, laser ablation
COC	Acids, bases	Some organic solvents	Injection molding, hot embossing
PDMS	Weak acids and bases	Strong acids, hydrocarbons	Soft-lithography, direct laser plotting
SU-8	Acids, bases, most solvents	-	Photolithography

In recent years, significant attention has been focused on bringing the fabrication processes used in research laboratories closer to the ones used in industry, by widening the range of polymers and fast prototyping techniques available for microfluidic applications.

A wide variety of polymers with different physico-chemical properties (e.g. chemical resistance, heat resistance, transparency, gas permeability, biocompatibility, etc.) and the corresponding fabrication techniques is now available. Common examples are poly(methyl methacrylate) (PMMA), poly(carbonate) (PC), poly(propylene) (PP), poly(styrene) (PS), cyclic olefin copolymer (COC), poly(dimethyl siloxane) (PDMS), and photoresist SU-8 (Tab. 5.1 and Tab. 5.2).

Tab. 5.2: Overview of advantages and disadvantages of fabrication techniques for polymer-based microfluidics. Adapted from [211] **and** [212]**.**

Fabrication method	Advantages	Disadvantages
Laser ablation	Rapid, cost-effective, large format production	Limited materials and resolution, difficult mass production
Hot embossing	Precise replication of microstructures, suitable for mass production	Restricted to thermoplastics, time-consuming
Injection molding	Mass production, good resolution, time-effective and highly automated	Restricted to thermoplastics, expensive instrumentation
Photolithography	Ideal for microscale features	Requires a flat surface to start with, need chemical treatment
Soft-lithography	Cost-effective, able to fabricate 3D geometries, high resolution	Pattern deformation, vulnerable to defect, not high-throughput
X-ray lithography	High resolution for fabrication of nanopatterns	Time-consuming, high cost, difficult master fabrication process

In conclusion, the choice of material and fabrication technique is influenced by the specific purpose and application. In **Paper III**, sample filtration was implemented by embedding a membrane between layers of PMMA and PSA tape, ideal for rapid prototyping through laser ablation. Considering the harsh chemicals used in LLE, a transparent grade of PP was chosen for its chemical resistance, transparency and availability, and used for the microfluidic LLE assay. In addition, injection molding was the reproducible and high-throughput method of choice for PP microfluidic slides, demonstrating the scalability of the presented LoD.

5.2.1 Filtration module: laser ablation and PSA cutting

For the implementation of the filtration part, laser ablation was used to rapidly cut PMMA layers (Axxicon Moulds, The Netherlands), which were assembled together with PSA layers, embedding a piece of cellulose acetate membrane. A table-top CO_2 laser cutter (Epilog Mini 18, 30 W, Epilog, CO, USA) was used to engrave channels and cut chambers into PMMA, which is a biocompatible and optically clear polymer, used for the fabrication of a wide range of microfluidic devices [213].

The ablation mechanism of PMMA is the result of a photothermal process [213]. In fact, the CO_2 laser continuously emits an infrared radiation at 10.6 μm, which is effectively absorbed by PMMA. When the laser beam meets the PMMA surface, the temperature rises rapidly above the polymer boiling temperature. The polymer is melted and immediately vaporized in its monomer form, so that the V-shaped cavity is not contaminated by any degradation component (Fig. 5.15a). However, in case of high power, part of the molten polymer tends to redeposit at the edge of the V-shaped groove (Fig. 5.15b). For this reason, laser power, laser speed and number of passes must be optimized according to the desired channel depth, width and shape.

Double-sided PSA tape (ARcare® 90106, Adhesive Research, Limerick, Ireland) was used to assemble together PMMA layers. The tape was composed by a layer of clear polyester covered by adhesive (MA-69 acrylic hybrid medical grade adhesive) and white polyester release films on both sides. A computer-programmed desktop cutter (Silhouette Cameo Plotter, Silhouette America Inc., Utah, US) was used to cut microfluidic features

through the tape. After cutting, the excess material was removed with the help of a sharp blade before use.

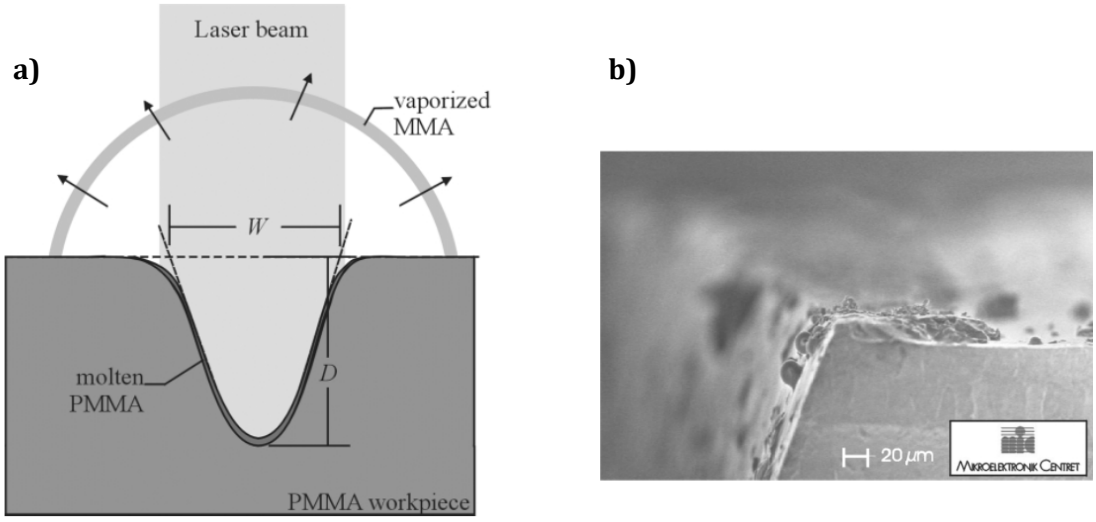

Fig. 5.15: (a) Scheme representing the mechanism of laser ablation of PMMA. (b) Edge of a laser-cut groove. Reprinted from [213] **with permission.**

5.2.2 Assay module: micromilling, injection molding and ultrasonic welding

The use of injection molding for low-cost fabrication of large volumes of microfluidic devices is now one of the many possibilities for microfluidic fabrication [214]. The injection molding of polymeric microfluidic components and total analysis devices has been reviewed in the last few years [215], [216], and examples have been reported of injection molded devices for LLE [217].

Injection molding is the process of heating and melting a thermoplastic material in the form of pellets inside a heated barrel. The molten polymer is forced and kept under pressure into a mold cavity, where a removable shim with the desired microfluidic features is located. After the polymer solidifies, the mold cavity is opened and the piece is ejected, before repeating the whole cycle. The optimization of the molding parameters (mold temperature, injection speed, holding pressure, holding time, demolding speed, etc.) results in the automated production of molded parts with short fabrication cycles. In case

of variotherm processes, in which a cooling system improves polymer demolding by actively cooling down the mold cavity, the time needed for temperature variation can significantly increase the cycle length up to a few minutes. In the case of the developed PP microfluidic slides (**Paper III**), the whole cycle, involving heating up of the mold, polymer injection, holding time until cooled down and demolding, lasted approximately two and a half minutes, enabling the production of approximately 100 pieces in 4 hours.

The PP flat slides were obtained through injection molding with a flat shim, whereas the microfluidic slides were molded with a milled aluminum shim.

Milling is defined as a subtractive manufacturing process that removes excess material from a workpiece through the use of rotary cutting tools [218]. Milling can be used to carve channels and chambers directly into the final microfluidic piece, or to create a negative mold to use in subsequent processing steps, such as hot embossing [219], soft-lithography [220] or, as in **Paper III**, injection molding. The use of milled shims for injection molding results in reproducible microfluidic structures with vertical walls, much closer to the desired size than with other techniques, such as laser ablation. This is particularly advantageous for fabrication of microfluidic features that need a precise and reproducible implementation, such as metering.

The process of milling is summarized in Fig. 5.16. The milling machine is essentially composed of a worktable moving in the xy plane, a spindle moving in the z direction, and a rotating cutting tool secured to the spindle. It is possible to regulate the spinning speed of the rotating tool and the x, y and z speed; in general, a lower translational speed generates a smoother surface, at the cost of a longer process. Increasing the spinning speed also helps with obtaining a smoother surface, but particular attention must be put in securing the workpiece to the worktable and in avoiding tool overheating with constant spraying of water or cutting oil.

In a typical milling process, once the 3D model is designed (with a 3D CAD software such as SolidWorks, Dassault Systèmes, France) and loaded as a suitable CNC code (with a CAD/CAM software such as CimatronE, Cimatron Group, Israel), the aluminum bulk piece is secured to the worktable through screws or a layer of heavy-duty double-sided tape. In this step it is important to keep the workpiece as flat as possible, since this is directly

related to the flatness of the shim. In fact, a significantly tilted shim creates undesired slots in the mold cavity and generates polymer flakes which make demolding difficult or impossible. Furthermore, non-flat pieces can significantly complicate the subsequent welding step.

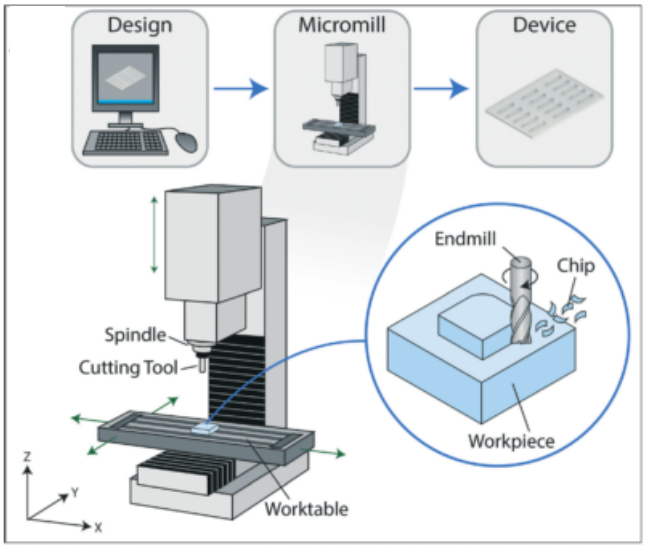

Fig. 5.16: Schematic drawing of the steps in the milling process (design, milling and finished piece). The main components of a milling machine are a worktable, a spindle and a rotating cutting tool. During milling, excess material is removed from the workpiece by the cutting tool (inset). Reprinted from [218] **with permission.**

The alignment of the rotating tool in the z direction is then performed manually, inevitably introducing an experimental error in the starting z position. For this reason, more reproducible devices can be obtained by using the same milled shim for molding several parts, rather than directly milling chambers and channels into each microfluidic part.

Finally, it is important to keep the cutting tool wet with cutting oil during milling, in order to avoid overheating and possible breakage of the tool.

Ultrasonic welding, used for the bonding of the injection molded parts, is an important and well-established fusion process for thermoplastics, commonly used in industry [221]. It is a thermal process where two parts are joined together through vibrational friction

heating at their interface [222]. Special structures, called *energy directors*, can be designed to direct the vibrational energy into predetermined spots across the surface. As depicted in Fig. 5.17, the welding of a flat and a microstructured surface is achieved by applying a short ultrasonic vibration to the parts through the sonotrode of an ultrasonic welder (Telsonic USP4700 20 kHz ultrasonic welder, Telsonic, Erlangen, Germany). In order to dampen vibrations and prevent slides from moving during welding, the slides are placed onto a flat steel block with a custom shape well (slightly bigger than a microscope slide, which is 25 x 75 mm). For a proper distribution of the vibrational energy it is important that the surfaces of the slides are parallel to the sonotrode; however, it is possible to compensate for slightly non-flat parts by placing small wedges at the bottom of the steel block. In this process, the main parameters to be optimized are the welding pressure, the welding time and the amplitude/energy of the vibration.

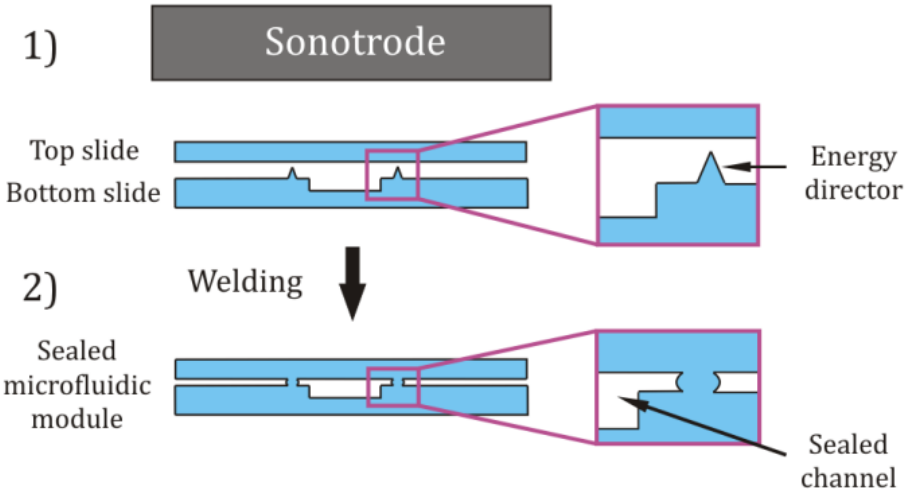

Fig. 5.17: Working principle of ultrasonic welding: (1) a flat slide and a microstructured slide with V-shaped energy directors are placed under a sonotrode. The channel is sealed by delivering a short ultrasonic vibration (2), which melts the energy directors (inset).

Ultrasonic welding is a fast technique for bonding polymers, it does not require any heating or soldering material, and it is easy to automate. Furthermore, thermal fusion is ideal for binding together inert polymers, such as PP.

In spite of its advantages, the use of ultrasonic welding is not established in the microfluidic field yet [223]–[226], probably due to the difficult implementation of energy directors in the microfluidic device. Poulsen *et al*. addressed this issue by developing a patented technique for fabrication of energy directors through injection molding [217], [222], [227], based on laser micromachining of triangular-shaped grooves along the microfluidic features on the aluminum shim. Thanks to this method, we were able to easily incorporate energy directors on the injection molded PP slides.

In **Paper III**, the combination of micromilling (2 – 3 h, just once), injection molding (4 – 5 h) and ultrasonic welding (1 – 2 h) enabled the fabrication of tens of PP microfluidic slides within one working day. Including the manual wetting of hydrophilic siphons with surfactant (1 – 2 h with drying), the cutting and assembly of PMMA and PSA layers for the filtration part (2 – 3 h), the opening of venting holes on PP through a soldering tool and the assembly of the slides on disc (0.5 h), the fabrication time of the complete discs was two working days.

6 Conclusions and future perspectives

The main goal of the Ph.D. project was to develop a centrifugal microfluidic platform to facilitate SERS sensing for quantitative screening of microbial strains.

In this work, we investigated Raman and SERS-based methods for screening of *E. coli* strains, demonstrating that (i) SERS can be effectively used as a robust quantitative technique, (ii) sample pre-treatment allows detection of one or more small compounds in complex supernatant samples, and (iii) the developed pre-treatment protocol can be implemented on a solvent-resistant LoD device, made with rapid fabrication techniques, also suitable for large scale production. In addition, we (iv) evaluated the usability of Raman spectroscopy for monitoring nutrients and metabolites in bacterial supernatant during a fermentation process (**Chapter 3**).

In the optimization process of engineered microbial strains for overproduction of valuable compounds, a specific, robust, fast and cost-effective detection technique would be ideal to speed up the testing step. Therefore, the aim of this Ph.D. project was to develop analytical approaches and platforms, enabling reliable, specific, time and cost efficient detection of bacterial metabolites, which have the potential to increase the throughput compared to the currently available methods, such as HPLC. In this context, SERS-based sensing presents significant advantages, providing molecule-specific spectral information, fast acquisition and high potential for miniaturization and automation, for instance with the integration of small active substrates into an automated microfluidic platform.

In order to discriminate between different strains based on the amount of the produced metabolites, the SERS-based sensing had to be optimized to achieve a robust and reproducible quantitative detection. The SERS substrates used in the project, based on gold-capped silicon nanopillars, had been previously developed in our group and had showed a good surface uniformity at a wafer scale, together with an excellent signal enhancement generated by the leaning of the nanopillars. The optimal enhancement is reached when the substrates are wetted by a droplet of organic sample and left to dry, causing the nanopillars to lean and create plasmonic hotspots. We investigated and

standardized the composition of the sample droplet (made of DCM or of water samples diluted with EtOH) and the sample volume needed to cover the SERS surface evenly, and thereby minimized the signal variability. Additionally, we developed and standardized a simple mapping method for 4x4 mm^2 SERS chips (described in **Chapter 3**) and investigated the reproducibility of SERS signal in-wafer, in-batch and batch-to-batch, observing an acceptable in-wafer variation of approximately 11% (**Paper II**). We addressed the higher in-batch and batch-to-batch variation either by collecting new calibration samples for each experiment, and using them for a different quantification every time (**Paper II** and **III**), or by accumulating data from several experiments in a PLS model to compensate for such variations (**Paper III** and **IV**).

Another important issue was the complexity of the matrix of real supernatant samples, containing salts, fouling the active surface, and molecules with vibrational peaks similar to the ones of the compounds of interest. In order to address this issue, we investigated the combination of SERS with two sample pretreatment techniques (LLE and SLM extraction), able to exclude salts and interfering compounds from the extracts. We characterized LLE in terms of extraction efficiency (**Paper II** and **V**) and SLM extraction in terms of enrichment and memory effect (**Paper V**), establishing the robustness of both the techniques with results validated by HPLC. In both cases, we demonstrated that the combination of SERS with a simple and robust pre-treatment step can significantly improve the sensitivity and specificity of detection while maintaining an easy-to-use experimental setup.

Based on the steps of the developed LLE protocol, we designed and developed a solvent-resistant, injection molded LoD device combining LLE and SERS sensing (**Paper III**). The chosen material (a clear grade of PP) was resistant to harsh chemicals such as HCl 32% and DCM, widening the applicability of the developed platform for various sample pre-treatment protocols. The fast and large-scale fabrication techniques involved (e.g. injection molding and ultrasonic welding) enabled the fabrication of tens of fluidic modules in two working days, demonstrating the possibility of a scalable, fast and low-cost production of the designed platform, increasing its potential as a commercial at-line monitoring tool.

Nevertheless, the applicability and the commercial value of the LLE/SERS LoD platform could be boosted through further improvements. Injection molding and ultrasonic welding of whole discs could significantly drop the fabrication time, whereas embedding injection-molded polymer SERS substrates in the microfluidic channels would overcome the integration issues of silicon chips presented in **Paper III**. Besides increasing the number of fluidic modules on a single disc, additional integrated features could make the LoD more appealing for biotechnologists, such as the detection of OD_{600}, a commonly used parameter in the study of *E. coli* growth and metabolism.

References

[1] J. Bailey, “Toward a science of metabolic engineering,” *Science*, vol. 252, no. 5013, pp. 1668–1675, Jun. 1991.

[2] J. Nielsen and J. D. Keasling, “Engineering Cellular Metabolism,” *Cell*, vol. 164, no. 6, pp. 1185–1197, Mar. 2016.

[3] P. Saling, “Eco-Efficiency Analysis of biotechnological processes,” *Appl. Microbiol. Biotechnol.*, vol. 68, no. 1, pp. 1–8, Jul. 2005.

[4] J. A. Dietrich, A. E. McKee, and J. D. Keasling, “High-Throughput Metabolic Engineering: Advances in Small-Molecule Screening and Selection,” *Annu. Rev. Biochem.*, vol. 79, no. 1, pp. 563–590, Jun. 2010.

[5] D. W. Shipp, F. Sinjab, and I. Notingher, “Raman spectroscopy: techniques and applications in the life sciences,” *Adv. Opt. Photonics*, vol. 9, no. 2, p. 315, Jun. 2017.

[6] L. A. Lyon, C. D. Keating, A. P. Fox, B. E. Baker, L. He, S. R. Nicewarner, S. P. Mulvaney, and M. J. Natan, “Raman Spectroscopy,” *Anal. Chem.*, vol. 70, no. 12, pp. 341–362, Jun. 1998.

[7] A. Rygula, K. Majzner, K. M. Marzec, A. Kaczor, M. Pilarczyk, and M. Baranska, “Raman spectroscopy of proteins: a review,” *J. Raman Spectrosc.*, vol. 44, no. 8, pp. 1061–1076, Aug. 2013.

[8] S. Wachsmann-Hogiu, T. Weeks, and T. Huser, “Chemical analysis in vivo and in vitro by Raman spectroscopy—from single cells to humans,” *Curr. Opin. Biotechnol.*, vol. 20, no. 1, pp. 63–73, Feb. 2009.

[9] Y. Xu, J. F. Ford, C. K. Mann, T. J. Vickers, J. M. Brackett, K. L. Cousineau, and W. G. Robey, “Raman measurement of glucose in bioreactor materials,” in *Biomedical Sensing, Imaging, And Tracking Technologies Ii*, 1997, vol. 2976, pp. 10–19.

[10] K. Kneipp, H. Kneipp, I. Itzkan, R. R. Dasari, and M. S. Feld, “Ultrasensitive Chemical Analysis by Raman Spectroscopy,” *Chem. Rev.*, vol. 99, no. 10, pp. 2957–2976, Oct. 1999.

[11] E. Smith and G. Dent, *Modern Raman Spectroscopy—A Practical Approach*, vol. 36, no. 8. John Wiley & Sons, Ltd, 2005.

[12] M. Navas-Moreno, M. Mehrpouyan, T. Chernenko, D. Candas, M. Fan, J. J. Li, M. Yan, and J. W. Chan, “Nanoparticles for live cell microscopy: A surface-enhanced Raman scattering perspective,” *Sci. Rep.*, vol. 7, no. 1, p. 4471, Dec. 2017.

[13] I-Fang Cheng, H.-C. Chang, T.-Y. Chen, C. Hu, and F.-L. Yang, "Rapid (<5 min) Identification of Pathogen in Human Blood by Electrokinetic Concentration and Surface-Enhanced Raman Spectroscopy," *Sci. Rep.*, vol. 3, no. 1, p. 2365, Dec. 2013.

[14] R. M. Jarvis, R. Goodacre, P. O. Box, S. Street, and M. Manchester, "Discrimination of bacteria using surface-enhanced Raman spectroscopy.," *Anal. Chem.*, vol. 76, no. 1, pp. 40–7, 2004.

[15] M. S. Schmidt, J. Hübner, and A. Boisen, "Large area fabrication of leaning silicon nanopillars for Surface Enhanced Raman Spectroscopy," *Adv. Mater.*, vol. 24, no. 10, pp. 11–18, 2012.

[16] C. T. Culbertson, T. G. Mickleburgh, S. A. Stewart-James, K. A. Sellens, and M. Pressnall, "Micro Total Analysis Systems: Fundamental Advances and Biological Applications," *Anal. Chem.*, vol. 86, no. 1, pp. 95–118, Jan. 2014.

[17] O. Strohmeier, M. Keller, F. Schwemmer, S. Zehnle, D. Mark, F. von Stetten, R. Zengerle, and N. Paust, "Centrifugal microfluidic platforms: advanced unit operations and applications," *Chem. Soc. Rev.*, 2015.

[18] R. Gorkin, J. Park, J. Siegrist, M. Amasia, B. S. Lee, J.-M. Park, J. Kim, H. Kim, M. Madou, and Y.-K. Cho, "Centrifugal microfluidics for biomedical applications," *Lab Chip*, vol. 10, no. 14, pp. 1758–1773, 2010.

[19] R. Burger, L. Amato, and A. Boisen, "Detection methods for centrifugal microfluidic platforms," *Biosens. Bioelectron.*, vol. 76, pp. 54–67, 2016.

[20] Y. Kim, S. N. Jeong, B. Kim, D. P. Kim, and Y. K. Cho, "Rapid and Automated Quantification of Microalgal Lipids on a Spinning Disc," *Anal. Chem.*, vol. 87, no. 15, pp. 7865–7871, 2015.

[21] A. Ribeiro, M. Estanqueiro, M. Oliveira, and J. Sousa Lobo, "Main Benefits and Applicability of Plant Extracts in Skin Care Products," *Cosmetics*, vol. 2, no. 2, pp. 48–65, 2015.

[22] N. Balasundram, K. Sundram, and S. Samman, "Phenolic compounds in plants and agri-industrial by-products: Antioxidant activity, occurrence, and potential uses," *Food Chem.*, vol. 99, no. 1, pp. 191–203, 2006.

[23] S. Y. Ou, J. W. Teng, Y. Y. Zhao, and J. Zhao, "p-Coumaric acid production from lignocelluloses," in *Phenolic Acids: Composition, Applications and Health Benefits*, 2012, pp. 63–71.

[24] A. Kim, S. J. Barcelo, R. S. Williams, and Z. Li, "Melamine sensing in milk products by using surface enhanced Raman scattering.," *Anal. Chem.*, vol. 84, pp. 9303–9, Nov. 2012.

[25] F. Sun, T. Bai, L. Zhang, J.-R. Ella-Menye, S. Liu, A. K. Nowinski, S. Jiang, and Q. Yu, "Sensitive and Fast Detection of Fructose in Complex Media via Symmetry Breaking

and Signal Amplification Using Surface-Enhanced Raman Spectroscopy," *Anal. Chem.*, vol. 86, no. 5, pp. 2387–2394, Mar. 2014.

[26] S. Boca-Farcau, M. Potara, T. Simon, A. Juhem, P. Baldeck, and S. Astilean, "Folic acid-conjugated, SERS-labeled silver nanotriangles for multimodal detection and targeted photothermal treatment on human ovarian cancer cells," *Mol. Pharm.*, vol. 11, no. 2, pp. 391–399, 2014.

[27] A. M. Giovannozzi, F. Rolle, M. Sega, M. C. Abete, D. Marchis, and A. M. Rossi, "Rapid and sensitive detection of melamine in milk with gold nanoparticles by Surface Enhanced Raman Scattering," *Food Chem.*, vol. 159, pp. 250–256, 2014.

[28] C. Weizmann and B. Rosenfeld, "The activation of the butanol-acetone fermentation of carbohydrates by Clostridium acetobutylicum (Weizmann).," *Biochem. J.*, vol. 31, no. 4, pp. 619–39, Apr. 1937.

[29] J. W. Foster and E. O. Karow, "Microbiological Aspects of Penicillin," *J. Bacteriol.*, vol. 49, no. 1, pp. 19–29, Sep. 1945.

[30] X. Chen, L. Zhou, K. Tian, A. Kumar, S. Singh, B. A. Prior, and Z. Wang, "Metabolic engineering of Escherichia coli: A sustainable industrial platform for bio-based chemical production," *Biotechnol. Adv.*, vol. 31, no. 8, pp. 1200–1223, 2013.

[31] H. Huttanus, J. Sheng, and X. Feng, "Metabolic Engineering for Production of Small Molecule Drugs: Challenges and Solutions," *Fermentation*, vol. 2, no. 1, p. 4, 2016.

[32] Y. Tsuge, H. Kawaguchi, K. Sasaki, and A. Kondo, "Engineering cell factories for producing building block chemicals for bio-polymer synthesis," *Microb. Cell Fact.*, vol. 15, no. 1, p. 19, 2016.

[33] C. T. Trinh, P. Unrean, and F. Srienc, "Minimal Escherichia coli Cell for the Most Efficient Production of Ethanol from Hexoses and Pentoses," *Appl. Environ. Microbiol.*, vol. 74, no. 12, pp. 3634–3643, 2008.

[34] S. Atsumi and J. C. Liao, "Directed Evolution of Methanococcus jannaschii Citramalate Synthase for Biosynthesis of 1-Propanol and 1-Butanol by Escherichia coli," *Appl. Environ. Microbiol.*, vol. 74, no. 24, pp. 7802–7808, Dec. 2008.

[35] C. R. Shen, E. I. Lan, Y. Dekishima, A. Baez, K. M. Cho, and J. C. Liao, "Driving Forces Enable High-Titer Anaerobic 1-Butanol Synthesis in Escherichia coli," *Appl. Environ. Microbiol.*, vol. 77, no. 9, pp. 2905–2915, May 2011.

[36] S. Atsumi, T.-Y. Wu, E.-M. Eckl, S. D. Hawkins, T. Buelter, and J. C. Liao, "Engineering the isobutanol biosynthetic pathway in Escherichia coli by comparison of three aldehyde reductase/alcohol dehydrogenase genes," *Appl. Microbiol. Biotechnol.*, vol. 85, no. 3, pp. 651–657, Jan. 2010.

[37] B. S. Dien, N. N. Nichols, and R. J. Bothast, "Fermentation of sugar mixtures using Escherichia coli catabolite repression mutants engineered for production of L -

lactic acid," *J. Ind. Microbiol. Biotechnol.*, vol. 29, no. 5, pp. 221–227, Nov. 2002.

[38] Y. Zhu, M. A. Eiteman, R. Altman, and E. Altman, "High Glycolytic Flux Improves Pyruvate Production by a Metabolically Engineered Escherichia coli Strain," *Appl. Environ. Microbiol.*, vol. 74, no. 21, pp. 6649–6655, Nov. 2008.

[39] T. B. Causey, S. Zhou, K. T. Shanmugam, and L. O. Ingram, "Engineering the metabolism of Escherichia coli W3110 for the conversion of sugar to redox-neutral and oxidized products: Homoacetate production," *Proc. Natl. Acad. Sci.*, vol. 100, no. 3, pp. 825–832, Feb. 2003.

[40] J. Báez-Viveros, N. Flores, K. Juárez, P. Castillo-España, F. Bolivar, and G. Gosset, "Metabolic transcription analysis of engineered Escherichia coli strains that overproduce L-phenylalanine," *Microb. Cell Fact.*, vol. 6, no. 1, p. 30, 2007.

[41] Z.-J. Zhao, C. Zou, Y.-X. Zhu, J. Dai, S. Chen, D. Wu, J. Wu, and J. Chen, "Development of l-tryptophan production strains by defined genetic modification in Escherichia coli," *J. Ind. Microbiol. Biotechnol.*, vol. 38, no. 12, pp. 1921–1929, Dec. 2011.

[42] L. Zhou, Z.-R. Zuo, X.-Z. Chen, D.-D. Niu, K.-M. Tian, B. A. Prior, W. Shen, G.-Y. Shi, S. Singh, and Z.-X. Wang, "Evaluation of Genetic Manipulation Strategies on d-Lactate Production by Escherichia coli," *Curr. Microbiol.*, vol. 62, no. 3, pp. 981–989, Mar. 2011.

[43] J. H. Park, K. H. Lee, T. Y. Kim, and S. Y. Lee, "Metabolic engineering of Escherichia coli for the production of L-valine based on transcriptome analysis and in silico gene knockout simulation," *Proc. Natl. Acad. Sci.*, vol. 104, no. 19, pp. 7797–7802, May 2007.

[44] H. S. Zahiri, S. H. Yoon, J. D. Keasling, S. H. Lee, S. Won Kim, S. C. Yoon, and Y. C. Shin, "Coenzyme Q10 production in recombinant Escherichia coli strains engineered with a heterologous decaprenyl diphosphate synthase gene and foreign mevalonate pathway," *Metab. Eng.*, vol. 8, no. 5, pp. 406–416, Sep. 2006.

[45] H. Mundhada, K. Schneider, H. B. Christensen, and A. T. Nielsen, "Engineering of high yield production of L-serine in Escherichia coli," *Biotechnol. Bioeng.*, vol. 113, no. 4, pp. 807–816, Apr. 2016.

[46] P. K. Ajikumar, W.-H. Xiao, K. E. J. Tyo, Y. Wang, F. Simeon, E. Leonard, O. Mucha, T. H. Phon, B. Pfeifer, and G. Stephanopoulos, "Isoprenoid Pathway Optimization for Taxol Precursor Overproduction in Escherichia coli," *Science*, vol. 330, no. 6000, pp. 70–74, 2010.

[47] K. Watanabe, K. Hotta, A. P. Praseuth, K. Koketsu, A. Migita, C. N. Boddy, C. C. C. Wang, H. Oguri, and H. Oikawa, "Total biosynthesis of antitumor nonribosomal peptides in Escherichia coli," *Nat. Chem. Biol.*, vol. 2, no. 8, pp. 423–428, 2006.

[48] W. Zhang, Y. Li, and Y. Tang, "Engineered biosynthesis of bacterial aromatic polyketides in Escherichia coli," *Proc. Natl. Acad. Sci.*, vol. 105, no. 52, pp. 20683–

20688, 2008.

[49] T. T. Eckdahl, A. M. Campbell, L. J. Heyer, J. L. Poet, D. N. Blauch, N. L. Snyder, D. T. Atchley, E. J. Baker, M. Brown, E. C. Brunner, S. A. Callen, J. S. Campbell, C. J. Carr, D. R. Carr, S. A. Chadinha, G. I. Chester, J. Chester, B. R. Clarkson, K. E. Cochran, S. E. Doherty, C. Doyle, S. Dwyer, L. M. Edlin, R. A. Evans, T. Fluharty, J. Frederick, J. Galeota-Sprung, B. L. Gammon, B. Grieshaber, J. Gronniger, K. Gutteridge, J. Henningsen, B. Isom, H. L. Itell, E. C. Keffeler, A. J. Lantz, J. N. Lim, E. P. McGuire, A. K. Moore, J. Morton, M. Nakano, S. A. Pearson, V. Perkins, P. Parrish, C. E. Pierson, S. Polpityaarachchige, M. J. Quaney, A. Slattery, K. E. Smith, J. Spell, M. Spencer, T. Taye, K. Trueblood, C. J. Vrana, and E. T. Whitesides, "Programmed evolution for optimization of orthogonal metabolic output in bacteria," *PLoS One*, vol. 10, no. 2, pp. 1–27, 2015.

[50] R. H. Dahl, F. Zhang, J. Alonso-Gutierrez, E. Baidoo, T. S. Batth, A. M. Redding-Johanson, C. J. Petzold, A. Mukhopadhyay, T. S. Lee, P. D. Adams, and J. D. Keasling, "Engineering dynamic pathway regulation using stress-response promoters," *Nat. Biotechnol.*, vol. 31, no. 11, pp. 1039–1046, 2013.

[51] J. E. Dueber, G. C. Wu, G. R. Malmirchegini, T. S. Moon, C. J. Petzold, A. V Ullal, K. L. J. Prather, and J. D. Keasling, "Synthetic protein scaffolds provide modular control over metabolic flux," *Nat. Biotechnol.*, vol. 27, no. 8, pp. 753–759, 2009.

[52] M. I. Chávez-Béjar, A. R. Lara, H. López, G. Hernández-Chávez, A. Martinez, O. T. Ramírez, F. Bolívar, and G. Gosset, "Metabolic engineering of Escherichia coli for L-tyrosine production by expression of genes coding for the chorismate mutase domain of the native chorismate mutase-prephenate dehydratase and a cyclohexadienyl dehydrogenase from Zymomonas mobilis," *Appl. Environ. Microbiol.*, vol. 74, no. 10, pp. 3284–3290, 2008.

[53] G. N. Vemuri, M. A. Eiteman, and E. Altman, "Succinate production in dual-phase Escherichia coli fermentations depends on the time of transition from aerobic to anaerobic conditions," *J. Ind. Microbiol. Biotechnol.*, vol. 28, no. 6, pp. 325–332, Jun. 2002.

[54] J. Le Yu, X. X. Xia, J. J. Zhong, and Z. G. Qian, "Direct biosynthesis of adipic acid from a synthetic pathway in recombinant escherichia coli," *Biotechnol. Bioeng.*, vol. 111, no. 12, pp. 2580–2586, 2014.

[55] C. B. Jendresen, S. G. Stahlhut, M. Li, P. Gaspar, S. Siedler, J. Förster, J. Maury, I. Borodina, and A. T. Nielsen, "Highly Active and Specific Tyrosine Ammonia-Lyases from Diverse Origins Enable Enhanced Production of Aromatic Compounds in Bacteria and Saccharomyces cerevisiae," *Appl. Environ. Microbiol.*, vol. 81, no. 13, pp. 4458–4476, Jul. 2015.

[56] C. J. Petzold, L. J. G. Chan, M. Nhan, and P. D. Adams, "Analytics for Metabolic Engineering," *Front. Bioeng. Biotechnol.*, vol. 3, pp. 1–11, Sep. 2015.

[57] R. Kelwick, J. T. MacDonald, A. J. Webb, and P. Freemont, "Developments in the

Tools and Methodologies of Synthetic Biology," *Front. Bioeng. Biotechnol.*, vol. 2, no. November, pp. 1–23, Nov. 2014.

[58] H. H. Wang, F. J. Isaacs, P. A. Carr, Z. Z. Sun, G. Xu, C. R. Forest, and G. M. Church, "Programming cells by multiplex genome engineering and accelerated evolution," *Nature*, vol. 460, no. 7257, pp. 894–898, Aug. 2009.

[59] M. Jinek, K. Chylinski, I. Fonfara, M. Hauer, J. A. Doudna, and E. Charpentier, "A Programmable Dual-RNA-Guided DNA Endonuclease in Adaptive Bacterial Immunity," *Science*, vol. 337, no. 6096, pp. 816–821, Aug. 2012.

[60] J. K. Rogers and G. M. Church, "Multiplexed Engineering in Biology," *Trends Biotechnol.*, vol. 34, no. 3, pp. 198–206, Mar. 2016.

[61] C. Wittmann and S. Y. Lee, *Systems Metabolic Engineering*. Springer Science & Business Media, 2012.

[62] T. van Rossum, S. W. M. Kengen, and J. van der Oost, "Reporter-based screening and selection of enzymes," *FEBS J.*, vol. 280, no. 13, pp. 2979–2996, Jul. 2013.

[63] L. Lepot, K. De Wael, F. Gason, and B. Gilbert, "Application of Raman spectroscopy to forensic fibre cases," *Sci. Justice*, vol. 48, no. 3, pp. 109–117, Sep. 2008.

[64] H. G. M. Edwards, A. F. Johnson, and I. R. Lewis, "Applications of Raman Spectroscopy to the Study of Polymers and Polymerization Processes," *J. Raman Spectrosc.*, vol. 24, no. 8, pp. 475–483, 1993.

[65] R. J. Young and S. J. Eichhorn, "Deformation mechanisms in polymer fibres and nanocomposites," *Polymer (Guildf).*, vol. 48, no. 1, pp. 2–18, Jan. 2007.

[66] B. H. Stuart, "Polymer crystallinity studied using Raman spectroscopy," *Vib. Spectrosc.*, vol. 10, no. 2, pp. 79–87, Jan. 1996.

[67] B. . Stuart, "The application of Raman spectroscopy to the tribology of polymers," *Tribol. Int.*, vol. 31, no. 11, pp. 687–693, Nov. 1998.

[68] V. Parchaňský, J. Kapitán, and P. Bouř, "Inspecting chiral molecules by Raman optical activity spectroscopy," *RSC Adv.*, vol. 4, no. 100, pp. 57125–57136, Oct. 2014.

[69] C. A. Damin, V. H. T. Nguyen, A. S. Niyibizi, and E. A. Smith, "Application of scanning angle Raman spectroscopy for determining the location of buried polymer interfaces with tens of nanometer precision," *Analyst*, vol. 140, no. 6, pp. 1955–1964, 2015.

[70] D. Fischer, K. Sahre, M. Abdelrhim, B. Voit, V. B. Sadhu, J. Pionteck, H. Komber, and J. Hutschenreuter, "Process monitoring of polymers by in-line ATR-IR, NIR and Raman spectroscopy and ultrasonic measurements," *Comptes Rendus Chim.*, vol. 9, no. 11–12, pp. 1419–1424, Nov. 2006.

[71] F. J. Yang, X. Cheng, Z. D. Zhou, and Y. Zhang, "An analysis of domain reorientation in

PLZT ceramics by in situ Raman spectroscopy," *J. Appl. Phys.*, vol. 106, no. 11, 2009.

[72] W. B. White and D. G. Minser, "Raman spectra and structure of natural glasses," *J. Non. Cryst. Solids*, vol. 67, no. 1–3, pp. 45–59, Sep. 1984.

[73] Z. Li, M. Deen, S. Kumar, and P. Selvaganapathy, "Raman Spectroscopy for In-Line Water Quality Monitoring—Instrumentation and Potential," *Sensors*, vol. 14, no. 9, pp. 17275–17303, Sep. 2014.

[74] H. Rosen and T. Novakov, "Raman scattering and the characterisation of atmospheric aerosol particles," *Nature*, vol. 266, no. 5604, pp. 708–710, Apr. 1977.

[75] H. G. M. Edwards and P. Vandenabeele, "Raman spectroscopy in art and archaeology," *Philos. Trans. R. Soc. A Math. Phys. Eng. Sci.*, vol. 374, no. 2082, p. 20160052, Dec. 2016.

[76] K. Czamara, K. Majzner, M. Z. Pacia, K. Kochan, A. Kaczor, and M. Baranska, "Raman spectroscopy of lipids: a review," *J. Raman Spectrosc.*, vol. 46, no. 1, pp. 4–20, Jan. 2015.

[77] J. M. Benevides, S. A. Overman, and G. J. Thomas, "Raman, polarized Raman and ultraviolet resonance Raman spectroscopy of nucleic acids and their complexes," *J. Raman Spectrosc.*, vol. 36, no. 4, pp. 279–299, Apr. 2005.

[78] J. F. Neault, M. Naoui, M. Manfait, and H. A. Tajmir-Riahi, "Aspirin-DNA interaction studied by FTIR and laser Raman difference spectroscopy," *FEBS Lett.*, vol. 382, no. 1–2, pp. 26–30, 1996.

[79] T. Huser and J. Chan, "Raman spectroscopy for physiological investigations of tissues and cells," *Adv. Drug Deliv. Rev.*, vol. 89, pp. 57–70, Jul. 2015.

[80] K. Kong, C. Kendall, N. Stone, and I. Notingher, "Raman spectroscopy for medical diagnostics — From in-vitro biofluid assays to in-vivo cancer detection," *Adv. Drug Deliv. Rev.*, vol. 89, pp. 121–134, Jul. 2015.

[81] R. Pandey, S. K. Paidi, T. A. Valdez, C. Zhang, N. Spegazzini, R. R. Dasari, and I. Barman, "Noninvasive Monitoring of Blood Glucose with Raman Spectroscopy," *Acc. Chem. Res.*, vol. 50, no. 2, pp. 264–272, Feb. 2017.

[82] M. S. Bergholt and S. Hassing, "Quantification of C-Reactive protein in human blood plasma using near-infrared Raman spectroscopy," *Analyst*, vol. 134, no. 10, p. 2123, 2009.

[83] S. Pahlow, S. Meisel, D. Cialla-May, K. Weber, P. Rösch, and J. Popp, "Isolation and identification of bacteria by means of Raman spectroscopy," *Adv. Drug Deliv. Rev.*, vol. 89, pp. 105–120, Jul. 2015.

[84] K. Golcuk, G. S. Mandair, A. F. Callender, N. Sahar, D. H. Kohn, and M. D. Morris, "Is photobleaching necessary for Raman imaging of bone tissue using a green laser?," *Biochim. Biophys. Acta - Biomembr.*, vol. 1758, no. 7, pp. 868–873, 2006.

[85] L. E. Kamemoto, A. K. Misra, S. K. Sharma, M. T. Goodman, H. Luk, A. C. Dykes, and T. Acosta, "Near-Infrared Micro-Raman Spectroscopy for in Vitro Detection of Cervical Cancer," *Appl. Spectrosc.*, vol. 64, no. 3, pp. 255–261, Mar. 2010.

[86] S. Nie, "Probing Single Molecules and Single Nanoparticles by Surface-Enhanced Raman Scattering," *Science*, vol. 275, no. 5303, pp. 1102–1106, Feb. 1997.

[87] S. Schlücker, B. Küstner, A. Punge, R. Bonfig, A. Marx, and P. Ströbel, "Immuno-Raman microspectroscopy:In situ detection of antigens in tissue specimens by surface-enhanced Raman scattering," *J. Raman Spectrosc.*, vol. 37, no. 7, pp. 719–721, Jul. 2006.

[88] D. Graham, R. Stevenson, D. G. Thompson, L. Barrett, C. Dalton, and K. Faulds, "Combining functionalised nanoparticles and SERS for the detection of DNA relating to disease," *Faraday Discuss.*, vol. 149, pp. 291–299, 2011.

[89] C. N. Kotanen, L. Martinez, R. Alvarez, and J. W. Simecek, "Surface enhanced Raman scattering spectroscopy for detection and identification of microbial pathogens isolated from human serum," *Sens. Bio-Sensing Res.*, vol. 8, pp. 20–26, May 2016.

[90] N. P. Ivleva, M. Wagner, A. Szkola, H. Horn, R. Niessner, and C. Haisch, "Label-Free in Situ SERS Imaging of Biofilms," *J. Phys. Chem. B*, vol. 114, no. 31, pp. 10184–10194, Aug. 2010.

[91] W. R. Premasiri, J. C. Lee, A. Sauer-Budge, R. Th?berge, C. E. Costello, and L. D. Ziegler, "The biochemical origins of the surface-enhanced Raman spectra of bacteria: a metabolomics profiling by SERS," *Anal. Bioanal. Chem.*, vol. 408, no. 17, pp. 4631–4647, Jul. 2016.

[92] B. Li, N. M. S. Sirimuthu, B. H. Ray, and A. G. Ryder, "Using surface-enhanced Raman scattering (SERS) and fluorescence spectroscopy for screening yeast extracts, a complex component of cell culture media," *J. Raman Spectrosc.*, vol. 43, no. 8, pp. 1074–1082, 2012.

[93] N. E. Marotta and L. A. Bottomley, "Surface-enhanced raman scattering of bacterial cell culture growth media," *Appl. Spectrosc.*, vol. 64, no. 6, pp. 601–606, 2010.

[94] A. Calvet and A. G. Ryder, "Monitoring cell culture media degradation using surface enhanced Raman scattering (SERS) spectroscopy," *Anal. Chim. Acta*, vol. 840, pp. 58–67, 2014.

[95] C. V. Raman and K. S. Krishnan, "A New Type of Secondary Radiation," *Nature*, vol. 121, pp. 501–502, Feb. 1928.

[96] R. Świsłocka, M. Kowczyk-Sadowy, M. Kalinowska, and W. Lewandowski, "Spectroscopic (FT-IR, FT-Raman, 1H and 13C NMR) and theoretical studies of p-coumaric acid and alkali metal p-coumarates," *Spectroscopy*, vol. 27, pp. 35–48, 2012.

[97] R. L. Mc Creery, *Raman spectroscopy for chemical analysis*. John Wiley & Sons, 2005.

[98] FDA, "Guidance for Industry PAT: A Framework for Innovative Pharmaceutical Development, Manufacuring, and Quality Assurance," *FDA Off. Doc.*, no. September, p. 16, 2004.

[99] ICH, "Pharmaceutical Development Q8," *ICH Harmon. Tripart. Guidel.*, vol. 8, no. August, pp. 1–28, 2009.

[100] P. O'Mara, A. Farrell, J. Bones, and K. Twomey, "Staying alive! Sensors used for monitoring cell health in bioreactors," *Talanta*, vol. 176, no. July 2017, pp. 130–139, Jan. 2018.

[101] P. Biechele, C. Busse, D. Solle, T. Scheper, and K. Reardon, "Sensor systems for bioprocess monitoring," *Eng. Life Sci.*, vol. 15, no. 5, pp. 469–488, Jul. 2015.

[102] "PROCELLICS™ In-Line and Real-Time Bioprocess Raman Analyzer." [Online]. Available: http://resolutionspectra.com/products/procellics/.

[103] "SUNIL-INA INSTRUMENT LTD. ® Raman RXN3 Analyzer." [Online]. Available: http://www.sunilina.com/rxn3-pilot.html.

[104] K. A. Esmonde-White, M. Cuellar, C. Uerpmann, B. Lenain, and I. R. Lewis, "Raman spectroscopy as a process analytical technology for pharmaceutical manufacturing and bioprocessing," *Anal. Bioanal. Chem.*, vol. 409, no. 3, pp. 637–649, 2017.

[105] T. B. Shope, T. J. Vickers, and C. K. Mann, "The direct analysis of fermentation products by Raman spectroscopy," *Appl. Spectrosc.*, vol. 41, no. 5, pp. 908–912, 1987.

[106] S. Sivakesava, J. Irudayaraj, and A. Demirci, "Monitoring a bioprocess for ethanol production using FT-MIR and FT-Raman spectroscopy," *J. Ind. Microbiol. Biotechnol.*, vol. 26, no. 4, pp. 185–190, 2001.

[107] B. Li, B. H. Ray, K. J. Leister, and A. G. Ryder, "Performance monitoring of a mammalian cell based bioprocess using Raman spectroscopy," *Anal. Chim. Acta*, vol. 796, pp. 84–91, Sep. 2013.

[108] C. Cannizzaro, M. Rhiel, I. Marison, and U. von Stockar, "On-line monitoring of Phaffia rhodozyma fed-batch process with in situ dispersive raman spectroscopy," *Biotechnol. Bioeng.*, vol. 83, no. 6, pp. 668–680, Sep. 2003.

[109] E. C. Le Ru, E. Blackie, M. Meyer, and P. G. Etchegoin, "Surface Enhanced Raman Scattering Enhancement Factors: A Comprehensive Study," *J. Phys. Chem. C*, vol. 111, no. 37, pp. 13794–13803, Sep. 2007.

[110] M. Fleischmann, P. J. Hendra, and A. J. McQuillan, "Raman spectra of pyridine adsorbed at a silver electrode," *Chem. Phys. Lett.*, vol. 26, no. 2, pp. 163–166, 1974.

[111] S.-Y. Ding, E.-M. You, Z.-Q. Tian, and M. Moskovits, "Electromagnetic theories of

surface-enhanced Raman spectroscopy," *Chem. Soc. Rev.*, vol. 46, no. 13, pp. 4042–4076, 2017.

[112] K. A. Willets and R. P. Van Duyne, "Localized Surface Plasmon Resonance Spectroscopy and Sensing," *Annu. Rev. Phys. Chem.*, vol. 58, no. 1, pp. 267–297, 2007.

[113] T. Chung, S.-Y. Lee, E. Y. Song, H. Chun, and B. Lee, "Plasmonic Nanostructures for Nano-Scale Bio-Sensing," *Sensors*, vol. 11, no. 12, pp. 10907–10929, Nov. 2011.

[114] N. D. Israelsen, C. Hanson, and E. Vargis, "Nanoparticle Properties and Synthesis Effects on Surface-Enhanced Raman Scattering Enhancement Factor: An Introduction," *Sci. World J.*, vol. 2015, pp. 1–12, 2015.

[115] E. Petryayeva and U. J. Krull, "Localized surface plasmon resonance: Nanostructures, bioassays and biosensing—A review," *Anal. Chim. Acta*, vol. 706, no. 1, pp. 8–24, Nov. 2011.

[116] P. L. Stiles, J. A. Dieringer, N. C. Shah, and R. P. Van Duyne, "Surface-Enhanced Raman Spectroscopy," *Annu. Rev. Anal. Chem.*, vol. 1, no. 1, pp. 601–626, 2008.

[117] L. P. Hackett, L. L. Goddard, and G. L. Liu, "Plasmonic nanocone arrays for rapid and detailed cell lysate surface enhanced Raman spectroscopy analysis," *Analyst*, 2017.

[118] A. H. Thilsted, J. Y. Pan, K. Wu, K. Zór, T. Rindzevicius, M. S. Schmidt, and A. Boisen, "Lithography-Free Fabrication of Silica Nanocylinders with Suspended Gold Nanorings for LSPR-Based Sensing," *Small*, vol. 12, no. 48, pp. 6745–6752, 2016.

[119] A. Reyer, A. Prinz, S. Giancristofaro, J. Schneider, D. Bertoldo Menezes, G. Zickler, G. R. Bourret, and M. E. Musso, "Investigation of Mass-Produced Substrates for Reproducible Surface-Enhanced Raman Scattering Measurements over Large Areas," *ACS Appl. Mater. Interfaces*, vol. 9, no. 30, pp. 25445–25454, Aug. 2017.

[120] K. Wu, T. Rindzevicius, M. S. Schmidt, K. B. Mogensen, A. Hakonen, and A. Boisen, "Wafer-Scale Leaning Silver Nanopillars for Molecular Detection at Ultra-Low Concentrations," *J. Phys. Chem. C*, vol. 119, no. 4, pp. 2053–2062, 2015.

[121] K. Wu, T. Rindzevicius, M. S. Schmidt, A. H. Thilsted, and A. Boisen, "Optimizing silver-capped silicon nanopillars to simultaneously realize macroscopic, practical-level SERS signal reproducibility and high enhancement at low costs," *J. Raman Spectrosc.*, no. August, pp. 1–11, Sep. 2017.

[122] K. Wu, T. Rindzevicius, M. S. Schmidt, K. B. Mogensen, S. Xiao, and A. Boisen, "Plasmon resonances of Ag capped Si nanopillars fabricated using mask-less lithography," *Opt. Express*, vol. 23, no. 10, p. 12965, 2015.

[123] L. Ramos, "Critical overview of selected contemporary sample preparation techniques," *J. Chromatogr. A*, vol. 1221, pp. 84–98, Jan. 2012.

[124] S. P. J. van Leeuwen, A. Kärrman, B. van Bavel, J. de Boer, and G. Lindström, "Struggle for Quality in Determination of Perfluorinated Contaminants in

Environmental and Human Samples," *Environ. Sci. Technol.*, vol. 40, no. 24, pp. 7854–7860, Dec. 2006.

[125] T. Hyötyläinen, "Critical evaluation of sample pretreatment techniques," *Anal. Bioanal. Chem.*, vol. 394, no. 3, pp. 743–758, Jun. 2009.

[126] K. Krygier, F. Sosulski, and L. Hogge, "Free, esterified, and insoluble-bound phenolic acids. 1. Extraction and purification procedure," *J. Agric. Food Chem.*, vol. 30, pp. 330–334, Mar. 1982.

[127] E. Müller, R. Berger, E. Blass, and D. Sluyts, "Liquid-Liquid Extraction," in *Ullmann's Encyclopedia of Industrial Chemistry*, Weinheim, Germany: Wiley-VCH Verlag GmbH & Co. KGaA, 2000, p. 54.

[128] J. D. Law and T. A. Todd, "Liquid-Liquid Extraction Equipment." Idaho National Laboratory (2008), INL-CON-08–15151.

[129] W. J. Groot, H. S. Soedjak, P. B. Donck, R. G. J. M. van der Lans, K. C. A. M. Luyben, and J. M. K. Timmer, "Butanol recovery from fermentations by liquid-liquid extraction and membrane solvent extraction," *Bioprocess Eng.*, vol. 5, no. 5, pp. 203–216, 1990.

[130] N. E. Markina, V. V. Shalabay, A. M. Zakharevich, and A. V. Markin, "Detection of sulfonamide drug in urine using liquid-liquid extraction and surface-enhanced Raman spectroscopy," 2016, vol. 9917, p. 99170X–1–5.

[131] V. V. Shalabay, N. E. Markina, V. V. Galushka, A. M. Zakharevich, A. V. Markin, and I. Y. Goryacheva, "Detection of rhodamine 6G in blood and urine using combination of surface-enhanced Raman spectroscopy and liquid-liquid extraction," in *Progress in Biomedical Optics and Imaging - Proceedings of SPIE*, 2017, vol. 10336, no. March, pp. 1033613-1–6.

[132] Z. Li, L. C. Romanoff, D. A. Trinidad, N. Hussain, R. S. Jones, E. N. Porter, D. G. Patterson, and A. Sjödin, "Measurement of Urinary Monohydroxy Polycyclic Aromatic Hydrocarbons Using Automated Liquid–Liquid Extraction and Gas Chromatography/Isotope Dilution High-Resolution Mass Spectrometry," *Anal. Chem.*, vol. 78, no. 16, pp. 5744–5751, Aug. 2006.

[133] J. Wang, C. Quan, X. Wang, P. Zhao, and S. Fan, "Extraction, purification and identification of bacterial signal molecules based on N-acyl homoserine lactones," *Microb. Biotechnol.*, vol. 4, no. 4, pp. 479–490, Jul. 2011.

[134] M. Patejko, J. Jacyna, and M. J. Markuszewski, "Sample preparation procedures utilized in microbial metabolomics: An overview," *J. Chromatogr. B*, vol. 1043, pp. 150–157, Feb. 2017.

[135] S. Tan, T. W. T. Rupasinghe, D. L. Tull, M. A. Augustin, and S. L. Gras, "Liquid–liquid extraction and liquid chromatography–mass spectrometry detection of curcuminoids from bacterial culture medium," *J. Chromatogr. B*, vol. 988, pp. 116–120, Apr. 2015.

[136] C. Nerín, J. Salafranca, M. Aznar, and R. Batlle, "Critical review on recent developments in solventless techniques for extraction of analytes," *Anal. Bioanal. Chem.*, vol. 393, no. 3, pp. 809–833, Feb. 2009.

[137] F. H. Quina and W. L. Hinze, "Surfactant-Mediated Cloud Point Extractions: An Environmentally Benign Alternative Separation Approach," *Ind. Eng. Chem. Res.*, vol. 38, no. 11, pp. 4150–4168, Nov. 1999.

[138] S. Oshite, M. Furukawa, and S. Igarashi, "Homogeneous liquid–liquid extraction method for the selective spectrofluorimetric determination of trace amounts of tryptophan," *Analyst*, vol. 126, no. 5, pp. 703–706, 2001.

[139] M. Rezaee, Y. Assadi, M.-R. Milani Hosseini, E. Aghaee, F. Ahmadi, and S. Berijani, "Determination of organic compounds in water using dispersive liquid–liquid microextraction," *J. Chromatogr. A*, vol. 1116, no. 1–2, pp. 1–9, May 2006.

[140] M. Zhang, X. Zhang, B. Qu, and J. Zhan, "Portable kit for high-throughput analysis of polycyclic aromatic hydrocarbons using surface enhanced Raman scattering after dispersive liquid-liquid microextraction," *Talanta*, vol. 175, no. July, pp. 495–500, Dec. 2017.

[141] D. Ciceri, J. M. Perera, and G. W. Stevens, "The use of microfluidic devices in solvent extraction," *J. Chem. Technol. Biotechnol.*, vol. 89, no. 6, pp. 771–786, Jun. 2014.

[142] K. Wang and G. Luo, "Microflow extraction: A review of recent development," *Chem. Eng. Sci.*, vol. 169, pp. 18–33, Sep. 2017.

[143] K. Sato, M. Tokeshi, T. Sawada, and T. Kitamori, "Molecular Transport between Two Phases in a Microchannel.," *Anal. Sci.*, vol. 16, no. 5, pp. 455–456, 2000.

[144] D. M. Fries, T. Voitl, and P. R. von Rohr, "Liquid Extraction of Vanillin in Rectangular Microreactors," *Chem. Eng. Technol.*, vol. 31, no. 8, pp. 1182–1187, Aug. 2008.

[145] H. Miyaguchi, M. Tokeshi, Y. Kikutani, A. Hibara, H. Inoue, and T. Kitamori, "Microchip-based liquid–liquid extraction for gas-chromatography analysis of amphetamine-type stimulants in urine," *J. Chromatogr. A*, vol. 1129, no. 1, pp. 105–110, Sep. 2006.

[146] A. Smirnova, K. Shimura, A. Hibara, M. A. Proskurnin, and T. Kitamori, "Application of a Micro Multiphase Laminar Flow on a Microchip for Extraction and Determination of Derivatized Carbamate Pesticides," *Anal. Sci.*, vol. 23, no. 1, pp. 103–107, 2007.

[147] J. Å. Jönsson and L. Mathiasson, "Membrane-based techniques for sample enrichment," *J. Chromatogr. A*, vol. 902, no. 1, pp. 205–225, 2000.

[148] J. Å. Jönsson and L. Mathiasson, "Liquid membrane extraction in analytical sample preparation: I. Principles," *TrAC Trends Anal. Chem.*, vol. 18, no. 5, pp. 318–325, May 1999.

[149] J. Å. Jönsson and L. Mathiasson, "Liquid membrane extraction in analytical sample preparation: II. Applications," *TrAC Trends Anal. Chem.*, vol. 18, no. 5, pp. 325–334, 1999.

[150] J. Lee, H. K. Lee, K. E. Rasmussen, and S. Pedersen-Bjergaard, "Environmental and bioanalytical applications of hollow fiber membrane liquid-phase microextraction: A review," *Anal. Chim. Acta*, vol. 624, no. 2, pp. 253–268, 2008.

[151] N. . van de Merbel, "The use of ultrafiltration and column liquid chromatography for on-line fermentation monitoring," *TrAC Trends Anal. Chem.*, vol. 16, no. 3, pp. 162–173, Mar. 1997.

[152] X. Wang, C. Saridara, and S. Mitra, "Microfluidic supported liquid membrane extraction," *Anal. Chim. Acta*, vol. 543, no. 1–2, pp. 92–98, 2005.

[153] B. Lindegård, H. Bjork, J. Å. Jonsson, L. Mathiasson, and A. M. Olsson, "Automated Column Liquid Chromatographic Determination of a Basic Drug in Blood Plasma Using the Supported Liquid Membrane Technique for Sample Pretreatment," *Anal. Chem.*, vol. 66, no. 24, pp. 4490–4497, 1994.

[154] P. Pantůčková and P. Kubáň, "In-line coupling of supported liquid membrane extraction to capillary electrophoresis for simultaneous analysis of basic and acidic drugs in urine," *J. Chromatogr. A*, vol. 1519, pp. 137–144, Oct. 2017.

[155] J. Å. Jönsson and L. Mathiasson, "Membrane extraction in analytical chemistry," *J. Sep. Sci.*, vol. 24, no. 7, pp. 495–507, Aug. 2001.

[156] A. Zwir-Ferenc and M. Biziuk, "Solid Phase Extraction Technique – Trends, Opportunities and Applications," *Polish J. Environ. Stud.*, vol. 15, no. 5, pp. 677–690, 2006.

[157] M.-C. Hennion, "Solid-phase extraction: method development, sorbents, and coupling with liquid chromatography," *J. Chromatogr. A*, vol. 856, no. 1–2, pp. 3–54, Sep. 1999.

[158] R. D. Oleschuk, L. L. Shultz-Lockyear, Y. Ning, and D. J. Harrison, "Trapping of Bead-Based Reagents within Microfluidic Systems: On-Chip Solid-Phase Extraction and Electrochromatography," *Anal. Chem.*, vol. 72, no. 3, pp. 585–590, Feb. 2000.

[159] V. Sahore, M. Sonker, A. V. Nielsen, R. Knob, S. Kumar, and A. T. Woolley, "Automated microfluidic devices integrating solid-phase extraction, fluorescent labeling, and microchip electrophoresis for preterm birth biomarker analysis," *Anal. Bioanal. Chem.*, pp. 1–9, Aug. 2017.

[160] J. Gao, B. T. Manard, A. Castro, D. P. Montoya, N. Xu, and R. M. Chamberlin, "Solid-phase extraction microfluidic devices for matrix removal in trace element assay of actinide materials," *Talanta*, vol. 167, no. January, pp. 8–13, May 2017.

[161] D. C. Harris, *Quantitative chemical analysis*, Sixth Edit. New York: W. H. Freeman and

Company, 2003.

[162] F. Gerber, M. Krummen, H. Potgeter, A. Roth, C. Siffrin, and C. Spoendlin, “Practical aspects of fast reversed-phase high-performance liquid chromatography using 3µm particle packed columns and monolithic columns in pharmaceutical development and production working under current good manufacturing practice,” *J. Chromatogr. A*, vol. 1036, no. 2, pp. 127–133, May 2004.

[163] R. D. McDowall, E. Doyle, G. S. Murkitt, and V. S. Picot, “Sample preparation for the HPLC analysis of drugs in biological fluids,” *J. Pharm. Biomed. Anal.*, vol. 7, no. 9, pp. 1087–1096, Jan. 1989.

[164] E. M. S. M. Gaspar and A. F. F. Lucena, “Improved HPLC methodology for food control – furfurals and patulin as markers of quality,” *Food Chem.*, vol. 114, no. 4, pp. 1576–1582, Jun. 2009.

[165] A. Kim, S. J. Barcelo, R. S. Williams, and Z. Li, “Melamine sensing in milk products by using surface enhanced Raman scattering.,” *Anal. Chem.*, vol. 84, no. 21, pp. 9303–9, Nov. 2012.

[166] C. M. Galanakis, V. Goulas, and V. Gekas, “Predicting the solubilization preference of natural phenols to different solvents,” in *11th International Congress on Engineering and Food*, 2011, pp. 1–6.

[167] M. Naczk and F. Shahidi, “Extraction and analysis of phenolics in food,” *J. Chromatogr. A*, vol. 1054, pp. 95–111, 2004.

[168] J. Dai and R. J. Mumper, “Plant phenolics: Extraction, analysis and their antioxidant and anticancer properties,” *Molecules*, vol. 15, pp. 7313–7352, 2010.

[169] P. Garcia-Salas, A. Morales-Soto, A. Segura-Carretero, and A. Fernández-Gutiérrez, “Phenolic-compound-extraction systems for fruit and vegetable samples,” *Molecules*, vol. 15, pp. 8813–8826, 2010.

[170] C. D. Stalikas, “Extraction, separation, and detection methods for phenolic acids and flavonoids,” *J. Sep. Sci.*, vol. 30, pp. 3268–3295, 2007.

[171] M. Knutsson, J. Lundh, L. Mathiasson, J. Å. Jönsson, and P. Sundin, “Supported Liquid Membranes for the Extraction of Phenolic Acids from Circulating Nutrient Solutions,” *Anal. Lett.*, vol. 29, no. 9, pp. 1619–1635, Jul. 1996.

[172] M. Putschögl, P. Zirak, and A. Penzkofer, “Absorption and emission behaviour of trans-p-coumaric acid in aqueous solutions and some organic solvents,” *Chem. Phys.*, vol. 343, no. 1, pp. 107–120, Jan. 2008.

[173] J. A. Cleveland, M. H. Benko, S. J. Gluck, and Y. M. Walbroehl, “Automated pKa determination at low solute concentrations by capillary electrophoresis,” *J. Chromatogr. A*, vol. 652, no. 2, pp. 301–308, Oct. 1993.

[174] J. Å. Jönsson, P. Lövkvist, G. Audunsson, and G. Nilvé, “Mass transfer kinetics for

analytical enrichment and sample preparation using supported liquid membranes in a flow system with stagnant acceptor liquid," *Anal. Chim. Acta*, vol. 277, no. 1, pp. 9–24, May 1993.

[175] D. R. Reyes, D. Iossifidis, P.-A. Auroux, and A. Manz, "Micro Total Analysis Systems. 1. Introduction, Theory, and Technology," *Anal. Chem.*, vol. 74, no. 12, pp. 2623–2636, Jun. 2002.

[176] E. K. Sackmann, A. L. Fulton, and D. J. Beebe, "The present and future role of microfluidics in biomedical research," *Nature*, vol. 507, no. 7491, pp. 181–189, Mar. 2014.

[177] W. Jung, J. Han, J.-W. Choi, and C. H. Ahn, "Point-of-care testing (POCT) diagnostic systems using microfluidic lab-on-a-chip technologies," *Microelectron. Eng.*, vol. 132, pp. 46–57, Jan. 2015.

[178] Y. Tang, M. Gan, Y. Xie, X. Li, and L. Chen, "Fast screening of bacterial suspension culture conditions on chips," *Lab Chip*, vol. 14, no. 6, p. 1162, 2014.

[179] S. Jang, B. Lee, H.-H. Jeong, S. H. Jin, S. Jang, S. G. Kim, G. Y. Jung, and C.-S. Lee, "On-chip analysis, indexing and screening for chemical producing bacteria in a microfluidic static droplet array," *Lab Chip*, vol. 16, no. 10, pp. 1909–1916, 2016.

[180] B. L. Wang, A. Ghaderi, H. Zhou, J. Agresti, D. A. Weitz, G. R. Fink, and G. Stephanopoulos, "Microfluidic high-throughput culturing of single cells for selection based on extracellular metabolite production or consumption.," *Nat. Biotechnol.*, vol. 32, no. 5, pp. 473–8, May 2014.

[181] H. S. Kim, T. L. Weiss, H. R. Thapa, T. P. Devarenne, and A. Han, "A microfluidic photobioreactor array demonstrating high-throughput screening for microalgal oil production.," *Lab Chip*, vol. 14, no. 8, pp. 1415–25, 2014.

[182] N. G. Anderson, "Computer Interfaced Fast Analyzers," *Science*, vol. 166, no. 3903, pp. 317–324, Oct. 1969.

[183] C. A. Burtis, J. C. Mailen, W. F. Johnson, C. D. Scott, T. O. Tiffany, and N. G. Anderson, "Development of a miniature fast analyzer.," *Clin. Chem.*, vol. 18, no. 8, pp. 753–761, 1972.

[184] M. Madou, J. Zoval, G. Jia, H. Kido, J. Kim, and N. Kim, "LAB ON A CD," *Annu. Rev. Biomed. Eng.*, vol. 8, no. 1, pp. 601–628, Aug. 2006.

[185] R. Burger, D. Kirby, M. Glynn, C. Nwankire, M. O'Sullivan, J. Siegrist, D. Kinahan, G. Aguirre, G. Kijanka, R. a Gorkin, and J. Ducrée, "Centrifugal microfluidics for cell analysis," *Curr. Opin. Chem. Biol.*, vol. 16, no. 3–4, pp. 409–414, Jul. 2012.

[186] F. Schuler, M. Trotter, M. Geltman, F. Schwemmer, S. Wadle, E. Domínguez-Garrido, M. López, C. Cervera-Acedo, P. Santibáñez, F. von Stetten, R. Zengerle, and N. Paust, "Digital droplet PCR on disk," *Lab Chip*, vol. 16, no. 1, pp. 208–216, 2016.

[187] Z. Noroozi, H. Kido, R. Peytavi, R. Nakajima-Sasaki, A. Jasinskas, M. Micic, P. L. Felgner, and M. J. Madou, "A multiplexed immunoassay system based upon reciprocating centrifugal microfluidics.," *Rev. Sci. Instrum.*, vol. 82, no. 6, p. 64303, Jun. 2011.

[188] A. Kazarine, M. C. R. Kong, E. J. Templeton, and E. D. Salin, "Automated Liquid–Liquid Extraction by Pneumatic Recirculation on a Centrifugal Microfluidic Platform," *Anal. Chem.*, vol. 84, no. 16, pp. 6939–6943, Aug. 2012.

[189] D. Choi, T. Kang, H. Cho, Y. Choi, and L. P. Lee, "Additional amplifications of SERS via an optofluidic CD-based platform.," *Lab Chip*, vol. 9, no. 2, pp. 239–43, Jan. 2009.

[190] O. Durucan, T. Rindzevicius, M. S. Schmidt, M. Matteucci, and A. Boisen, "Nanopillar Filters for Surface-Enhanced Raman Spectroscopy," *ACS Sensors*, Sep. 2017.

[191] H. Cho, H. Y. Kim, J. Y. Kang, and T. S. Kim, "How the capillary burst microvalve works," *J. Colloid Interface Sci.*, vol. 306, no. 2, pp. 379–385, 2007.

[192] M. Amasia and M. Madou, "Large-volume centrifugal microfluidic device for blood plasma separation," *Bioanalysis*, vol. 2, no. 10, pp. 1701–1710, Oct. 2010.

[193] M. Czugala, R. Gorkin III, T. Phelan, J. Gaughran, V. F. Curto, J. Ducrée, D. Diamond, and F. Benito-Lopez, "Optical sensing system based on wireless paired emitter detector diode device and ionogels for lab-on-a-disc water quality analysis," *Lab Chip*, vol. 12, no. 23, p. 5069, 2012.

[194] K. Sanger, K. Zór, C. Bille Jendresen, A. Heiskanen, L. Amato, A. Toftgaard Nielsen, and A. Boisen, "Lab-on-a-disc platform for screening of genetically modified E. coli cells via cell-free electrochemical detection of p-Coumaric acid," *Sensors Actuators, B Chem.*, vol. 253, pp. 999–1005, 2017.

[195] M. Karle, J. Wohrle, F. von Stetten, R. Zengerle, and D. Mark, "Axial centrifugal filtration - a novel approach for rapid bacterial concentration from a large volume," in *2013 Transducers & Eurosensors XXVII: The 17th International Conference on Solid-State Sensors, Actuators and Microsystems (TRANSDUCERS & EUROSENSORS XXVII)*, 2013, vol. M, pp. 1235–1238.

[196] E. J. Templeton and E. D. Salin, "A novel filtration method integrated on centrifugal microfluidic devices," *Microfluid. Nanofluidics*, vol. 17, no. 1, pp. 245–251, Jul. 2014.

[197] D. Mark, P. Weber, S. Lutz, M. Focke, R. Zengerle, and F. von Stetten, "Aliquoting on the centrifugal microfluidic platform based on centrifugo-pneumatic valves," *Microfluid. Nanofluidics*, vol. 10, no. 6, pp. 1279–1288, Jun. 2011.

[198] P. Andersson, G. Jesson, G. Kylberg, G. Ekstrand, and G. Thorsen, "Parallel nanoliter microfluidic analysis system," *Anal. Chem.*, vol. 79, no. 11, pp. 4022–4030, Jun. 2007.

[199] J. Steigert, T. Brenner, M. Grumann, L. Riegger, S. Lutz, R. Zengerle, and J. Ducrée, "Integrated siphon-based metering and sedimentation of whole blood on a

hydrophilic lab-on-a-disk," *Biomed. Microdevices*, vol. 9, no. 5, pp. 675–679, Oct. 2007.

[200] L. Riegger, M. M. Mielnik, A. Gulliksen, D. Mark, J. Steigert, S. Lutz, M. Clad, R. Zengerle, P. Koltay, and J. Hoffmann, "Dye-based coatings for hydrophobic valves and their application to polymer labs-on-a-chip," *J. Micromechanics Microengineering*, vol. 20, no. 4, p. 45021, Apr. 2010.

[201] J. Ducrée, S. Haeberle, S. Lutz, S. Pausch, F. Von Stetten, and R. Zengerle, "The centrifugal microfluidic Bio-Disk platform," *J. Micromechanics Microengineering*, vol. 17, no. 7, pp. S103–S115, Jul. 2007.

[202] J. Siegrist, R. Gorkin, L. Clime, E. Roy, R. Peytavi, H. Kido, M. Bergeron, T. Veres, and M. Madou, "Serial siphon valving for centrifugal microfluidic platforms," *Microfluid. Nanofluidics*, vol. 9, no. 1, pp. 55–63, 2010.

[203] D. C. Duffy, H. L. Gillis, J. Lin, N. F. Sheppard, and G. J. Kellogg, "Microfabricated centrifugal microfluidic systems: Characterization and multiple enzymatic assays," *Anal. Chem.*, vol. 71, no. 20, pp. 4669–4678, 1999.

[204] M. La, S. J. Park, H. W. Kim, J. J. Park, K. T. Ahn, S. M. Ryew, and D. S. Kim, "A centrifugal force-based serpentine micromixer (CSM) on a plastic lab-on-a-disk for biochemical assays," *Microfluid. Nanofluidics*, vol. 15, no. 1, pp. 87–98, Jul. 2013.

[205] R. Gorkin, L. Clime, M. Madou, and H. Kido, "Pneumatic pumping in centrifugal microfluidic platforms," *Microfluid. Nanofluidics*, vol. 9, no. 2–3, pp. 541–549, 2010.

[206] N. Godino, R. Gorkin, A. V. Linares, R. Burger, and J. Ducrée, "A centrifugo-pneumatic cascade for fully integrated and multiplexed biological analysis," *Proc. IEEE Int. Conf. Micro Electro Mech. Syst.*, no. February, pp. 989–992, 2012.

[207] S. Smith, K. Land, M. Madou, and H. Kido, "Rapid, Low-Cost Prototyping Of Centrifugal Microfluidic Devices For Effective Implementation Of Various Microfluidic Components," *South African J. Ind. Eng.*, vol. 26, no. 1, pp. 179–190, May 2015.

[208] P. N. Nge, C. I. Rogers, and A. T. Woolley, "Advances in Microfluidic Materials, Functions, Integration, and Applications," *Chem. Rev.*, vol. 113, no. 4, pp. 2550–2583, Apr. 2013.

[209] H. Becker and C. Gärtner, "Polymer microfabrication technologies for microfluidic systems," *Anal. Bioanal. Chem.*, vol. 390, no. 1, pp. 89–111, 2008.

[210] D. C. Duffy, J. C. McDonald, O. J. A. Schueller, and G. M. Whitesides, "Rapid Prototyping of Microfluidic Systems in Poly(dimethylsiloxane)," *Anal. Chem.*, vol. 70, no. 23, pp. 4974–4984, Dec. 1998.

[211] R. O. Rodrigues, R. Lima, H. T. Gomes, and A. M. T. Silva, "Polymer microfluidic devices: an overview of fabrication methods," *U.Porto J. Eng.*, vol. 1, no. 1, pp. 67–79,

2015.

[212] J. Wu and M. Gu, “Microfluidic sensing: state of the art fabrication and detection techniques,” *J. Biomed. Opt.*, vol. 16, no. 8, p. 80901, 2011.

[213] H. Klank, J. P. Kutter, and O. Geschke, “CO2-laser micromachining and back-end processing for rapid production of PMMA-based microfluidic systems,” *Lab Chip*, vol. 2, no. 4, p. 242, 2002.

[214] U. M. Attia, S. Marson, and J. R. Alcock, “Micro-injection moulding of polymer microfluidic devices,” *Microfluid. Nanofluidics*, vol. 7, no. 1, pp. 1–28, Jul. 2009.

[215] C. Zhang, J. Xu, W. Ma, and W. Zheng, “PCR microfluidic devices for DNA amplification,” *Biotechnol. Adv.*, vol. 24, no. 3, pp. 243–284, May 2006.

[216] G. Fiorini and D. Chiu, “Disposable microfluidic devices: fabrication, function, and application,” *Biotechniques*, vol. 38, no. 3, pp. 429–446, Mar. 2005.

[217] C. E. Poulsen, R. C. R. Wootton, A. Wolff, A. J. DeMello, and K. S. Elvira, “A Microfluidic Platform for the Rapid Determination of Distribution Coefficients by Gravity-Assisted Droplet-Based Liquid–Liquid Extraction,” *Anal. Chem.*, vol. 87, no. 12, pp. 6265–6270, Jun. 2015.

[218] D. J. Guckenberger, T. E. de Groot, A. M. D. Wan, D. J. Beebe, and E. W. K. Young, “Micromilling: a method for ultra-rapid prototyping of plastic microfluidic devices,” *Lab Chip*, vol. 15, no. 11, pp. 2364–2378, 2015.

[219] P. I. Okagbare, J. M. Emory, P. Datta, J. Goettert, and S. A. Soper, “Fabrication of a cyclic olefincopolymer planar waveguide embedded in a multi-channel poly(methyl methacrylate) fluidic chip for evanescence excitation,” *Lab Chip*, vol. 10, no. 1, pp. 66–73, 2010.

[220] M. E. Wilson, N. Kota, Y. Kim, Y. Wang, D. B. Stolz, P. R. LeDuc, and O. B. Ozdoganlar, “Fabrication of circular microfluidic channels by combining mechanical micromilling and soft lithography,” *Lab Chip*, vol. 11, no. 8, p. 1550, 2011.

[221] R. S. Soloff and S. G. Linsley, “Sonic method of welding thermoplastic parts,” US Pat., US 3224916 A, 1965.

[222] K. Kistrup, C. E. Poulsen, M. F. Hansen, and A. Wolff, “Ultrasonic welding for fast bonding of self-aligned structures in lab-on-a-chip systems,” *Lab Chip*, vol. 15, no. 9, pp. 1998–2001, 2015.

[223] R. Truckenmüller, Y. Cheng, R. Ahrens, H. Bahrs, G. Fischer, and J. Lehmann, “Micro ultrasonic welding: joining of chemically inert polymer microparts for single material fluidic components and systems,” *Microsyst. Technol.*, vol. 12, no. 10–11, pp. 1027–1029, Sep. 2006.

[224] K. G. Lee, S. Shin, B. Il Kim, N. H. Bae, M.-K. Lee, S. J. Lee, and T. J. Lee, “Ultrasonic bonding method for heterogeneous microstructures using self-balancing jig,” *Lab*

Chip, vol. 15, no. 6, pp. 1412–1416, 2015.

[225] M. Matteucci, A. Heiskanen, K. Zór, J. Emnéus, and R. Taboryski, "Comparison of Ultrasonic Welding and Thermal Bonding for the Integration of Thin Film Metal Electrodes in Injection Molded Polymeric Lab-on-Chip Systems for Electrochemistry," *Sensors*, vol. 16, no. 12, p. 1795, Oct. 2016.

[226] J. Sackmann, K. Burlage, C. Gerhardy, B. Memering, S. Liao, and W. K. Schomburg, "Review on ultrasonic fabrication of polymer micro devices," *Ultrasonics*, vol. 56, pp. 189–200, Feb. 2015.

[227] C. E. Poulsen, A. Wolff, N. K. Andersen, K. Kistrup, and R. Taboryski, "Micro-Scale Energy Directors For Ultrasonic Welding," IPC No.: B29C 65/ 08 A I. Patent No.: WO2016075272, 2016.

Appendix: Publications

Please see the attachment “Papers and unpublished material” for links and content.

Published by:
DTU Nanotech
Department of Micro- and Nanotechnology
Technical University of Denmark
Ørsteds Plads, building 345C
DK-2800 Kgs. Lyngby